X-615-67-452

NASA TM X-55925

THE ANALYSIS OF TOPSIDE IONOGRAMS

J. E. JACKSON

SEPTEMBER 1967

NASA

GODDARD SPACE FLIGHT CENTER

GREENBELT, MARYLAND

X-615-67-452

THE ANALYSIS OF TOPSIDE IONOGRAMS

BY

J. E. Jackson

September 1967

Goddard Space Flight Center

Greenbelt, Maryland

TABLE OF CONTENTS

THE ANALYSIS OF TOPSIDE IONOGRAMS

by

John E. Jackson
Laboratory for Space Sciences
NASA Goddard Space Flight Center
Greenbelt, Maryland

ABSTRACT

The relatively simple N-h analysis techniques used for the reduction of Alouette I ionograms (obtained from a height of 1000 km) were found inadequate for the reduction of high altitude ionograms from Alouette II (3000 km apogee). In some cases the Alouette II N-h profiles calculated with the Alouette I reduction techniques were in error by as much as 50 km in altitude. The techniques discussed in this report have improved the accuracy of the Alouette II N-h analysis by at least one order of magnitude. The improved N-h program is based upon a parabolic-in-log-N lamination technique, the actual values of the earth magnetic field at all heights, a change in variable which renders the integrand finite at the reflection point (and varying sufficiently slowly elsewhere to be calculated very accurately with a 3-point Gaussian integration technique), and iteration until successive calculations agree to within 0.01 km. A new technique is described which insures and accelerates the convergence of the iteration process. The selection of data points is discussed and it is shown that accurate results can be obtained with typically ten to twenty properly selected h'-f values. An important area where great care is required is in the actual scaling of ionograms, particularly when critical portions of the traces are hidden by local resonance effects. Although the N-h profiles are normally derived from the extraordinary trace, significant improvements in scaling accuracy can be achieved by making use of all the information

available on the ionograms. The identification on the ionograms of local effects (plasma resonances and propagation phenomena at the sounder) has been considerably simplified by making use of special tables computed for this purpose. These local effects are used to verify the interpretation of the extraordinary trace and, when desired, the resulting N-h profile is checked with the aid of the Z- and O- traces. The topside sounder parameters, capabilities and limitations are discussed in detail and illustrated with graphs indicating the temporal and geographic coverage available.

THE ANALYSIS OF TOPSIDE IONOGRAMS

by

J. E. JACKSON

I. INTRODUCTION

The ionospheric sounder (ionosonde) is the most powerful tool for the synoptic determination of the ionospheric electron density N, as a function of altitude h and of geographic location. Although an ionosonde does not yield directly the N-h function, the ionosonde data can be converted to N-h data by making use of the magneto-ionic theory. This theory is concerned with the propagation of radio waves in an ionized medium in the presence of a magnetic field. This subject is sufficiently broad to be the major (and sometimes exclusive) topic of a number of textbooks (Budden 1961, Kelso 1964, Ratcliffe 1959). However, for the specific task of reducing ionosonde data to N-h curves, only a few basic concepts and formulas are required. Consequently, the present report will restrict itself to the theoretical considerations actually used in the N-h analysis described. Although this report is based mainly upon experience with topside ionograms, much of the discussion is applicable to ionograms obtained from ground-based sounders.

An ionospheric sounder is essentially a swept low-frequency radar used to obtain echoes from the ionosphere. The sounder yields the apparent range of these ionospheric echoes, as a function of the sounder frequency (typically 1 to 15 MHz). The apparent range is one half of the measured round-trip time multiplied by the velocity of light in vacuo. Actually, in the ionosphere, the velocity of the sounding signals is less than the velocity of light, therefore the apparent range is greater than the true range. If the ionospheric horizontal gradients

and localized irregularities are small, the soundings can be considered to be vertical. Hence the apparent range is normally the apparent height for a ground-based sounder, and the apparent depth for a satellite-borne (or topside) sounder. In the subsequent discussion, it will be assumed that the soundings are vertical and that the ionograms provided by the sounder yield the apparent height h' as a function of frequency, keeping in mind that this apparent height can be measured either upward from the ground, or downward from a satellite. The apparent height h' is related to the true height h by the formula:

$$h' = \int_0^h n' \, dh \qquad (1)$$

where n', the group refractive index, is a function of the medium and of the sounding frequency. The property of the medium which control n' are the electron density, the intensity of the terrestrial magnetic field and the angle of magnetic dip. Since these parameters are height-dependent, it is quite appropriate to use height as the variable in formula (1). It is worth mentioning, however, that some authors are in favor of using apparent depth d' to describe topside ionograms. This leads to the very awkward notation $d' = \int_0^d n' \, dd'$! Others favor a general designation such as apparent path (P') which would apply to echoes from any direction. In this report the h'-f notation will be used, for the reasons given earlier, and also because this notation is consistent with the traditional terminology of ground-based soundings. Furthermore oblique echoes cannot be used for N-h analysis, unless the propagation path is known from other considerations. Hence, conventional N-h analysis is restricted to h'-f (or d'-f) curves.

One additional characteristic of the n' function is the fact that it has two values, one for each of the two possible

modes of propagation in the ionosphere. These two modes of propagation, called respectively ordinary (o) and extraordinary (x), yield separate echoes with different round-trip times. Hence an ionogram exhibits two distinct traces. one for the ordinary ray and one for the extraordinary ray. These two rays not only propagate with different velocities, but they also reflect under different conditions. An ordinary ray with a frequency f (MHz) reflects at a density N_R given by:

$$N_R = 12{,}400\ f^2 \text{ electrons/cc} \tag{2}$$

The frequency f defined by Equation (2) is known as the plasma frequency (fN) for the density N_R.
An extraordinary ray with a frequency f (MHz) reflects at a density N_R given by:

$$N_R = 12{,}400\ f(f-fH) \text{ electrons/cc} \tag{3}$$

where:

$$fH = (2.8)B \text{ MHz} \tag{4}$$

The quantity fH is known as the gyrofrequency and B is the induction in gausses of the earth's magnetic field at the reflection point. It is seen that the magnetic field influences the reflection condition only for the extraordinary ray. However B affects the propagation velocities of both magneto-ionic modes, the effect being more pronounced upon the extraordinary ray than upon the ordinary ray. In principle, either trace could be used to derive an N-h profile. An analysis based upon the ordinary trace is somewhat simpler, because the reflection density is independent of the magnetic field. A more important consideration, however, is the relative quality of the (o) and (x) data. In the lower portion of the ionosphere (D and E regions), the collisions between electrons and neutral particles causes low frequency waves

to be attenuated. The absorption is more severe for the (x) mode than for the (o) mode. Consequently on ground-based ionograms the (o) trace is usually more complete and therefore it is the one used in N-h analysis. The situation is different on topside ionograms. The relative quality of the (o) and (x) data is no longer due to differential absorption. The controlling factors are now the sounder antennas and the fact that reflection at a given density occurs at a higher frequency for the (x) mode than for the (o) mode. For example, if N_R = 1240 el/cc and fH = 1.0 MHz, it is seen from formulas (2) and (3) that the (o) ray reflects at f = 0.316 MHz and that the (x) ray reflects at f = 1.09 MHz. Although the antennas used in a topside sounder satellite are physically very long, they are electrically short (and hence difficult to match to the transmitter) at the low-frequency end of the sweep. Based upon this consideration alone, transmissions at 0.316 MHz would be considerably weaker than at 1.09 MHz. However, the situation is made even worse due to the fact that the antennas are immersed in the ionosphere. This causes a change in antenna impedance, which is particularly severe near the plasma frequency. The net result of the above considerations is that the low-frequency end of the (o) trace is usually missing on topside ionograms. Hence, on topside ionograms, the (x) trace is normally used for N-h analysis. It will be understood in the subsequent development that formula (1) refers only to one of the two possible modes. The discussion however applies to the analysis of either mode, unless otherwise indicated.

One should mention also the frequent presence of a Z trace on topside ionograms, for which the reflection condition is N_R = 12,400 f (f+fH) el/cc. However there is only a small range of frequencies (See page A-9 of Appendix A) at which the Z mode can propagagate from the satellite, and consequently the Z mode becomes cut off at the satellite long before it can penetrate down to the maximum of the F2 region. The Z trace is therefore not very useful for N-h analysis.

The above introductory comments can be summarized as follows. The ordinary (or extraordinary) trace of an ionogram, which is used in N-h analysis represents the function h'(f) given by:

$$h'(f) = \int_{h_0}^{h_R(f)} n'[N(h), f, B(h), \theta(h)]\, dh \qquad (5)$$

where:

- h' = virtual height with respect to the sounder (h' is considered negative on a topside ionogram)
- h = actual height
- h_0 = height of sounder (satellite altitude for a topside sounder)
- h_R = height at which reflection occurs for frequency f
- n' = group index of refraction
- N = ionospheric electron density
- B = induction of terrestrial magnetic field, a function of geographic location and altitude
- θ = dip angle of the terrestrial magnetic field, a function of geographic location, but relatively constant with altitude over usual altitude range of soundings.

It should be noted that Equation (5) does not give the function n' in explicit form. The actual formula for n' is quite complicated, and really not needed for the present discussion. The formula can be found in Appendix A. Tables giving values of n' under a wide range of conditions have been published (Becker, 1960).

II. OUTLINE OF THE LAMINATION CONCEPT

For a given geographic location and a given N-h distribution, it is a relatively straight forward matter to evaluate the integral shown in Equation (5). For a given frequency f,

the density N_R at the reflection point is known from either Equation (2) or Equation (3), and the integration limit h_R follows immediately from the known N-h function. The magnetic field parameters are known as a function of altitude. Thus all the required quantities are known in the group height integral of Equation (5). Although the integration cannot in general be performed analytically, it is nevertheless relatively simple, when N(h) is known, to compute h'(f) by a numerical integration technique. The basic problem involved in the analysis of an ionogram is to perform the opposite conversion, namely to derive the N(h) function from a knowledge of the h'(f) function. It is however, generally impossible to invert analytically the group height integral. The method used is to find a general model for N(h), with many adjustable parameters, which will satisfy Equation (5) for selected values of the h'(f) function. The number of parameters which can be determined is the same as the number of h'(f) values selected for the analysis. With the lamination model used in this report the N(h) function is represented by a number of points (N_j,h_j) connected by simple analytic curves. More specifically, in a given height interval (h_{j-1} to h_j), the profile is assumed to be of the form:

$$h = h_{j-1} + F_j\ (N) \qquad (6)$$

where $F_j(N)$ is a simple analytic function of density and where N_j would be the density at h_j. The actual use of the lamination concept can be more readily visualized in terms of a specific example. Let us assume that the h'-f function under analysis is the ordinary trace of a topside ionogram (negative virtual height) and that the laminations are assumed to be linear. Equation (6) becomes:

$$h = h_{j-1} + a_j\ (N-N_{j-1}) \qquad (7)$$

from which

$$dh = a_j \, dN \tag{8}$$

Writing Equation (5) in terms of the laminations shown in Equation (7) and changing from the variable h to the variable N yields:

$$h'(f_j) = \sum_{i=1}^{i=j} a_i \int_{N_{i-1}}^{N_i} n' \, dN \tag{9}$$

where N_j is the density at which reflection occurs at the frequency f_j, i.e. N_j is given by Equation (2). The right hand of Equation (9) represents an integration over (j-1) laminations. For the first lamination, i.e. the lamination nearest to the topside sounder:

$$h'(f_1) = a_1 \int_{N_0}^{N_1} n'(N,f_1,B,\theta) \, dN \tag{10}$$

For a given geographical location the variation of θ with altitude is negligible, while the magnetic intensity changes typically by 4 percent over a 100 km interval. The integral in Equation (10), however, is not very sensitive to the value of B and it can be evaluated with adequate accuracy by assuming B to be constant and equal to its value at the satellite. Hence a_1 is completely defined by Equation (10) and from Equation (7) it follows that:

$$h_1 = h_0 + a_1 \, (N_1 - N_0)$$

where: h_0 = height of the satellite

N_0 = electron density at satellite (given by Equation (2) and using for frequency, the exit frequency of the ordinary ray).

For the second lamination:

$$h'(f_2) = a_1 \int_{N_0}^{N_1} n'(N,f_2,B_0,\theta)dN + a_2 \int_{N_1}^{N_2} n'(N,f_2,B_1,\theta)dN \qquad (11)$$

where N_2 is related to f_2 by formula (2). It should be noted that the integral associated with a_1 is now for the frequency f_2, and also that the value of B used in the second integral corresponds to the altitude h_1 (which is obviously a more correct estimate of B in the second lamination). Equation (11) yields a_2 since this is the only unknown quantity, and consequently:

$$h_2 = h_1 + a_2 \ (N_2-N_1)$$

This step-by-step procedure is continued until the entire profile is determined. The relatively simple procedure described above has been used for the analysis of ionograms obtained from ground-based sounders (Jackson 1956). The techniques used for the reduction of topside ionograms are basically refinements of the simple lamination concept outlined above. Section III gives a general discussion of these refinements, and Section IV indicates the improvements in accuracy resulting from these refinements. The detailed discussion of the N-h reduction technique is given in Appendices A, B, C and D. These Appendices are concerned with the formulas used, the scaling procedure, the method of analysis and the accuracy of calculations.

III. DISCUSSION OF THE LAMINATION METHOD

The lamination procedure implies that values of h' have been selected from the ionogram at specific values of frequencies. In fact there is a one-to-one correspondence

between the successive values of f and the boundaries of the laminations. A question which arises naturally is how to select the h'-f values which enter in the analysis. A basic, but post-factum, criterion is that the resulting profile is adequately described by the calculated lamination. A rough criterion for the minimum number of h'-f values is that the selected points should permit an accurate reconstruction of the original h'-f graph. Usually twenty points are sufficient. The actual GSFC criterion for selecting data points is discussed in Appendix B.

Closely related to the number of points used in the analysis is the model used in the lamination technique. If a large number of points are used, then the resulting profile will be fairly accurate, even with the simple linear model used in the earlier example. However, the number of numerical integrations required increases as the square of the number of h'-f values used in the calculations. With a more elaborate model fewer points can be used in the calculation with an attending reduction in the computer time required, or a greater accuracy can be achieved using the same number of h'-f points in the calculations. Actually, in the topside ionosphere the electron density profile is represented more accurately by a succession of exponential segments, (Fitzenreiter and Blumle, 1964), i.e. the height increments are almost linear in log N, namely:

$$\Delta h = a_j \, (\ln N - \ln N_{j-1}) \tag{12}$$

One objection to the linear-in-N or linear-in-log N representation is that the assumed profile has discontinuous derivatives at each of lamination boundaries. This difficulty is readily overcome by assuming that the height increments are parabolic with continuous slopes at the boundaries. The parabolic-in-log N assumption (Paul and Wright, 1963) yields:

$$\Delta h = a_j \, \ln N/N_{j-1} + b_j \, [\ln N/N_{j-1}]^2 \tag{13}$$

with the slope continuity yielding:

$$a_{j+1} = a_j + 2b_j \ln (N_j/N_{j-1}) \tag{14}$$

It should be noted that the parabolic-in-log (fN) assumption (Doupnik and Schmerling, 1965) is equivalent to the parabolic-in-log N assumption. The parabolic-in-log (fN) assumption leads to:

$$\Delta h = a'_j \ln(fN/fN_{j-1}) + b'_j [\ln(fN/fN_{j-1})]^2$$

From the definition of fN (Eq.2), this reduces to:

$$\Delta h = \tfrac{1}{2}a'_j \ln(N/N_{j-1}) + \tfrac{1}{4} b'_j [\ln(N/N_{j-1})]^2$$

which is identical to Equation (13).

It is also noted that the analysis yields as answers the values of heights and densities corresponding to the top and bottom of the laminations. These are the values which appear in published tables of N-h data derived from ionograms. The heights and densities thus obtained are quite arbitrary and very awkward to use for any synoptic studies of the ionosphere. Although some authors include interpolated values of standard heights (or densities), there has been some feeling that these interpolated numbers are less accurate than the "calculated" values at the top and bottom of the laminations. Actually as indicated earlier, the calculations yield the parameters which defines the lamination. There is no basis for saying that the end points on the lamination are more accurate than any other point defined by the equation of the lamination. Hence if the calculated lamination equation is used (such as Equation (7) for the example shown), the interpolated values are just as valid as the so-called computed points which are simply the end points of these laminations.

The last group of comments is concerned with the method used for evaluating an integral such as the one shown in

Equation (10). There are three types of problems to be considered, the first one involves the parameters used in the integrand, the second one is concerned with the limits of integration, and the third one is the integration technique itself. These problems will be examined in the order listed above. The procedure suggested for evaluating the integral in Equation (10) was to assume that B was constant. This yields a fairly accurate value of the height h_1 and consequently of the altitude interval over which the integration is performed. Having determined the parameter a_1, the altitude and the value of B are known for each value of N used in the numerical integration. Hence the integral can be evaluated again, this time associating a more accurate value of B with each value of N used in the integration. This will yield a slightly differenct value of a_1 and h_1. The process however converges very rapidly and after a couple of iterations there are no further significant changes in the final answer.

The principle of iteration is also involved, but in a slightly more complicated way when extraordinary data are used in the calculations, since in this case it is not only the integrand which is affected but also the upper integration limit. If Equation (10) referred to a virtual height for the extraordinary ray, then the upper limit of integration N_1 would be given by Equation (3) namely:

$$N_1 = 12{,}400\ f_1\ (f_1 - 2.8B_1)$$

The value of B_1 is not known, and it would have to be initially estimated by letting $B_1 = B_0$. Solving Equation (10) with this assumption would yield a fairly good estimate of h_1 and hence B_1. The procedure could then be repeated, using not only a more accurate value of the integration limit N_1, but also more representative values of B within the integrand. It is natural to anticipate that iteration should be more important for the extraordinary ray than for the ordinary ray. Further discussion of this point is given in Appendix D.

The final point is concerned with the integration technique. The problem which arises here is the fact that the integrand is infinite at the reflection point. Although it has been known for at least 15 years (Poeverlein, 1951; Shinn , 1951; Jackson, 1956) that this infinity can be removed by means of a suitable change of variable, the importance of this transformation has not fully been appreciated. It was believed by some experimenters that a 16-point Gaussian integration technique could yield an accurate answer for an integral such as the one appearing in Equation (10). It turns out that a 16-point integration technique is both inefficient and inaccurate for the evaluation of the integral shown in Equation (10). For a typical lamination, including the reflection point, a direct evaluation of the group retardation in this lamination will be in error by 5.5% using a 7-point Gaussian and by 2.5% using a 16-point Gaussian, whereas the error is less than 0.005% if the same integral is evaluated numerically after making the suggested change of variable and using only a 3-point Gaussian integration technique! The author keeps the integrand finite at the reflection point by using the following change of variable:

$$t^2 = 1-X \qquad \text{for the ordinary ray}$$

$$t^2 = 1-X/(1-Y_R) \qquad \text{for the extraordinary ray}$$

where:

$X = 80.6\ N/f^2$

Y_R= value of Y at reflection point

$Y = f_H/f$

The detailed discussion of the accuracy achieved in the integration by using the above transformations is given in Appendix C.

IV. DISCUSSION OF ERRORS

There are three broad areas in which errors can arise: First in the instrumentation itself (for a topside sounder this includes both satellite and ground-based equipment), Second in the scaling of ionograms, Third in the method used to accomplish h'-f to N-h conversion. This section will be concerned only

with the problem of converting accurate topside h'-f values tothe correct N-h profile. Some comments and suggestions for the scaling of topside ionograms will be given in appendix B. A discussion of the instrumentation used to obtain h'-f records is certainly needed for an overall assessment of errors. To perform this task for the topside sounders would require inputs from the many engineering teams who have designed the satellite electronics, the telemetry system, the tape - to film processing equipment, etc. . . . Although these considerations will not be included in this report, it is hoped that the information will eventually be available from other sources.

It was pointed out in section III that the accurate analysis of topside ionograms require special care in a number of areas, such as the selection of data points, the choice of lamination technique, the use of iteration in the calculations, and the method used for the numerical evaluation of the group height integral.

The importance of these considerations will be now illustrated quantitatively, in terms of two extraordinary ray ionograms calculated from two theoretical (but representative) electron density profiles. The electron density profiles used are based upon Bauer's model for a ternary ion mixture topside ionogram (Bauer, 1962). The two models have the same shape, but at all altitudes there is a 5-to-1 ratio in density between the high and the low density models. It is assumed that the ionograms were obtained from an altitude of 3000 km (which corresponds to the apogee of Alouette II) and that the local electron densities were respectively

1000 el/cc for the low density model and 5000 el/cc for the high density model. For this theoretical situation it was assumed that the gyro-frequency at the satellite was 0.38 Mc and that the magnetic field varied with altitude according to an inverse cube law. The profiles and the corresponding ionograms are shown in Fig. B-4, B-5 and B-6 of Appendix B. To compute the ionograms, the profiles were divided into linear-in-log N laminations 5 km thick. The scaling criterion discussed in Appendix B was applied to the set of 520 h'-f values thus obtained, yielding the points (open and solid) shown on the ionograms. The solid points illustrate a less detailed scaling in which approximately half of the data points would be eliminated. Based upon additional calculations of the virtual heights, using 10 km and 20 km laminations, it was concluded that the errors in the virtual heights (obtained with the 5 km laminations) were less than 1 km.

The normal GSFC procedure for reducing an ionogram is to use the data points given by the scaling criterion, to assume laminations parabolic-in-log N, to iterate until the successive altitudes differ by less than 0.01 km, and to integrate with a 3-point Gaussian after making the change of variable $t^2 = 1-X/(1-Y_R)$. Using this procedure, the maximum error in altitude is about 1 km for both the high-density and the low-density models. This error is small compared to the errors due to uncertainties in the scaling of ionograms. Even on excellent ionograms the scaling error on the virtual heights is at least 5 km. Hence the recommended calculation procedures will not contribute significantly to the total error in the ionogram reduction process. Furthermore, even if scaling errors could be made negligible, a maximum error

of 1 km would not be significant, particularly on a profile extending from 400 to 3000 km. Deviations from the recommended procedure, however, can sometimes introduce large errors as will be shown in the following discussion.

1. Selection of data points.

   The criterion used for the selection of data points is not optimum for all types of ionogram. In some cases it might provide too many points, and lead to a slight reduction in efficiency from the standpoint of computer time. Typically the processing of an ionogram requires about 4 seconds if 20 data points are used and 8 seconds if 30 points are used. On the other hand the criterion will very seldom yield an insufficient number of points. For example, on the low density model the criterion yields 24 data points and a maximum error in altitude of 1 km. If the calculations are done with only 13 data points the maximum error becomes equal to 6 km, which is still relatively small. The error for these two cases is shown as a function of altitude on Fig. 1 and 2 (graphs labelled: parabolic).

   There results indicate that the number of points given by the scaling criterion is not marginal, since it is possible to eliminate approximately half of these points and still achieve a satisfactory accuracy.

2. Choice of lamination model.

   Performing the same calculations with the low density model, but assuming laminations linear in log N, yields a maximum error of 20 km for the 24 point analysis, and 50 km for the 13 point analysis. The error for the linear lamination calculation is also shown in Fig. 1 and 2 (graphs labelled: linear). Similar graphs were obtained for the high density model. In this case the linear-in-log N lamination yielded a maximum error in altitude of 15 km using the 28 points provided by the

scaling criterion. The maximum error is 40 km when only 15 points are used in the calculations.

This leads to the conclusion that the parabolic lamination method yields results about 10 times more accurate than those obtained with the linear lamination method. Furthermore the use of the linear laminations causes the profile to be too high.

3. Importance of iteration.

Failure to iterate will cause the profile to be too low, the effect being most pronounced at the higher altitudes (See Fig. 3). Also illustrated in Fig. 3, is the combined effect of using linear in log N laminations and no iterations. In this case the two effects tend to compensate causing the upper portion of the profile to be too low and the lower portion of the profile to be too high. The results shown in Fig. 3 correspond to the high density model. It is seen that the error curve is very smooth when linear laminations are used, but quite erratic with the parabolic lamination method. This illustrates one characteristic of the parabolic method, namely the fact that it is much more critical than the linear method. In other words, the error at a given point produces not only a incorrect starting point but also an incorrect initial slope. This situation can lead to densities decreasing with depth, making the integration calculations impossible with the techniques used in the N-h program. (See Appendix D, section 4). This is precisely what happened when the no-iteration test was performed with the low density model. Consequently the error curve for the low density model cannot be shown.

In terms of a given lamination, and assuming a correct starting point, the altitude at the bottom of the lamination (or equivalently the thickness of the lamination) can easily be in error by 1 km prior

to the iteration. Each iteration tends to reduce this error by roughly a factor of 10, giving as successive errors 0.1, 0.01, 0.001, 0.0001, etc. Since the iteration is carried out until the successive heights differ by less than 0.01 km,* the process would stop after the 3rd iteration for the above example. In actual practice most calculations require 3 ± 1 iterations, the iterations being of course performed only with the lamination having the reflection point at its lower boundary. Referring to Fig. 3, it is seen that for the parabolic method, the point obtained at 2800 km (using no iteration) is actually in error by about 10 km, whereas the same point obtained with the linear method is in error by less than 1 km. It should be noted also that in both cases the same starting point is used, since the first lamination is always calculated by the linear method (in view of the fact that a matching of slopes is not feasible at that stage). It is seen that the linear method provides a much better initial estimate of the lamination thickness. Consequently even for the parabolic method the first calculation of the unknown lamination is based upon the linear lamination method. This provides a good starting point for the parabolic technique which is then used in the iteration process. This method speeds up the convergence process and also helps in preventing the parabolic calculations from going astray.

4. Choice of integration technique.

To show the importance of the change of variable in performing the integration, the ionogram for the low density model was analyzed using the parabolic-in-log N lamination technique, iteration until Δh was less than 0.01 km, but omitting the change of variable.

* The 0.01 km criterion refers only to the internal consistency of the calculations. Scaling errors and assumptions made in the analysis will cause the computed N-h profile to have errors much greater than 0.01 km.

The integration was performed with both a 7-point Gaussian and a 16-point Gaussian. The error is shown as a function of altitude in Fig. 4. It is seen that even with a 16-point Gaussian an error of 22 km can take place. The errors are such as to make the profile appear to be too low.

5. Comparable observations using actual Alouette II ionograms.

Three Alouette II ionograms were selected by the ISIS Working Group to compare the results of N-h reductions as performed by the various agencies participating in the ISIS Program. Actually the ionograms came from different agencies, each agency scaling its own ionogram, according to its own scaling criterion. The scaling criterion suggested in this report was not used on any of these three ionograms. The error obtained, if either a change of variable is not made, or iterations are not performed, is shown in Fig. 5 as a function of altitude. Since two of the test ionograms were for near-apogee conditions, only one high altitude case is illustrated. Actually the resulting errors were very similar for both ionograms. For the high altitude ionograms used to obtain the data in Fig. 5, the satellite altitude was 2873 km and the local density was 1260 el/cc. The third ionogram was taken from an altitude of 958 km and is similar to the type of ionograms obtained with Alouette I. The error was determined by assuming that the parabolic-in-log N technique yielded the correct answer. It is seen that the errors on the high altitude ionogram are comparable to the errors found with the low density Bauer model. It should be mentioned that in Fig. 5 curve C was smoothed on the error graph for the high altitude ionogram. Prior to smoothing, curve C was similar to the corresponding curve in Fig. 3.

It is also seen that the errors are much smaller for a low altitude topside ionogram. In particular, iteration is not nearly as important for a low altitude ionogram as for a high altitude ionogram. It should be pointed out that for an actual ionogram, the magnetic field variation with altitude is calculated not from an inverse cube law, but from a refined field model, (September 1965, Daniels and Cain model). Errors obtained when an inverse cube law is used (Instead of the more accurate field values) have been investigated in these three test ionograms. The maximum error resulting from the use of an inverse cube field model was 10.4 km for the high altitude profiles and 0.22 km for the low altitude profile. It was also found that no significant error is introduced if the magnetic variation is assumed to follow the inverse cube law within each lamination. Although a 7-point Gaussian integration was used to calculate curve C, the same results would be obtained with a 3-point Gaussian integration.

V. CONCLUDING REMARKS AND ILLUSTRATIVE EXAMPLES

The N-h analysis discussed in this report assumes rather ideal sounding conditions into a spherically stratified ionosphere. The sounder is also assumed stationary during the complete sounding. Actually the horizontal distance changes typically by a few tens of kilometers during a sounding and on Alouette II the satellite altitude also changes by a few kilometers during a complete sounding. Large errors in scaling can also be present when the ionograms exhibit heavy spread conditions.

Work is currently under way to evaluate (and hopefully minimize) some of the errors arising from the above assumptions and uncertainties. This effort must be based upon both

theoretical considerations (such as ray path analysis) and experimental data (such as making maximum use of the orbital data and of the total information actually present on the ionograms). It has been stressed earlier that N-h analysis of topside ionograms is done almost exclusively with the extraordinary ray. The initial portion of the ordinary trace is usually difficult to scale or completely missing. Conversely, the low frequency end of the Z trace terminates when $X = (1 - Y^2)/(1 - Y_L^2)$. Both of these traces however, can provide useful checks on the validity of the extraordinary ray analysis. Consequently, the author also makes use of O mode and Z mode data to check the profile derived from the extraordinary trace. At the present state of the art, this approach can either show that the results are consistent and hence give greater confidence in the X-trace interpretation or reveal disagreements and give some indication of the possible errors present in the computed N-h profiles. Another way to check the analysis of a given ionogram is to make use of adjacent ionograms. This is particularly helpful on Alouette II, since successive soundings are usually obtained from significantly different altitudes. Incorrect interpretation of the ionogram echoes on successive ionograms taken from different heights is very likely to yield inconsistent N-h results.

The following examples illustrate the two types of consistency checks discussed above.

Example I. The Alouette II ionogram of Figure 6 exhibits excellent Z, O and X traces, and it was therefore selected for simultaneous analysis of the three traces. The results of the analysis are shown in Figure 7. It is seen that good agreement was obtained by the three methods. The Z trace yielded the profile from the satellite altitude

(950 km) down to 515 km. Analysis of Z traces have been found to give good results provided the steepest portion of the trace (near Z infinity) is not used. In this case the last point used was at the 0.90 MHz frequency marker. The infinity of the Z trace (fzI) occurs at 0.97 MHz which is consistent with the condition $X = (1 - Y^2)/(1 - Y_L^2)$ and with the assumption that the propagation was vertical. The resolution is such that a 3 degree departure from vertical propagation could have been detected. Figure 6 shows a good example of the Z' trace (Calvert, 1966) which is an additional Z trace originating from the plasma resonance. Also visible on Fig. 6 are echoes due to the side responses of the transmitted pulse (See Appendix B). There is one response below the main spectrum and two responses above. These are very clearly seen on the Z' trace.

A search was conducted in order to see whether or not any exception could be found to the general rule that the Z trace on Alouette II does not extend down to the maximum of the F2 region. Theoretical considerations (See Appendix A) show that the Z mode could reach hmaxF2 if f_oF2 is very low, if the magnetic dip is not close to 90^o, and if the satellite is near perigee. Very low values of f_oF2 (combined with dip angles less than 65 degrees) occur at high Southern latitudes during the months of June, July and August. Since Alouette II perigee was near the South Point of the orbit during the first two weeks of July 1966, it seemed that the requirements could be met on some of the ionograms obtained from SOLANT (the South Atlantic Station) for the period June 1 to August 31, 1966. Approximately 450 Alouette II ionograms were obtained from SOLANT during this period and for satellite altitudes ranging from 500 to 800 km. (Ionograms taken from

altitudes greater than 800 km were discarded as being unlikely to exhibit complete Z traces.) Most of the low altitude ionograms had very good Z traces ending at fzI. Three had Z traces terminating at F2max, but only one ionogram could be found where the Z trace extended continuously from the satellite all the way down to F2max. This very unusual Alouette ionogram, obtained on day 191 of 1966 at 000659 GMT, exhibits a complete X trace, an almost complete O trace, and a continuous Z trace corresponding to reflections from the satellite down to F2max. Electron density profiles derived from these three traces were found to be in excellent agreement. It should be noted that this ionogram was obtained near the Southern end of the SOLANT coverage. It is quite possible that such ionograms are more common over Antarctica and that additional examples could be found among the data acquired at the Byrd telemetry station. Data from this station were not available to the author at the time of this writing.

For N-h calculations based upon the ordinary ray, a change of variable $t^2=1-X$ is used. A 3-point Gaussian integration technique is satisfactory if the dip is less than 50 degrees. If the angle of magnetic dip is greater than 50 degrees, a higher order Gaussian must be used on the last lamination.

Example 2. Consistency of results obtained from the analysis of consecutive ionograms is best indicated by plotting electron density contours as a function of latitude (or dip angle). An example of a pole-to-pole Alouette II pass is given by Fig. 8, which shows the altitude of constant density lines. One striking feature of this presentation is the high degree of uniformity indicated by the N-h analysis at altitudes between 400 and 600 km, when one considers the fact that these density levels are viewed from sounder heights ranging from 600 km to 2700 km, and also considering the fact that the distribution changed considerably at altitudes above

1000 km on successive ionograms. The high altitude portion of the profiles changed quite rapidly as the dip increased from 60 to 75 degrees. This is illustrated more clearly by Fig. 9, which shows some of the profiles used to produce Fig. 8. Another presentation of the same pole-to-pole data is given by the constant height contours of Fig. 10. This Figure shows that the densities at 500 and 600 km were relatively constant as the dip increased from 40 to 80 degrees, whereas the densities at 1500 km decreased by one order of magnitude as the dip increased from 60 to 80 degrees. This effect is much less pronounced at the 800 and 1000 km levels and it would therefore be much less noticeable on Alouette I ionograms. On the other hand, Alouette I would have provided a more complete picture South of the magnetic equator.

ACKNOWLEDGMENTS

I am greatly indebted to Mr. Joseph Bredekamp for doing most of the ionogram analyses, computer calculations and illustrations used in this report. Mr. Bredekamp worked on this project during his senior year at the University of Maryland. I am very grateful for the helpful comments and suggestions which have been provided by Lawrence Colin of ARC, and for the information provided by Leroy Nelms and Glenn Lockwood of DRTE. I must also acknowledge many stimulating discussions held with the above mentioned colleagues, with Siegfried Bauer, Leo Blumle and Richard Fitzenreiter of GSFC, and with David Eccles of RSRS.

References

Bauer, S. J., On the structure of the topside ionosphere, Journal of the Atmospheric Sciences, Vol. 19, No. 3, pp. 276-278, May 1962.

Becker, W., Tables of ordinary and extraordinary refractive indices, group refractive indices and $h'_{O,X}(f)$ - curves for standard ionospheric layer models, Mitteilungen aus dem Max-Plank-Institut fur Aeronomie, 1960.

Budden, K. G., Radio waves in the ionosphere, University Press, Cambridge, England, 1961.

Calvert, W., Oblique z-mode echoes in the topside ionosphere, Journal of Geophysical Research, Vol. 71, No. 23, pp. 5579-5583, December 1, 1966.

Doupnik, J. R. and Schmerling, E. R., The reduction of ionograms from the bottomside and topside, Journal of Atmospheric and Terrestrial Physics, Vol. 27, pp. 917 to 941, September 1965.

Fitzenreiter, R. J. and Blumle, L. J., Analysis of topside sounder records, Journal of Geophysical Research, Vol. 69, No. 3, pp. 407-415, February 1, 1964.

Jackson, John E., A new method for obtaining electron density profiles from P'-f records, Journal of Geophysical Research, Vol. 61, No. 1, pp. 107-127, March 1956.

Kelso, John M., Radio ray propagation in the ionosphere, McGraw-Hill, Inc., 1964.

Paul, A. K. and Wright, J. W., Some results of a new method for obtaining ionospheric N(h) profiles and their bearing on the structure of the lower F region, Journal of Geophysical Research, Vol. 68, No. 19, pp. 5413-5420, October 1, 1963.

Poeverlein, H., Z. angew. Phys. 1951, 3, 135.

Ratcliffe, J. A., The magneto-ionic theory, University Press, Cambridge, England, 1962.

Shinn, D. H. and Whale, H. A., Group velocities and group heights from the magneto-ionic theory, Journal of Atmospheric and Terrestrial Physics, Vol. 2, pp. 85-105, 1952.

Figure Captions

Fig. 1. Relative accuracy of parabolic-in-log N and linear in log N techniques for 24-point analysis.

Fig. 2. Relative accuracy of parabolic-in-log N and linear in log N techniques for 13-point analysis.

Fig. 3. Errors introduced when iteration is not used.

Fig. 4. Errors introduced when the group height integrals are evaluated without making the change of variable $t^2 = 1 - X/(1-Y_R)$.

Fig. 5. Errors introduced in ionogram analysis when either the integrand is infinite at the reflection point, or when iteration is not performed. Hs is the satellite altitude.

Fig. 6. Example of an Alouette II ionogram with excellent Z, O and X traces.

Fig. 7. Electron densities obtained from the ionogram of Figure 6, doing independent N-h analysis on each of the Z, O and X traces. The points shown on the graph were selected from the computed points. For the sake of clarity, overlapping points were omitted, except at the ends of the profile.

Fig. 8. Electron density contours over the American continents derived from Alouette II ionograms.

Fig. 9. Typical electron density profiles used to obtain the contours of Fig. 8.

Fig. 10. Same data as Fig. 8, but presented in terms of density at constant heights.

Fig. B-1. Typical Alouette II ionogram and graph showing the relative frequencies of the cut-off and resonance conditions. The dashed line on the graph shows the conditions corresponding to the ionogram shown.

Fig. D-1. Lamination Model.

Fig. D-2. Computed altitude for the bottom of a lamination as a function of gyrofrequency. The minimum gyrofrequency is the value at the satellite, and the maximum gyrofrequency is based upon an essentially constant density within the lamination. The actual gyrofrequency as a function of altitude is also indicated. The correct value of gyrofrequency at the bottom of the lamination is the intersection of the two curves. The purpose of the iteration process is to find this intersection point.

Fig. E-1. Local Mean Times for Alouettes I and II and position of Alouette II perigee. Data are for year 1966, but apply also to other years in the case of Alouette I.

Fig. E-2. Shows how the Alouette I equatorial crossings are evenly spaced when plotted for a one week period. The crossings drift slowly as illustrated for a period of eleven weeks.

Fig. E-3. Local mean time and position of perigee for Alouette II during 1967.

Fig. E-4. Altitude of Alouette II as a function of latitude when the argument of perigee is 0, 90, 180, and 270 degrees.

FIGURE 1

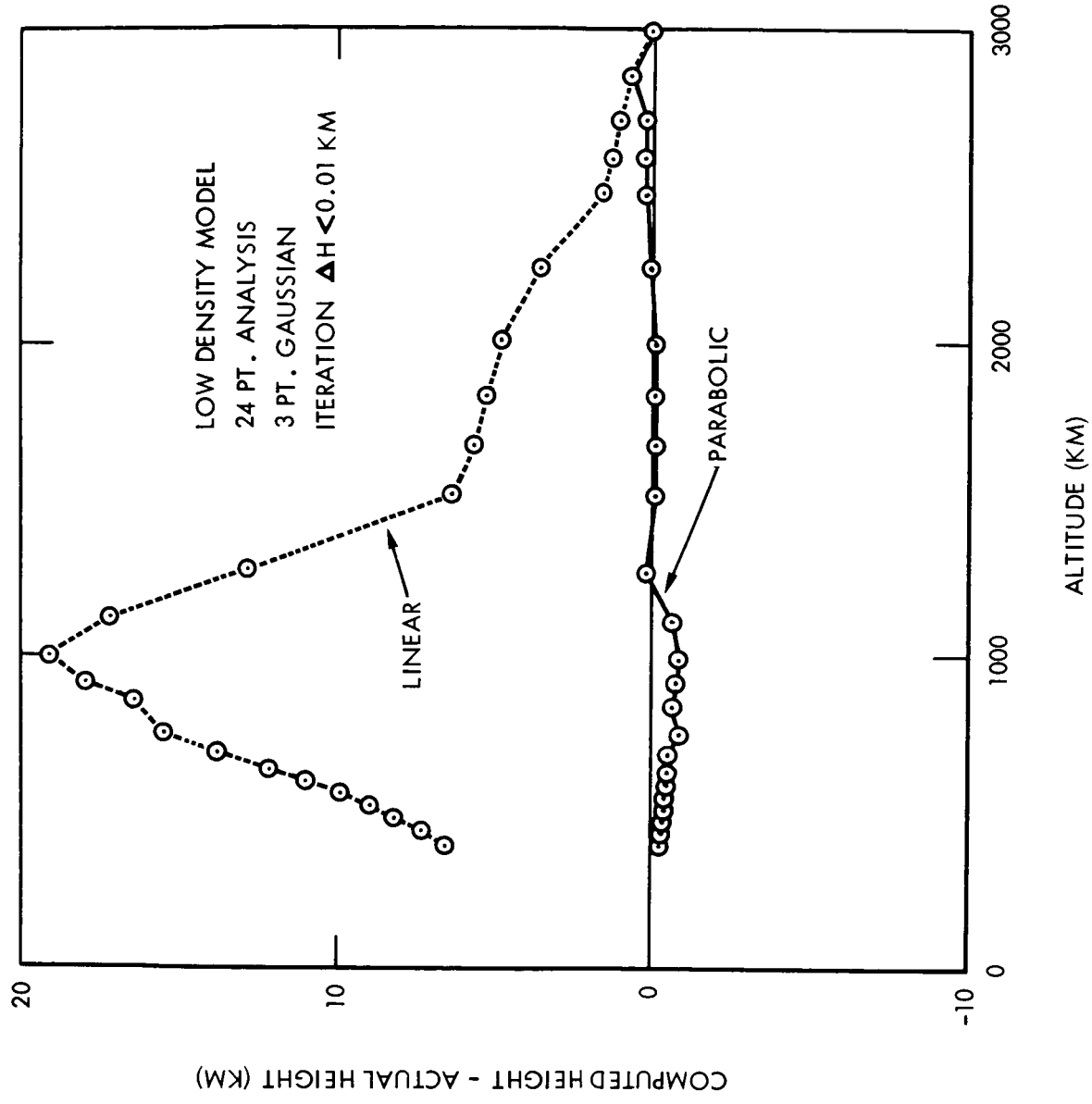
LOW DENSITY MODEL
24 PT. ANALYSIS
3 PT. GAUSSIAN
ITERATION ΔH <0.01 KM
LINEAR
PARABOLIC
COMPUTED HEIGHT - ACTUAL HEIGHT (KM)
ALTITUDE (KM)
20
10
0
-10
0
1000
2000
3000

FIGURE 2

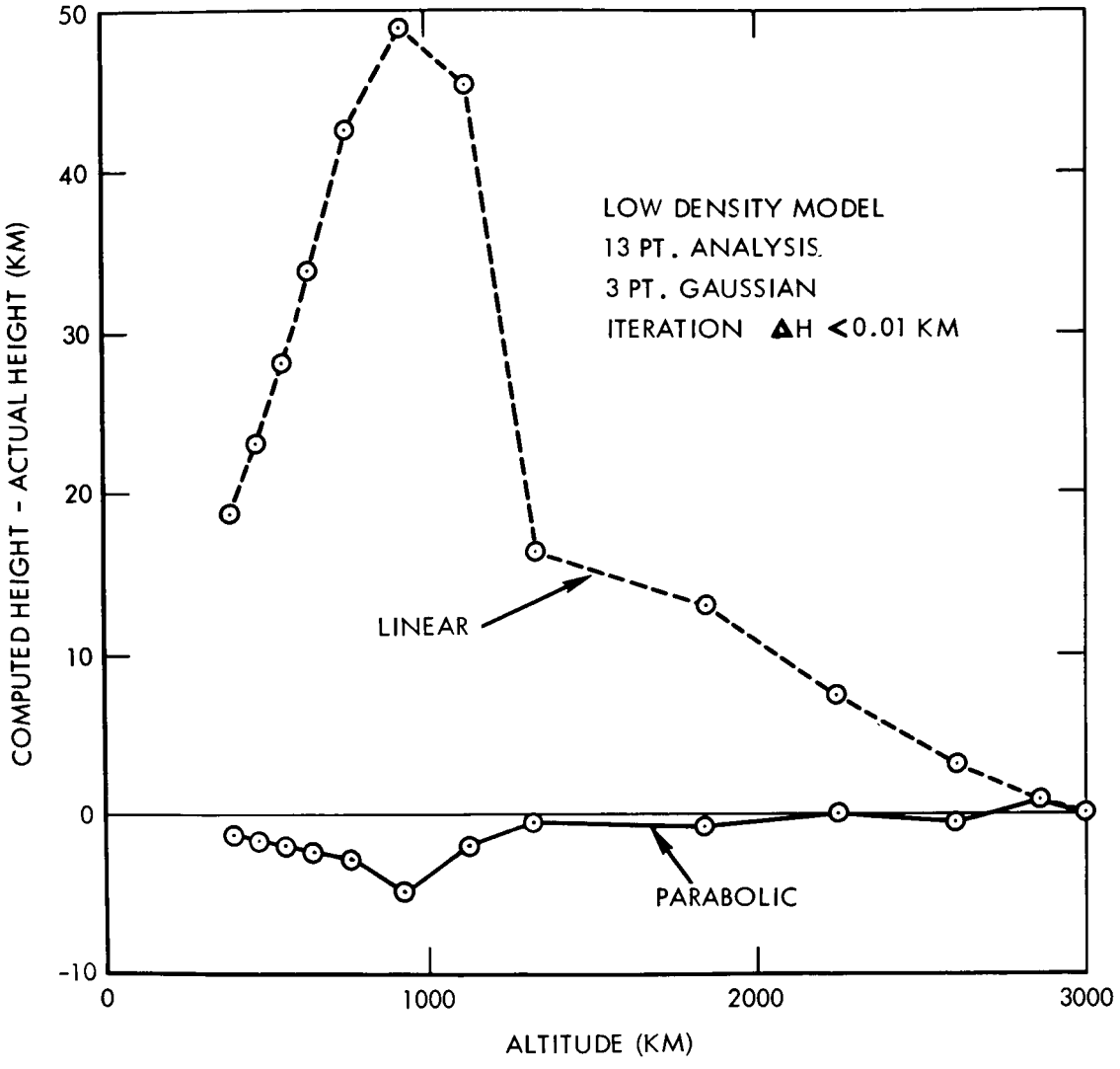
50
40
30
20
10
0
-10
0
1000
2000
3000
COMPUTED HEIGHT - ACTUAL HEIGHT (KM)
ALTITUDE (KM)
LOW DENSITY MODEL
13 PT. ANALYSIS
3 PT. GAUSSIAN
ITERATION ΔH <0.01 KM
LINEAR
PARABOLIC

FIGURE 3

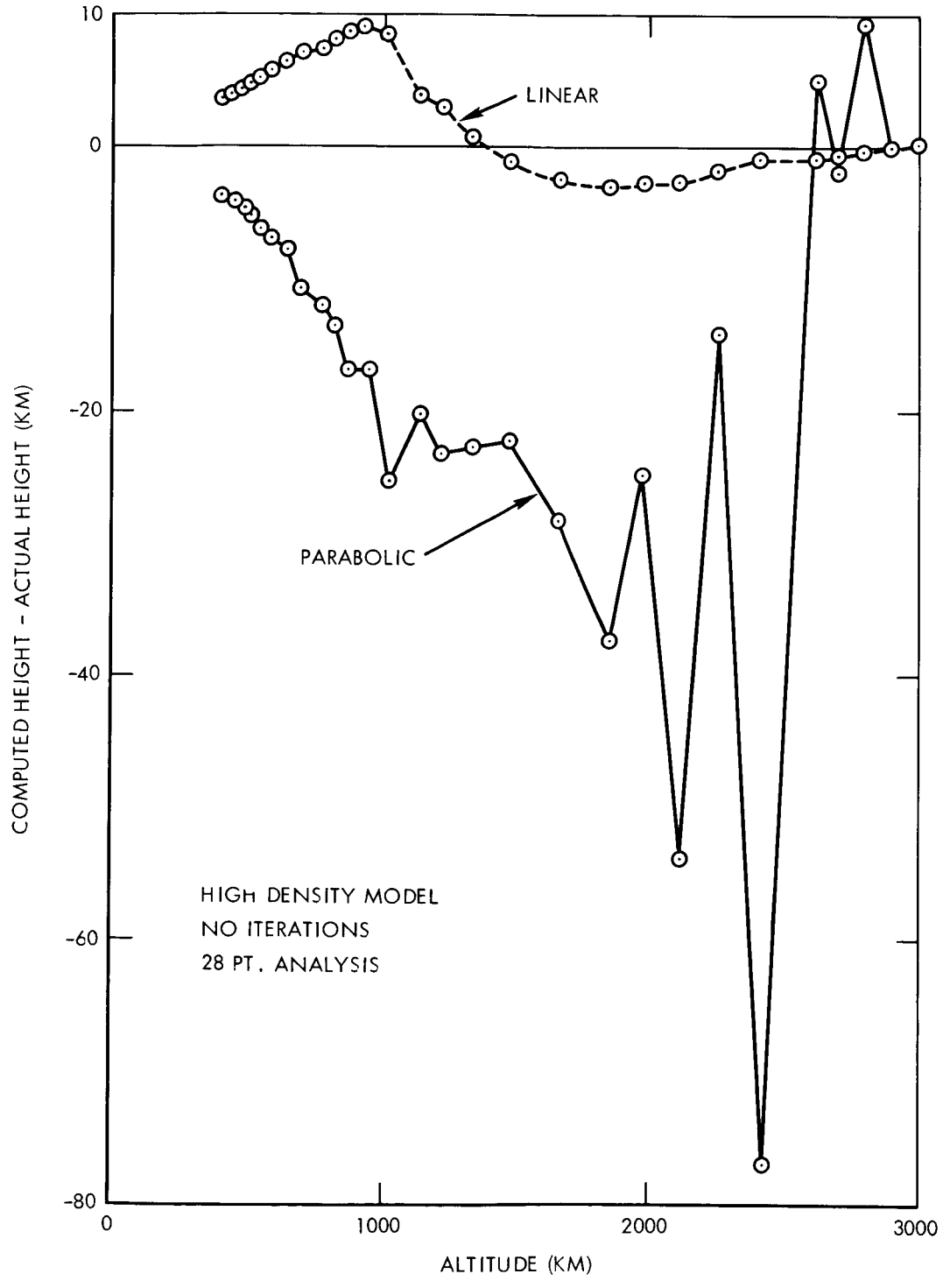
10
0
-20
-40
-60
-80
0
1000
2000
3000
LINEAR
PARABOLIC
HIGH DENSITY MODEL
NO ITERATIONS
28 PT. ANALYSIS
COMPUTED HEIGHT - ACTUAL HEIGHT (KM)
ALTITUDE (KM)

FIGURE 4

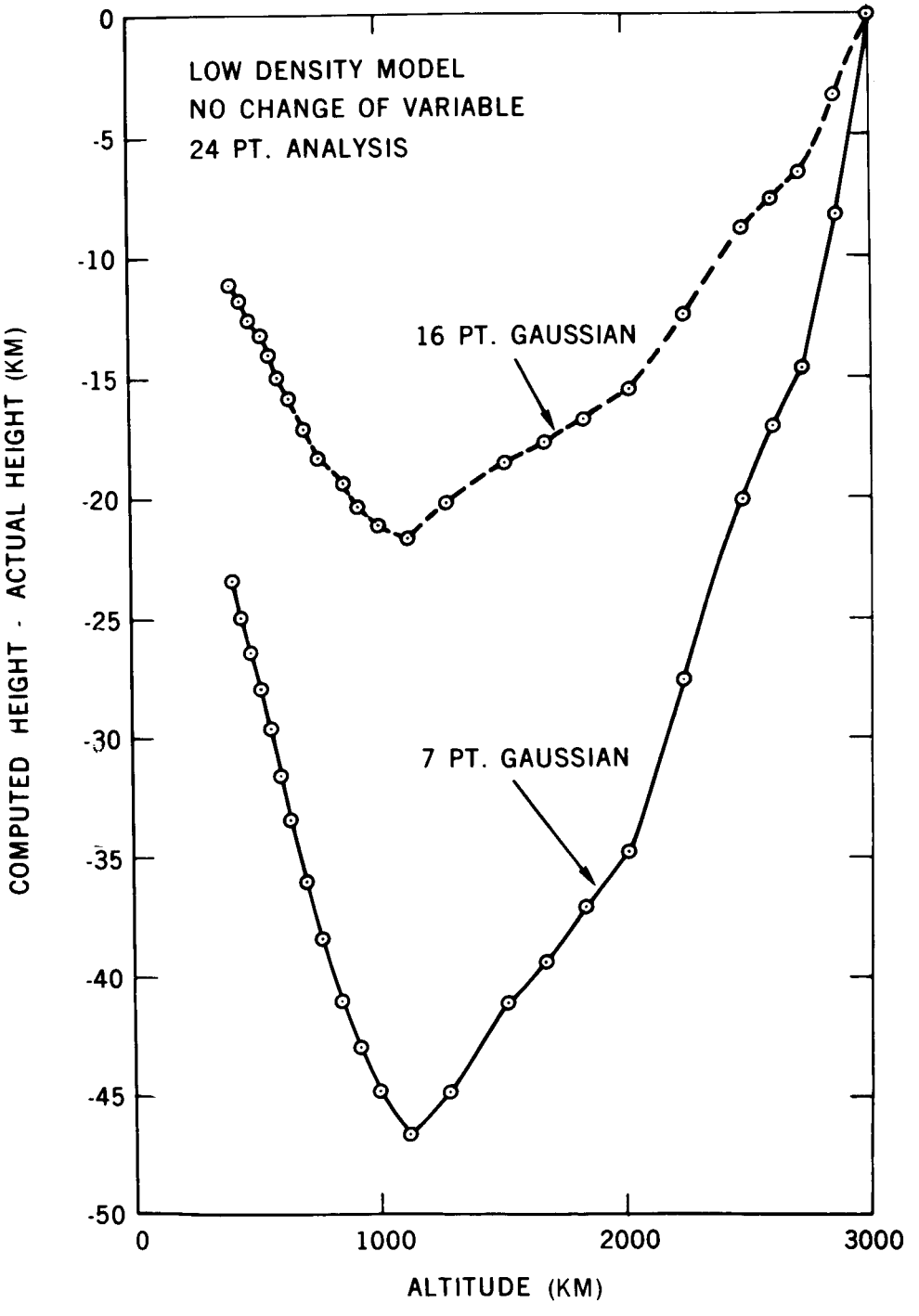
LOW DENSITY MODEL
NO CHANGE OF VARIABLE
24 PT. ANALYSIS
16 PT. GAUSSIAN
7 PT. GAUSSIAN
COMPUTED HEIGHT - ACTUAL HEIGHT (KM)
ALTITUDE (KM)
0
-5
-10
-15
-20
-25
-30
-35
-40
-45
-50
0
1000
2000
3000

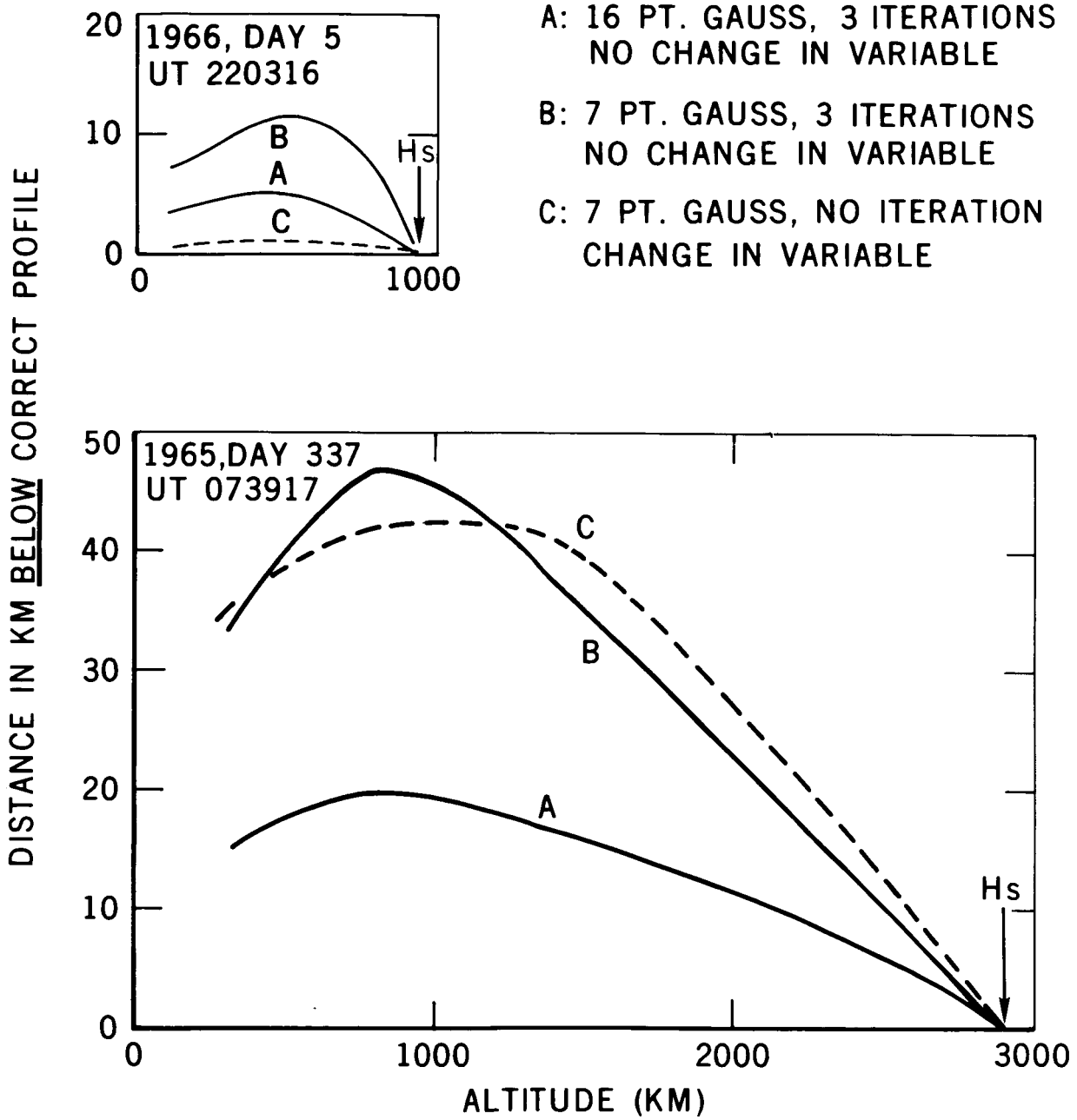

FIGURE 5. ERRORS INTRODUCED IN IONOGRAM ANALYSIS WHEN EITHER THE INTEGRAND IS INFINITE AT THE REFLECTION POINT, OR WHEN ITERATION IS NOT PERFORMED. Hs IS THE SATELLITE ALTITUDE.

FIGURE 6

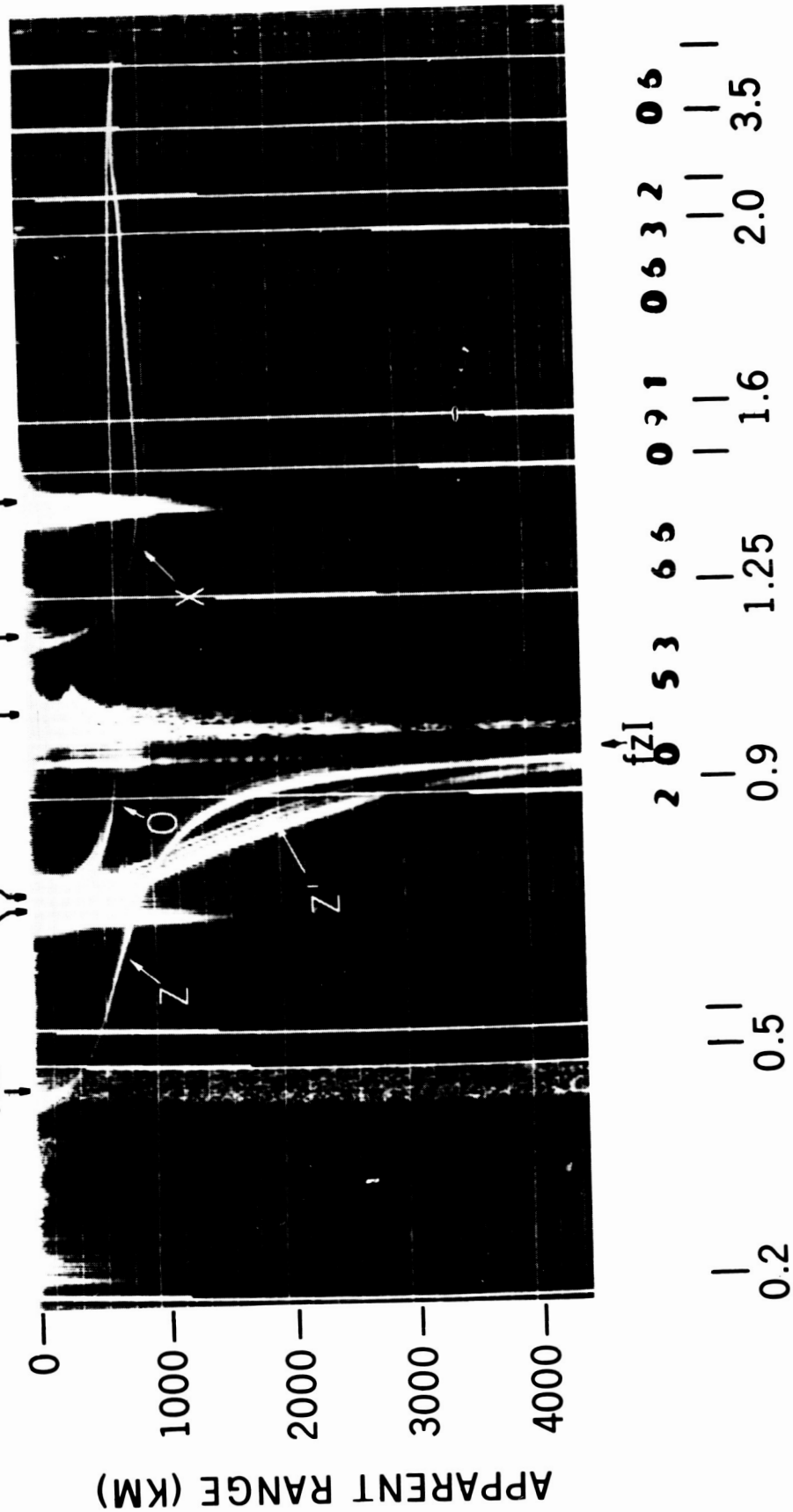
fzS
fH
fN
fT
fxS
2fH
Z
O
Z'
fz1
0
1000
2000
3000
4000
APPARENT RANGE (KM)
0.2
0.5
0.9
1.25
1.6
2.0
3.5
FREQUENCY (MHz)

FIGURE 7

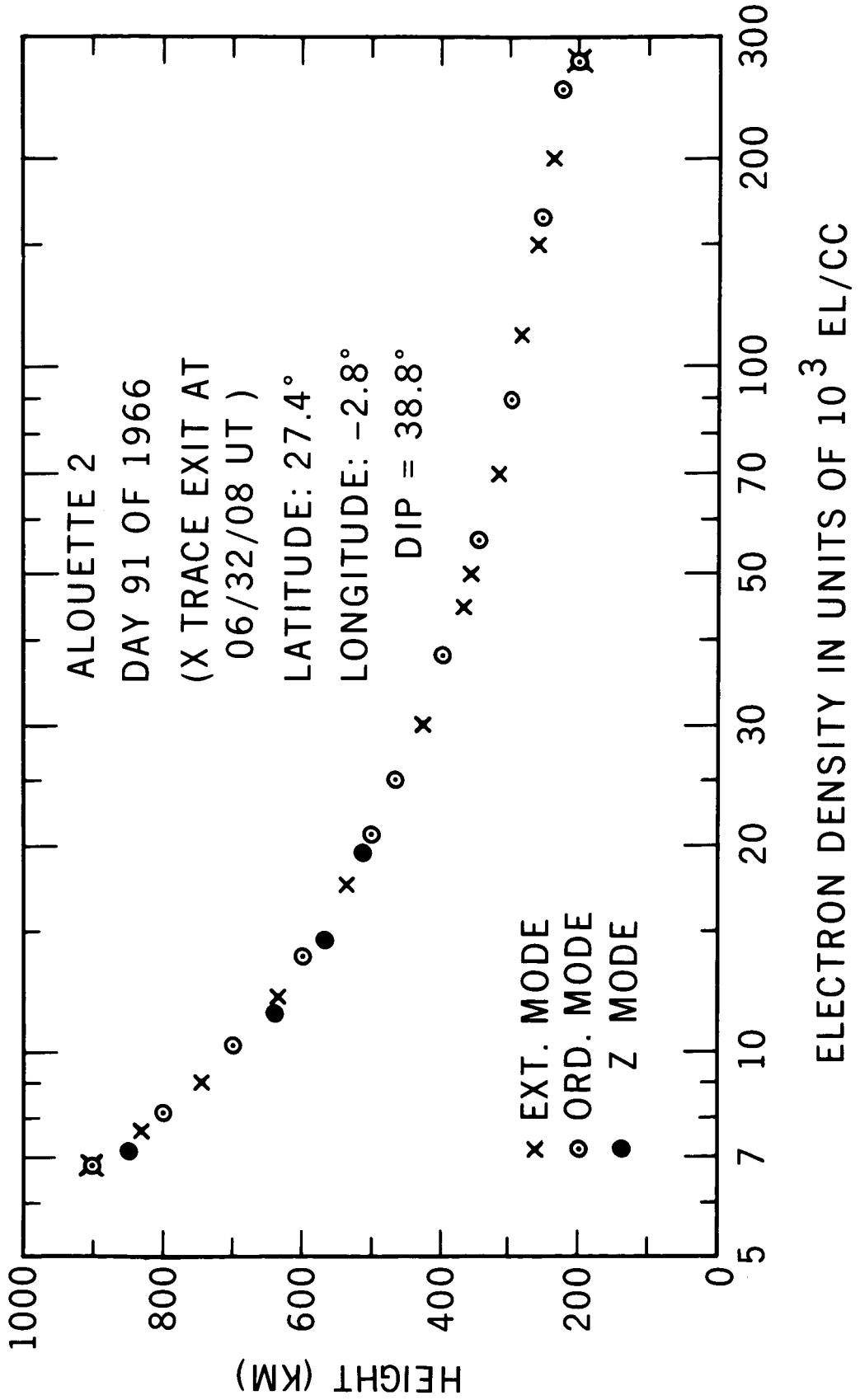
ALOUETTE 2
DAY 91 OF 1966
(X TRACE EXIT AT
06/32/08 UT)
LATITUDE: 27.4°
LONGITUDE: -2.8°
DIP = 38.8°
× EXT. MODE
⊙ ORD. MODE
● Z MODE
HEIGHT (KM)
1000
800
600
400
200
0
5
7
10
20
30
50
70
100
200
300
ELECTRON DENSITY IN UNITS OF 10^3 EL/CC

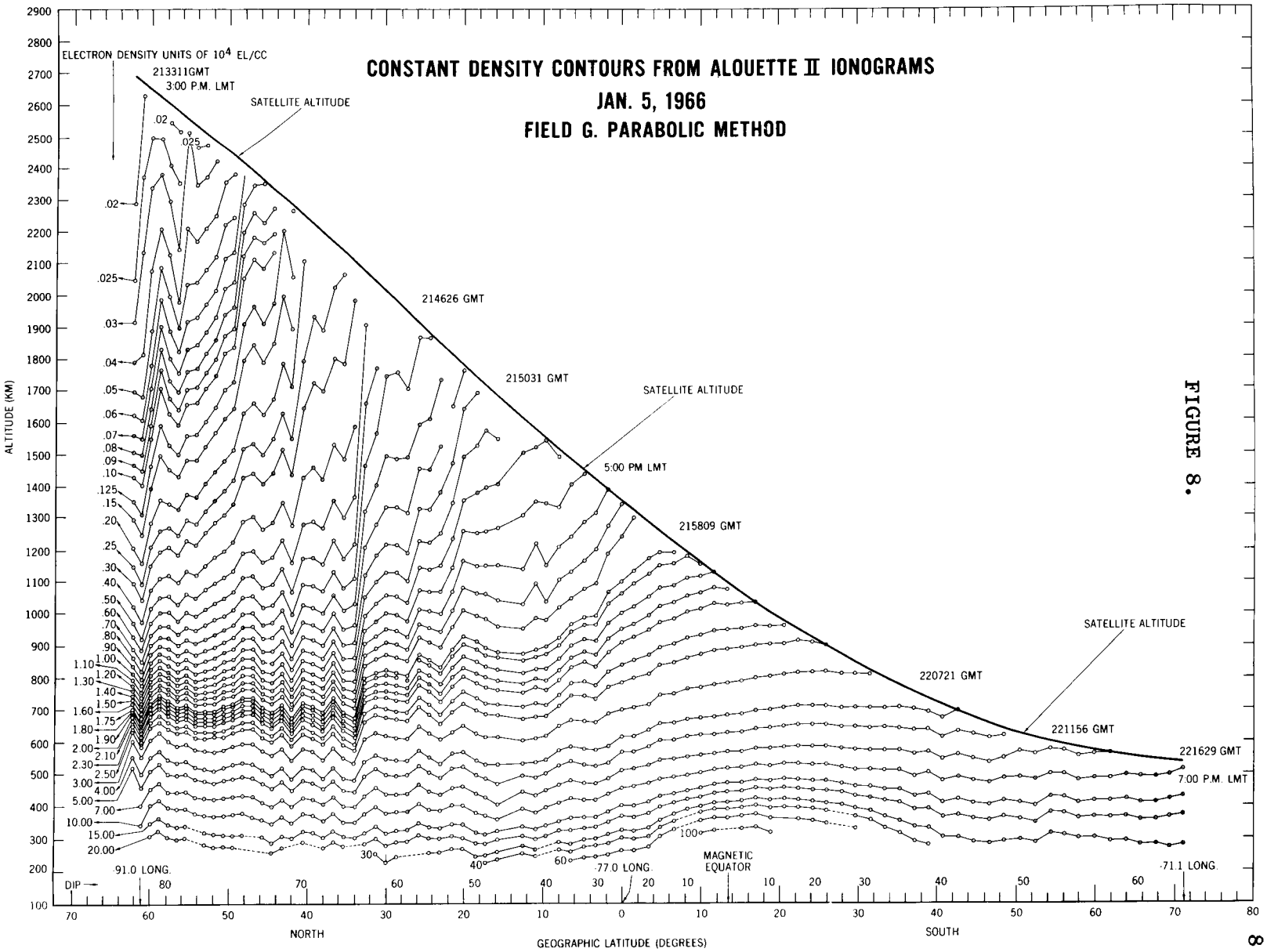
CONSTANT DENSITY CONTOURS FROM ALOUETTE II IONOGRAMS
JAN. 5, 1966
FIELD G. PARABOLIC METHOD
ELECTRON DENSITY UNITS OF 10^4 EL/CC
213311GMT
3:00 P.M. LMT
SATELLITE ALTITUDE
214626 GMT
215031 GMT
SATELLITE ALTITUDE
5:00 PM LMT
215809 GMT
SATELLITE ALTITUDE
220721 GMT
221156 GMT
221629 GMT
7:00 P.M. LMT
ALTITUDE (KM)
91.0 LONG.
77.0 LONG.
MAGNETIC EQUATOR
71.1 LONG.
DIP
NORTH
SOUTH
GEOGRAPHIC LATITUDE (DEGREES)

FIGURE 8.

FIGURE 9.

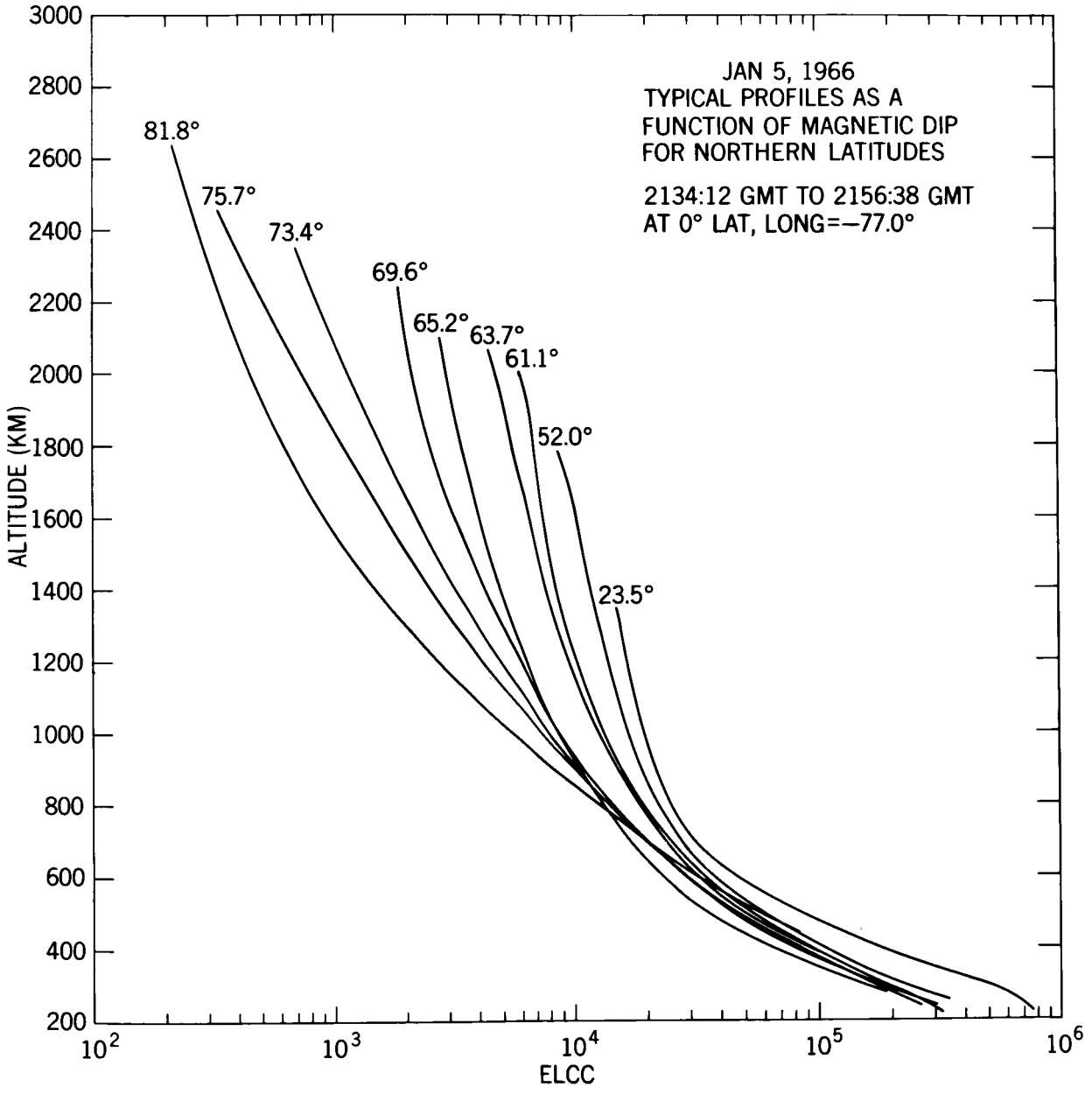
JAN 5, 1966
TYPICAL PROFILES AS A
FUNCTION OF MAGNETIC DIP
FOR NORTHERN LATITUDES
2134:12 GMT TO 2156:38 GMT
AT 0° LAT, LONG=−77.0°
81.8°
75.7°
73.4°
69.6°
65.2°
63.7°
61.1°
52.0°
23.5°
ALTITUDE (KM)
3000
2800
2600
2400
2200
2000
1800
1600
1400
1200
1000
800
600
400
200
10^2
10^3
10^4
10^5
10^6
ELCC

FIGURE 10.

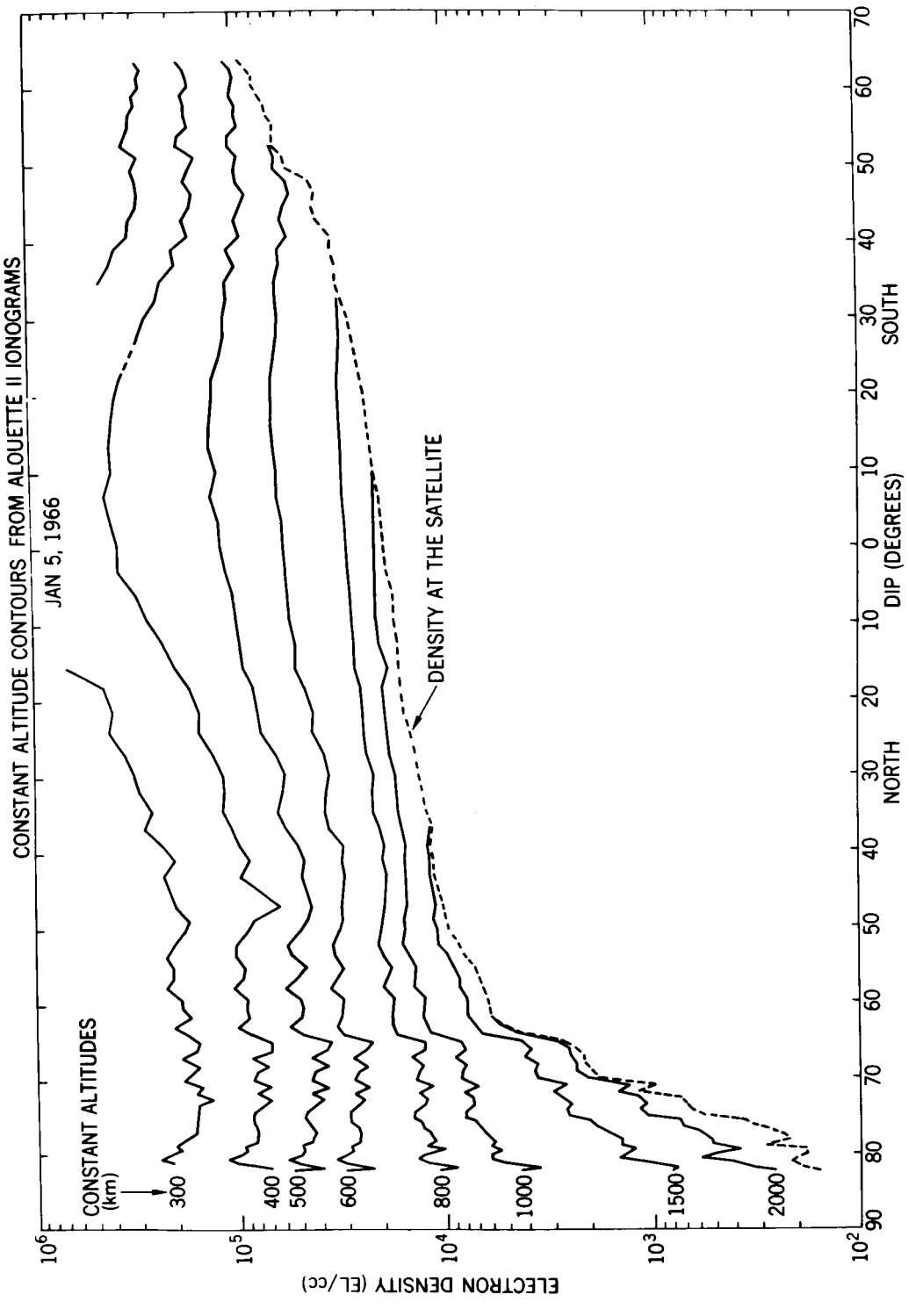
CONSTANT ALTITUDE CONTOURS FROM ALOUETTE II IONOGRAMS
JAN 5, 1966
CONSTANT ALTITUDES (km)
300
400
500
600
800
1000
1500
2000
DENSITY AT THE SATELLITE
ELECTRON DENSITY (EL/cc)
10^6
10^5
10^4
10^3
10^2
90 80 70 60 50 40 30 20 10 0 10 20 30 40 50 60 70
NORTH
DIP (DEGREES)
SOUTH

APPENDIX A

FORMULAS FOR GROUP AND REFRACTIVE INDICES

APPENDIX A

1. Basic Formulas

The group refractive index n' for a radio wave of frequency f is defined as the free space velocity of light divided by the group velocity of the wave. The fundamental formula for n' is:

$$n' = n + f \frac{\partial n}{\partial f} \qquad \text{(A-1)}$$

where n is the real part of the refractive index of the medium. The index n is given by the well known Appleton Hartree formula, namely:

$$n = \sqrt{1 - \frac{X}{1 - \frac{Y_T^2}{2(1-X)} \pm \sqrt{\left[\frac{Y_T^2}{2(1-X)}\right]^2 + Y_L^2}}} \qquad \text{(A-2)}$$

where

$X = N/(12,400f^2) = \frac{fN^2}{f^2}$

N = electrons/cc

f = frequency in Mc/s

$Y = fH/f$

fH = 2.8B Mc/s

B = (terrestrial) magnetic induction in gausses

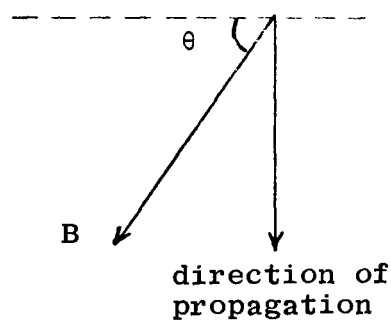

Fig. A.1

θ = angle of magnetic dip (see Fig. A.1)

$Y_T = Y \cos \theta$

$Y_L = Y \sin \theta$

$\pm$ = positive sign in front of square root is for ordinary ray; negative sign is for extraordinary ray

The reflection conditions are X=1 for the ordinary ray (except when θ is exactly 90^0) and X=1-Y for the extraordinary ray.

The evaluation of $\frac{\partial n}{\partial f}$ is fairly complicated since n is a function of X and Y and both of these parameters are functions of f. The calculations are simplified considerably, however, when θ is either 0 or 90 degrees, i.e. when the earth's magnetic field is either perpendicular to (transverse propagation) or parallel to (longitudinal propagation) the direction of the wave propagation. For these two limiting cases it is also possible to evaluate analytically the group height integral $\int n\, dh$ and hence check the accuracy of the numerical integration technique which is needed for the general case (i.e. θ neither 0, nor 90 degrees).

2. Special Cases

a. Transverse Propagation (θ=0; Y_T=Y; Y_L=0)

In this case formulas (A-2) and (A-1) give:

for the ordinary ray:

$$n = \sqrt{1-X} \qquad \text{(A-3)}$$

$$n' = 1/n \qquad \text{(A-4)}$$

for the extraordinary ray:

$$n = \sqrt{1 - \frac{X(1-X)}{1-X-Y^2}} \qquad \text{(A-5)}$$

$$n' = \frac{1}{n}\left[1 + \frac{XY^2}{(1-X-Y^2)^2}\right] \qquad (A-6)$$

b. Longitudinal Propagation ($\theta=90^o$, $Y_L=Y$, $Y_T=0$)

In this case formulas (A-2) and (A-3) give:

for the ordinary ray:

$$n = \sqrt{1 - X/(1+Y)} \qquad (A-7)$$

$$n' = \frac{1}{n}\left[1 - \frac{XY}{2(1+Y)^2}\right] \qquad (A-8)$$

for the extraordinary ray:

$$n = \sqrt{1 - X/(1-Y)} \qquad (A-9)$$

$$n' = \frac{1}{n}\left[1 + \frac{XY}{2(1-Y)^2}\right] \qquad (A-10)$$

3. Comments on Index Computation Procedures

a. The function nn'

For the special cases discussed above:

$$nn' = F(X,Y) \qquad (A-11)$$

where F(X,Y) is a function of X and Y, which is positive and finite for every point along either an ordinary or an extraordinary trace on a topside ionogram. More specifically F(X,Y) is finite when:

$0 \leq X \leq 1$ ⟵ for the ordinary ray, and

$0 \leq X \leq 1-Y$ ⟵ for the extraordinary ray.

It can be seen from formulas (A-4) and (A-8) that this statement is obviously true for the ordinary ray. It is also true of the extraordinary ray, because the denominators appearing in formulas (A-6) and (A-10) can never become equal to zero. On the extraordinary trace of a topside ionogram the parameter Y is always less than unity because on the extraordinary trace f is always greater than fH. This fact, plus the relationship $X \leq 1-Y$, implies that the condition $X < 1-Y^2$ is also satisfied.

The fact that nn' is always finite is true for the general case ($\theta \neq 0^o$, $\theta \neq 90^o$). In fact, the general formula for n' is of the form

$$n' = \frac{1}{n} F(X,Y,\theta)$$

where $F(X,Y,\theta)$ is positive and finite everywhere. Since n=0 at the reflection point, the value of the group index n' becomes infinite as n approaches zero. Thus, the accuracy of the group index calculations near the reflection point depends upon the accuracy of the corresponding refractive index calculations. The need for special care in the calculation can be illustrating by showing what happens to Equation A-2 for the ordinary ray when X approaches unity. In this case Equation A-2 takes the form:

$$n = \sqrt{1 - \frac{X}{1-M+\sqrt{M^2+Y_L{}^2}}}$$

where M is a quantity which becomes infinite when X approaches unity. The quantity $\sqrt{M^2+Y_L^2}-M$ cannot be evaluated accurately (in the given form) because it is the difference between two large and almost equal numbers. For example if M=1000 and $Y_L^2 = 0.5$, the difference (assuming an 8 significant figure accuracy in the computer) would be: 1000.0002-1000.0000, yielding only one significant figure in the answer. The method used by Becker (1960) is based upon the formula:

$$\sqrt{M^2+Y_L^2}-M = \frac{Y_L^2}{\sqrt{M^2+Y_L^2}+M}$$

For the same numerical example as above, Becker's formula would yield as a difference $(0.5)/2000$, with an accuracy of at least 7 significant figures!

Doupnik (private communication) suggested the use of the following trigonometric substitution:

$$\tan \alpha = \frac{M}{Y_L}$$

yielding:

$$\sqrt{M^2+Y_L^2} - M = Y_L \frac{(1-\sin\alpha)}{\cos\alpha}$$

$$= Y_L \frac{\cos\alpha}{1+\sin\alpha}$$

Noting that $\cos\alpha = \frac{Y_L}{\sqrt{M^2+Y_L^2}}$ and $\sin\alpha = \frac{M}{\sqrt{M^2+Y_L^2}}$,

it is readily seen that Doupnik's transformation is equivalent

to Becker's. Doupnik's trigonometric transformation, however, leads to much simpler formulas than Becker's transformation, and for this reason it has been used in most of the topside N-h programs.

4. Doupnik's Formulas for the Group Index.

Substituting the value of M from Equation A-2 into the expression for tan α gives:

$$\tan \alpha = \frac{Y_T^2}{2Y_L(1-X)} \qquad \text{(A-12)}$$

and evaluating equation A-1 yields:

$$n' = \frac{1}{n}\left[1 + \frac{X(1-S)}{2S^2}\left(1+e\,\frac{1+X}{1-X}\,\text{Sin}\,\alpha\right)\right] \qquad \text{(A-13)}$$

where:

$$n = \sqrt{1-\frac{X}{S}} \qquad \text{(A-14)}$$

$S = 1+Y_L \frac{\text{Cos}\alpha}{1+\text{Sin}\alpha}$ for the ordinary ray

$e = -1$ for the ordinary ray

$S=1-Y_L \frac{1+\text{Sin}\alpha}{\text{Cos}\alpha}$ for the extraordinary ray

$e = +1$ for the extraordinary ray

The above formulas are not valid for $Y_L = 0$. In this case formulas (A-3), (A-4), (A-5) and (A-6) are used in lieu of (A-12), (A-13) and (A-14).

5. Expressions for n and n' Near the Reflection Point

The value of n near the reflection point is obtained by expanding the Equation (A-14) with a Taylor series. It is found that:

$$n_{(ord.)} \rightarrow \frac{\sqrt{1-X}}{\cos\theta} \text{ when } x \rightarrow 1 \qquad \text{(A-15)}$$

and

$$n_{(ext.)} \rightarrow \sqrt{1 - \frac{X}{1-Y}}\left(\sqrt{\frac{2}{1+\sin^2\theta}}\right) \text{ when } x \rightarrow 1-Y \qquad \text{(A-16)}$$

It can also be shown with Equation (A-13) that:
for the ordinary ray:

$$\left[nn'\right]_{x=1} = \frac{1}{\cos^2\theta} \qquad \text{(A-17)}$$

and for the extraordinary ray:

$$\left[nn'\right]_{x=1-Y} = \frac{2-Y}{(1-Y)(1+\sin^2\theta)} \qquad \text{(A-18)}$$

From Equations (A-15) and (A-17) it is seen that:

$$n'_{(ord.)} \rightarrow \frac{1}{(\sqrt{1-X})\cos\theta} \text{ when } x \rightarrow 1 \qquad \text{(A-19)}$$

Hence for the ordinary ray:

$$\lim_{x\rightarrow 1}(n't) = \frac{1}{\cos\theta} \qquad \text{(A-20)}$$

where

$$t = \sqrt{1-X} \qquad \text{(A-21)}$$

Formulas (A-15),(A-17),(A-19) and (A-20) do not hold for $\theta = 90^{o}$, since in this case the reflection point occurs for the ordinary ray at X = 1+Y. This situation can arise with oblique (field-aligned) propagation paths (a case excluded from the present report) or near the magnetic poles (and even then only over a small portion of a vertical propagation path).

Similarly, Equation (A-16) and (A-18) yield

$$n'(\text{ext.}) \rightarrow \frac{(2-Y)}{\left(\sqrt{1-\frac{X}{1-Y}}\right)\sqrt{2}(1-Y)\sqrt{1+\text{Sin}^2\theta}} \qquad \text{when } x \rightarrow 1-Y \qquad \text{(A-22)}$$

Hence for the extraordinary ray

$$\lim_{x \rightarrow 1-Y}(n't) = \frac{2-Y}{\sqrt{2}(1-Y)\sqrt{1+\text{Sin}^2\theta}} \qquad \text{(A-23)}$$

$$\text{where } t = \sqrt{1-\frac{X}{1-Y}} \qquad \text{(A-24)}$$

Thus the substitutions given by Equation (A-21) and (A-24) yield , in the group height formulas, an integrand which is everywhere finite. It is of interest to note that for the ordinary ray the value of n't at the reflection point is a function of θ but not Y, whereas in the case of the extraordinary ray, the value of n't at the reflection point depends upon both θ and Y. In the analysis of topside ionograms, allowance is made for the variation of Y within the interval of integration. Hence Equation (A-23) is not correct when Y is also a variable. If the limit given by Equation (A-23) is represented by L(Y) then, for a variable Y, Equation A-23 becomes:

$$\lim_{\substack{x \rightarrow 1-Y \\ Y \rightarrow Y_L}} = L(Y_L)\sqrt{\frac{1}{1+\left(\frac{dY}{dX}\right)_{\substack{X=1-Y_L \\ Y=Y_L}}}} \qquad \text{(A-25)}$$

For the evaluation of $\frac{dY}{dX}$ we write:

$$\frac{dY}{dX} = \frac{dY}{dh}\frac{dh}{dX}$$

and make use of the lamination model used to calculate $\frac{dh}{dX}$. The variation of Y with altitude ($\frac{dY}{dh}$) can be approximated satisfactorily within a lamination by assuming an inverse cube relationship between Y and h.

6. Z Mode

(a) General Comments

The presence of a Z trace is very common on topside ionograms. The exit frequency of the Z trace (fzS) can be used together with the exit frequency of the (x) trace, (fxS) to compute the gyrofrequency (fHS) and the plasma frequency (fNS) at the satellite since:

$$fHS = fxS - fzS \qquad \text{(A-26)}$$

and

$$(fNS)^2 = (fxS)\ (fzS). \qquad \text{(A-27)}$$

The Z mode, however, is not used for routine N-h analysis, because usually it cannot propagate from an Alouette satellite down to the peak of the F2 region (F2max). The Z trace terminates at a frequency fzI corresponding to $X = (1-Y^2)/(1-Y_L^2)$ at which point the trace becomes vertical. If propagation is vertical, the frequency fzI can provide an additional check on fN, since the condition for fzI can also be written:

$$fN^2/fzI^2 = [1-fH^2/fzI^2]/[1-fH^2\ Sin^2\theta/fzI^2]$$

from which fN can readily be computed. This measurement of fN is independent of fzS, fxS and fNS and is useful in cases when none of these quantities can be can be scaled accurately on the ionogram. Even in cases where the direction of propagation is uncertain, the value of fzI gives an upper limit for the value

of fN. Also if there is evidence that fN = fzI and if the magnetic dip is less than 80 degrees, then propagation is probably occurring along field-aligned irregularities. If the dip is greater than 80 degrees, the difference between fN and fzI is too small to be resolved when propagation is vertical.

The N-h analysis with the Z trace is done by keeping in mind that the phase and group index formulas for the Z trace are the same as for the ordinary ray if X is greater than unity and they are the same as for the extraordinary ray if X is less than unity, when the index formula is written in form shown by Equation (A-2). The change at X = 1 does not take place when Equation (A-2) is written so that (1-X) does appear below Y_T^2. (See Kelso page 160). Also at X = 1 Equation A-2 is indeterminate. However, when X = 1, the phase index is unity for the Z mode and the group index n' is:

$$n' = (1+Y_T^2)/Y_T^2$$

(b) Propagation Conditions for the Z Mode

In order to avoid the trivial case in which perigee and the maximum of the F2 region are at comparable altitudes (yielding vanishing h'-f traces), it will be assumed that hmaxF2 is 300 km, i.e. at least 200 km below the Alouette II perigee.

The Z mode can propagate downward from the satellite provided the sounder frequency (f) satisfies the following conditions:

$$fzS < f < fzI \qquad \text{(A-28)}$$

where: $fzS = -\frac{fH}{2} + \frac{1}{2}\sqrt{4fN^2 + fH^2}$

$$fzI = \sqrt{\frac{fH^2 + fN^2 + \sqrt{(fH^2 + fN^2)^2 - 4fN^2\, fH^2\, \sin^2\theta}}{2}}$$

fH = gyrofrequency at the satellite, and

fN = plasma frequency at the satellite.

The lower limit fzS shown in equation (A-28) is the Z mode exit frequency at the satellite, i.e. the Z mode reflection condition at the satellite. The formula for fzS is derived from the condition X=1+Y at the satellite. In order to be seen on an Alouette II ionogram the frequency fzS must be greater than 0.2 MHz, i.e.

$$-\frac{fH}{2} + \frac{1}{2}\sqrt{4fN^2 + fH^2} > 0.2$$

This yields this condition:

$$fN^2 > 0.2fH + 0.04 \qquad \text{(A-29)}$$

The upper limit fzI (fz, infinity) is the frequency at which the phase index at the satellite becomes infinite in the vertical direction. The formula for fzI is derived from the following condition at the satellite:

$$X = \frac{1-Y^2}{1-Y_L^2} \quad \text{and} \quad Y < 1$$

This condition on X yields two positive values of fzI, but only one for which Y is less than unity.

If the Z mode can propagate downward, it will reflect at a level where the plasma frequency f_P is defined by:

$$f_P^2 = f_z^2 + fzfH_R$$

where fH_R is the gyrofrequency at the reflection point. To simplify the discussion, it will be assumed that fH_R = fHS. The maximum value of f_P occurs when fz = fzI and when fzI is itself maximum, i.e. when fzI = fT.

Thus

$$(f_P^2)_{max} = fN^2 + fH^2 + fH\sqrt{fN^2 + fH^2}$$

or

$$(f_P^2)_{max} = fH^2\ (1+k+\sqrt{1+k}) \qquad (A-30)$$

where

$$k = fN^2/fH^2.$$

The maximum electron density ratio r over which Z mode echoes can be received at the satellite is therefore:

$$r = \frac{(f_P^2)_{max}}{fN^2} = \frac{1 + k + \sqrt{1+k}}{k} \qquad (A-31)$$

from which it is readily seen that r is maximum when k is minimum. The minimum value of k is determined by equation (A-29) which can be written:

$$k > (0.2\ fH + 0.04)/fH^2 \qquad (A-32)$$

Thus the smallest value of k corresponds to the maximum value of fH. At 500 km the maximum value of fH is 1.4 MHz, giving $(fN)_{min}$ = 0.565 MHz and k_{min} = 0.16. Substituting into equations (A-30) and (A-31) yields r = 14 and $(f_P)_{max}$ = 2.09 MHz.

Thus for Alouette II the maximum electron density ratio (over which Z echoes can be received at the satellite) is approximately equal to 14. This would occur when the satellite is at 500 km and at a location where fH = 1.4 MHz. A similar calculation for Alouette I (minimum fzS = 0.5 MHz, maximum fH = 1.2) yields a maximum ratio of 4.8. In order to have a Z trace corresponding

to the electron density distribution from the satellite down to the maximum of the F2 region, the ratio of the maximum density at hmaxF2 to the density at the satellite must be less than 14 for Alouette II at 500 km and less than 4.8 for Alouette I at 1000 km. Since the density at 1000 km is typically one order of magnitude smaller than the density at hmaxF2 the above requirement cannot be met with Alouette I. However, the required minimum ratio is by no means prohititive when Alouette II is near its perigee of 500 km. The real restriction is due to the fact that the critical frequency (foF2) of the F2 region must be extremely low. For the example given foF2 would have to be less than 2.09 MHz. The maximum permissible value of foF2 can be made somewhat larger by letting this ratio r be smaller. For example, letting fN = 1.5 MHz gives f_P = 2.66 and r = 3.1. It is estimated that the ratio r should be at least equal to 3, and therefore foF2 would have to be less than 2.66. Such low values of foF2 occur only at high magnetic latitudes, where allowance must be made for the fact that Y_L is large, causing fzI to be significantly lower than fT. Hence, the upper limit of foF2 is probably 2.3 MHz. Maps showing the world-wide distribution of foF2 indicate that such low values of foF2 are most likely to occur in the southern hemisphere at geographic latitudes greater than 60 degrees and during the months of June, July or August.

Thus, very special circumstances have to be postulated in order for the Z trace to define completely the electron density distribution from the satellite down to the maximum of the F2 region. Although, in general the Z trace does not extend all the way down to hmaxF2, it is sometimes possible for the Z trace to define the electron density profile over a large altitude range. For example, when Alouette II is at

2000 km, where FHS is typically 0.56, the portion of the electron density profile which can be defined by the Z trace is usually less than 5 to 1 in terms of electron density ratio, however, in terms of altitude range it could extend from 2000 km down to 1000 km.

from which it is readily seen that:

$$fT^2 = fN^2 + fH^2$$

It is similarly shown that:

$$fx = + \frac{fH}{2} + \tfrac{1}{2}\sqrt{4fN^2 + fH^2}\ , \qquad \text{(B-1)}$$

and that:

$$fz = - \frac{fH}{2} + \tfrac{1}{2}\sqrt{4fN^2 + fH^2} \qquad \text{(B-2)}$$

Another useful relation following from Eq. (B-1) and (B-2) is:

$$fx - fz = fH \qquad \text{(B-3)}$$

2. Identification of Features on Topside Ionograms

The frequencies listed in Table B-1 can be represented graphically (Fitzenreiter and Blumle, 1964) by normalizing the coordinates to fH as shown in the lower half of Fig. B-1. This graph reveals a number of interesting facts. For example, the following relation is always true:

$$fz < fN < fT < fx \qquad \text{(B-4)}$$

The sequence revealed in Equation (B-4) is a fixed pattern. The second harmonic of fT, which is sometimes seen, was not shown on Fig. B-1. Whenever 2fT is present, it is always much greater than fx and therefore it will not be considered in the discussion of pattern identification. Superimposed upon the fixed pattern is the gyrofrequency and its harmonics. It is seen from Fig. B-1 that the position of fH and nfH with respect to the sequence shown in Equation (B-4), depends upon the ration fN/fH. For example, if this ratio is less than unity, the sequence is as follows:

$$fz < fN < fH < fT < fx < 2fH$$

This sequence will be referred to as pattern 1. When the ratio of fN/fH is equal to unity fH and fN obviously occur at the

same frequency. This will be called pattern 2. As the fN/fH ratio continues to increase, fH will be next between fz and fN (pattern 3), and then equal to fz (pattern 4). When fH is equal to fz, 2fH is equal to fx. Further increases in the ratio fN/fH will cause 2fH to move through fT, fN and fz, generating higher order patterns. The first 8 of these patterns is illustrated schematically in Fig. B-2.

For the ionogram shown in the upper portion of Fig. B-1, the ratio of fN/fH at the satellite is equal to 1.17. The sequence would then correspond to the vertical dashed drawn for an abscissa of 1.17, giving:

$$fz < fH < fN < fT < fx < 2fH,$$

which is indeed what is seen on the ionogram. The actual identification of these characteristic frequencies is relatively easy on the ionogram shown, since fxS and fzS are clearly seen The other frequencies are then readily obtained.
Equation (B-3) yields:

$$fH = fxS - fzS$$

Combining Equations (2) and (3) yields:

$$fN = \sqrt{fxS(fxS-fH)}$$

and finally

$$fT = \sqrt{fN^2 + fH^2}$$

Other features which can be seen on the ionogram of Fig. B-1 are the earth echoes for the (o) and (x) waves. At frequencies greater than the critical frequency of the F2 region, the satellite soundings can penetrate down to the earth. Although these soundings still experience some retardation in the ionosphere, this effect decreases with frequency, and at the high-frequency end of the earth echoes the apparent range is only slightly greater than the satellite altitude. One should also note on

on the ionogram of Fig. B-1 the surprisingly long apparent ranges at the high-frequency end of the z trace. This is due to the fact that the z trace retardation becomes infinite for a frequency fzI (fz "infinity") corresponding to:

$$X = (1-Y^2)/(1-Y_L^2)$$

3. Scaling fxS

For routine N-h analysis, the extraordinary trace is usually the only data which is scaled on a topside ionogram. This trace is easily recognized. If the exit point fxS is clearly seen and if fxS is at least 0.5 MHz greater than fH, it is usually not necessary to identify other features such as fH, fN or fT. However, the exit point fxS is sometimes difficult to read accurately due either to a spreading of the x trace or to a nearby resonance masking the precise position of fxS. In such cases, (and also when the value of fxS is close to that of fH) it is desirable to locate the resonances and to compute fxS, making use of the resonance data. To avoid the numerical calculations, which would slow down the scaling procedure, the identification is performed at GSFC with the aid of tabulated data (fxS tables). The tables provide fN, fz and fT as a function of fH (varying from 0.20 MHz to 1.40 MHz in 0.01 MHz steps) and as a function of fxS (varying from fH + 0.02 MHz to fH + 2.81 MHz in 0.01 MHz steps). A typical page of the fxS tables is shown in Fig. B-3. The page was selected for fH = 0.95 MHz to represent the gyrofrequency corresponding to the ionogram of Fig. B-1. For this ionogram fxS is equal to 1.68 MHz, hence it is readily seen from the tables that fN = 1.11, fzS = 0.73 and fT = 1.46 MHz. The last entry in the table is the pattern number, which indicates the ionogram of Fig. B-1 follows pattern 3, namely:

$$fz < fH < fN < fT < fxS < 2fH$$

To facilitate further the identification of features on the ionogram, another table is used which gives fH at the satellite as a function of date and universal time. This fH table is

compiled from an orbit program and a magnetic field program. Hence the fH table gives immediately the correct value of gyrofrequency for the ionogram being scaled, which of course specifies which page should be used in the fxS tables. Incidentally, even if the magnetic field program yields a slightly incorrect value of fH, the determination of fxS in terms of this fH and of the actual fN will yield the correct density at the satellite, since the same magnetic field program (and hence the same fH) is used in the N-h analysis.

The main use of these tables is to improve the accuracy of the fxS scaling, particularly when the local densities are low ($N < 10^4$ el/cc). The procedure is to read the date and time of the ionogram, find the appropriate fH from the fH tables, read fxS on the ionogram, find in the fxS table the corresponding fN, check fN on the ionogram and correct its value if necessary, and finally read in the fxS tables the correct fxS corresponding to the actual fN. Since ionograms are usually scaled in sequence, the data for the next ionogram is usually found either on the same pages of the tables (as were used for the previous ionogram) or on adjacent pages. The entire procedure requires usually less than one minute of time per ionogram on the part of the ionogram scaling technician. The first ionogram of a sequence usually takes a little longer, since it is advisable to check it more thoroughly and make sure that the identification of fN is consistent with the other resonances. Since the pattern changes slowly from one ionogram to the next, the operator can usually recognize immediately the resonances on the next ionogram, and proceed much more rapidly with the precise scaling of the next fxS. The procedure will of course fail with Alouette II records if fN is less than the minimum transmitter frequency (0.2MHz).

4. Selection of Data Points

A criterion for the selection of h'-f values (from the extraordinary trace) to be used in the analysis of ionograms was developed empirically at GSFC, based upon experience with the scaling of Alouette II ionograms. The criterion can be used as a guide for manual scaling. However, it was prepared primarily for the purpose of selecting from the automatically-scaled h'-f values (roughly 200 points per ionogram), the h'-f data which would be fed to the computer (roughly 20 to 30 points per ionogram.) The test is therefore part of the editing process which is programmed between the scaler output and the computer input. The minimum frequency spacing corresponds to approximately 0.2 inch on the viewer of the scaler.

The first data point is the exit frequency of the extraordinary ray. The other points are taken in the following manner:

a) the next 4 points at 0.02 Mc intervals,

b) the next 5 points at 0.05 Mc intervals,

c) the next 5 points at 0.10 Mc intervals,

d) the next 5 points at 0.20 Mc intervals,

e) the remaining points at 0.50 Mc intervals. This will define the entire ionogram, except for the cusp at the penetration frequency. The remainder of the procedure is for the purpose of defining this cusp.

f) If the virtual heights for the last two points (f_{n-1}, h_{n-1} and f_n, h_n) obtained by the above procedure differ by more than 100 km, take one additional point at a frequency $(f_{n-1} + f_n)/2$. This will become the $n^{\underline{th}}$ point and the previous $n^{\underline{th}}$ will become

the $(n + 1)^{th}$ point. Regardless of whether or not this additional point is inserted, proceed with the next step.

g) The last data point to be kept will be scaled point corresponding to the maximum scaled frequency (for an ideal case this would be the critical frequency: f max). Compare this last point with the last point obtained under step f). If the virtual heights differ by more than 100 km, insert one additional point at the midpoint (frequency-wise).

The use of this criterion is illustrated with reference to the electron density model used in section IV of this report. The Bauer topside electron density distribution used is shown in fig. B-4 and the corresponding extraordinary ionograms are shown in fig. B-5 and B-6. The h'-f data points shown in fig. B-5 and B-6 were obtained by using the above criterion for the selection of data points. The corresponding N-h points are shown on fig. B-4. It is seen that the criterion corresponds to a fairly good choice of laminations for the actual profile, or equivalently to a fairly good distribution of N-h values on the actual profile.

The density ratios within a lamination depend upon fH, fxS and the selection sequence. Typical density ratios for the successive laminations (as obtained by the GSFC data point selection) are shown in Fig. B-7. It is seen that the maximum ratio is less than 1.6. In fact, most of the density ratios are less than 1.4. The importance of having a small density ratio within the lamination is discussed in Appendix C where it is shown that the error in the group height calculations increase rapidly with the value of this density ratio. However, if the density ratio does not exceed 1.6, then the errors in group height calculations are typically less than 1 part in 10,000, which is completely negligible compared to scaling inaccuracies.

5. Date and Time Identification of Topside Ionograms

Ionograms obtained with ground-based sounders are normally filmed at the time when the ionospheric soundings are taken. Consequently the format for a particular ionogram is established at that time. Topside ionograms are not produced at the time of data acquisition, but instead they are derived at a later date from tape recordings of the telemetered topside sounder A-scans. Furthermore since the tapes are preserved after the ionograms are filmed, it is possible to re-film topside ionograms many years later using improved data processing techniques. Since the number of available topside ionograms is well in excess of 10^6, re-filming all these ionograms would be a very expensive and time consuming procedure. It was therefore decided that modifications which did not change the inherent quality of ionograms, but merely resulted in improved formats, would not justify the re-processing and replacement of old topside ionograms. However these modifications were incorporated in subsequent ionograms. As a result of this policy, there are at least 3 different formats for the topside ionograms deposited in data centers, the difference being primarily in the method used for providing date and time identification.

a) A dot code was used in the early Alouette I ionograms produced by DRTE (Defence Research Telecommunications Establishment, Ottawa, Canada). The decimal digits appearing in the ionogram identification are given in a binary code (see Figure B-8). The time (Greenwich Mean Time) printed on the right hand side of the ionogram (07/31/28) is measured 15 seconds after the 2MHz frequency marker. When ionograms are consecutive they are 18 seconds apart. Hence for consecutive ionograms, the time shown to the left of the ionogram (07/31/10) is 3 seconds earlier than the 2MHz marker. The Alouette I ionograms processed by DRTE prior to July 1965 used the DRTE Code for identification of the telemetry station used to obtain the topside sounder

data. A Single line was used on the dot code for station identification. Thus, Woomera (station 12 in DRTE code) was written as 4 and 8 one line. The NASA station code number was used on topside ionograms processed after July 1965.

To read the dot code it is necessary to know the position of the unit dots (right or left of identification block). Furthermore if either the 8 or the 1 column is not required for the ionogram identification (such as 1962, day 006, 08 hr., 42 min., 06 sec., station 8) the "2" column could be interpreted as a "1" column, assuming that the "8" column was missing.

b) To prevent these ambiguities, the dots were subsequently replaced by numbers. One line was added for the satellite identification and two lines were provided for the telemetry station identification. Thus Alouette I, 1964, day 296, 23 hr., 36 min., 40 sec., station 7 (DRTE code for Quito) would be abbreviated: 1/4/296/23/36/40/07 and written:

```
1       1       1 1             1
    2     2 2 2 2 2             2
  4       4           4 4       4
          8
```

c) The binary representation of digits was eliminated with the next improvement in format. This format was introduced with the Alouette II ionograms (See Fig. B-1). The identification is provided at the bottom of the ionograms, near the center, using a decimal code. Thus Alouette II, Ottawa (NASA code 50), 1956, day 37, 17 hr., 02 min., 30 sec., would be written:

20 50 66 037 1702 30

Dots are used at the bottom of the ionogram to indicate the successive seconds of time, a double dot being used every 5 seconds. The printed time 17/02/30 corresponds to the dot nearest to the beginning of the identification. In the above example there would be a double dot above the initial number 2, since the indicated second (30) is a multiple of 5.

6. Frequency and Height Markers

On Alouette I the frequency range extends from 0.5 MHz to 11.5 MHz. The frequency is increased almost linearly at a rate of 1Mhz/per second. Frequency markers are provided at 1 MHz intervals, beginning at 0.5 MHz. These markers are derived from pulses generated within the sounder and initiated whenever the swept frequency reaches one of the reference frequencies. The marker is not synchronized with the transmitted pulse, i.e. the marker can start anywhere during a given pulse period. To insure that the frequency markers will appear across the entire ionogram, the duration of these markers were made slightly longer than the transmitter pulse period. To assist in the identification of these markers, additional markers were provided at 2.0 and 7.0 MHz. Furthermore these two additional markers were made somewhat longer in duration and consequently on the ionograms the 2.0 and the 7.0 MHz markers are broader than the other markers. The two additional frequency markers reduce considerably the uncertainty which could exist on ionograms when the markers are not too clear, due to noise or plasma resonances, or when a marker is missing (For example the 0.5 MHz is often missing on ionograms). The standard virtual height scale is 1500 km. with height markers at every 100 km., zero height being the leading edge of the transmitted pulse. Hence virtual heights must be scaled at the leading edge of the echo.

For Alouette II (see Fig. B-1) the frequency range extends

from 0.12MHz to 14MHz. A linear sweep with a rate of 0.125MHz per second is used below 2.0MHz and a linear sweep with a rate of 1.0MHz per second is used above 2.0MHz. The ionograms are 32 seconds apart. The frequency markers provided below 2.0MHz are indicated in Fig. B-5 and B-6. Above 2.0MHz the frequency markers are the same as on Alouette I, except that additional markers are provided at 12.5 and 13.5 MHz. The standard virtual height scale is 4600 km with height markers every 200 km. Darker height markers are provided at 1000, 2000, 3000 and 4000 km. Sometimes (when the Alouette II ionograms were obtained at altitudes comparable to or less than the Alouette I altitudes) a 2000 km height scale is used with height markers every 100 km. This format is illustrated in Fig. B-1.

7. Pulse Characteristics

The topside sounder transmits pulsed r-f signals. Rectangular pulses, 100 microsecond in duration, are used on both Alouette I and Alouette II. The pulse repetition rate is 67 Hz on Alouette I and 30 Hz on Alouette II. Thus the spacing between pulses is at least 150 times greater than the pulse width (w). In the absence of pulse broadening (due to either the receiver or the ionosphere) the corresponding ionogram trace should have a width equivalent to 15 km.

The transmitted r-f pulse has a frequency spectrum centered at the carrier frequency f. The envelope of the spectrum has an amplitude $S(\Delta f)$ given by:

$$S(\Delta f) = A_o \left| \frac{\mathrm{Sin}[\pi(\Delta f)w]}{[\pi(\Delta f)w]} \right|$$

where A_o = amplitude of spectrum at the carrier frequency (for a single impulse). The function $S(\Delta f)$ is equal to A_o when $\Delta f=0$, and it has zero amplitude when $(\Delta f)w = \pm k$, where k is an integer. Since $w = 10^{-4}$, these nulls occur at multiples of 10 kHz. The subsequent peaks in the spectrum occur approximately half-way between these nulls with amplitudes

$A_o/\pi(\Delta f)w$. Sufficient bandwidth must be provided in the receiver in order to reproduce such a pulse, without excessive broadening. The minimum bandwidth is usually considered to be 2/w (i.e. 20 kHz for a 100 microsecond pulse). With this bandwidth the received pulse is almost triangular in shape, the base of the triangle having a width of about 170 microseconds. With the bandwidth used in the topside sounder (33 kc in Alouette I and 37 kc in Alouette II) the pulse shape is more nearly trapezoidal and the pulse broadening is less than 40 percent (i.e. the width of the ionogram trace would at most be 20 km).

When a radio-frequency pulse is transmitted through the ionosphere, the various portions of its r-f spectrum are delayed according to their actual frequencies. In a region where the virtual range increases rapidly with frequency this leads not only to a considerable broadening of the received echoes, but also in some cases to side responses in the Fourier spectrum appearing as separate echoes. These separate echoes are particularly strong on certain high altitude Alouette II ionograms. Nelms, G. L. (private communication) showed that in such cases the received signal consists of four separate components. An A-scan (i.e. a presentation of echo amplitudes vs time for a single sounding pulse) reveals four separate components, corresponding to the main (center) spectrum, the first <u>two</u> secondary peaks on the <u>low</u> frequency side, and the first secondary peak on the <u>high</u> frequency side. On the conventional ionogram presentation the echoes produced by the low frequency side of the spectrum will normally experience less delay and appear above the main trace. Consequently, on the ionogram the traces due to the low frequency side of the spectrum will seem to be on the high frequency side of the main trace.

This asymmetry is due to the fact that the center frequency of the Alouette II receiver is 10 kHz lower than the transmitter frequency. Nelms also pointed out that unless special care is taken during processing, the side lobes may not appear as separate traces, but instead the three side responses and the main echo appear as a single broad trace. It is therefore important to take this into consideration when high altitude Alouette II ionograms are scaled.

FIGURE B-1

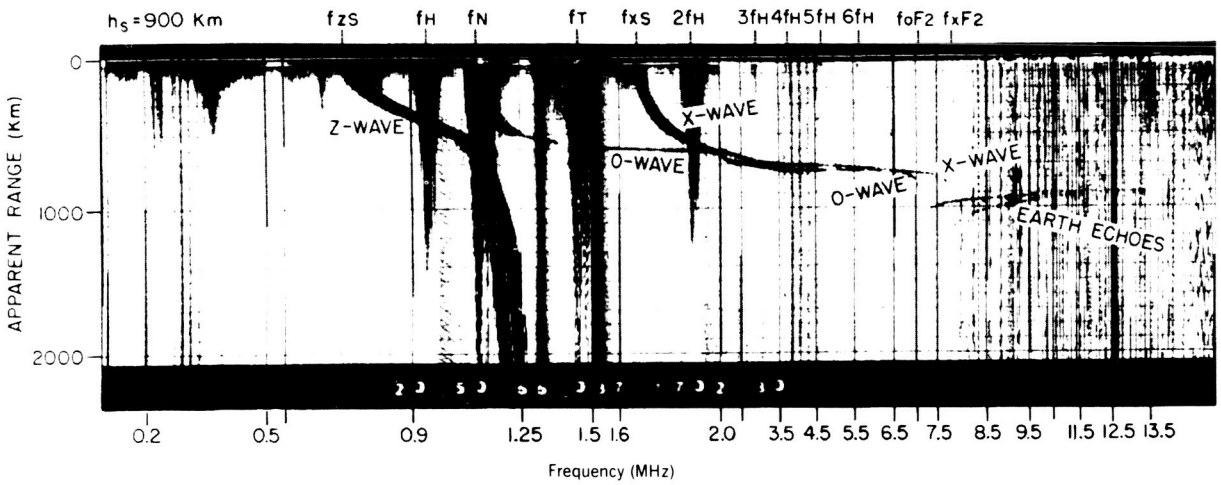

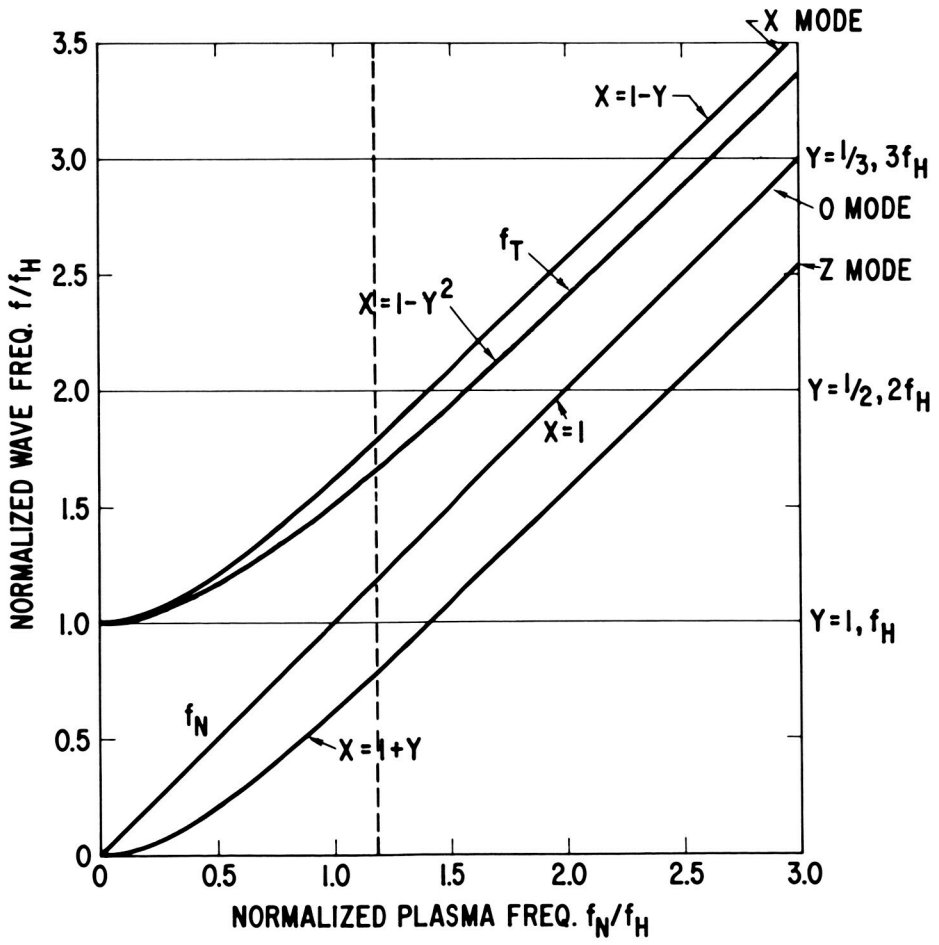

Cut-Off and Resonance Conditions in a Magnetoionic Medium.

FIGURE B-2

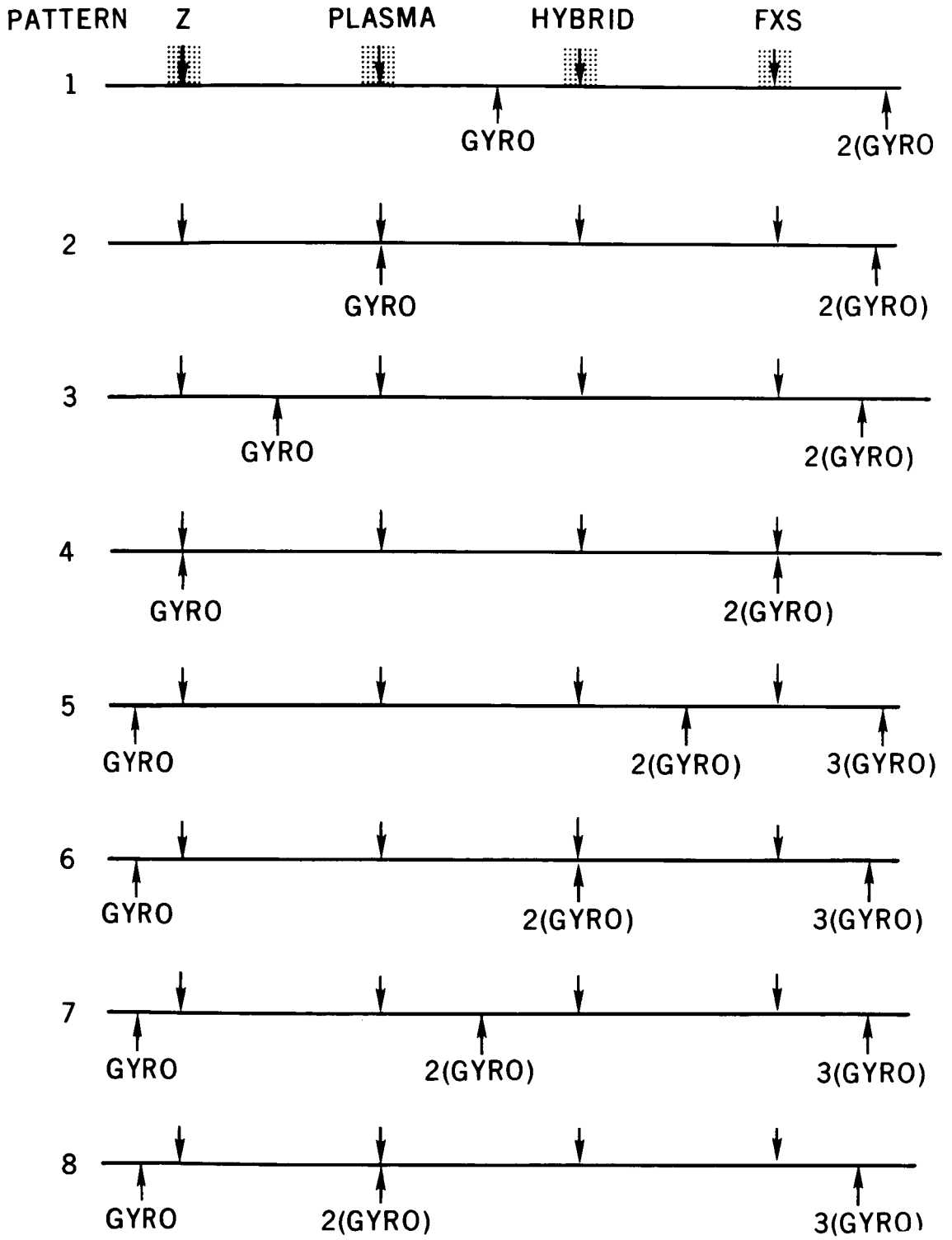
PATTERN
Z
PLASMA
HYBRID
FXS
1
GYRO
2(GYRO
2
GYRO
2(GYRO)
3
GYRO
2(GYRO)
4
GYRO
2(GYRO)
5
GYRO
2(GYRO)
3(GYRO)
6
GYRO
2(GYRO)
3(GYRO)
7
GYRO
2(GYRO)
3(GYRO)
8
GYRO
2(GYRO)
3(GYRO)

GYRO=0.95 2(GYRO)=1.90 3(GYRO)=2.85 4(GYRO)=3.80

FXS=	0.97	0.98	0.99	1.00	1.01	1.02	1.03	1.04	1.05	1.06	1.07	1.08	1.09	1.10	1.11	1.12	1.13	1.14	1.15	1.16
PLASMA=	0.14	0.17	0.20	0.22	0.25	0.27	0.29	0.31	0.32	0.34	0.36	0.37	0.39	0.41	0.42	0.44	0.45	0.47	0.48	0.49
ZMODE=	0.02	0.03	0.04	0.05	0.06	0.07	0.08	0.09	0.10	0.11	0.12	0.13	0.14	0.15	0.16	0.17	0.18	0.19	0.20	0.21
HYBRID=	0.96	0.97	0.97	0.98	0.98	0.99	0.99	1.00	1.00	1.01	1.02	1.02	1.03	1.03	1.04	1.05	1.05	1.06	1.06	1.07
PATTERN=	1	1	1	1	1	1	1	1	1	1	1	1	1	1	1	1	1	1	1	1

FXS=	1.17	1.18	1.19	1.20	1.21	1.22	1.23	1.24	1.25	1.26	1.27	1.28	1.29	1.30	1.31	1.32	1.33	1.34	1.35	1.36
PLASMA=	0.51	0.52	0.53	0.55	0.56	0.57	0.59	0.60	0.61	0.62	0.64	0.65	0.66	0.67	0.69	0.70	0.71	0.72	0.73	0.75
ZMODE=	0.22	0.23	0.24	0.25	0.26	0.27	0.28	0.29	0.30	0.31	0.32	0.33	0.34	0.35	0.36	0.37	0.38	0.39	0.40	0.41
HYBRID=	1.08	1.08	1.09	1.10	1.10	1.11	1.12	1.12	1.13	1.14	1.14	1.15	1.16	1.17	1.17	1.18	1.19	1.19	1.20	1.21
PATTERN=	1	1	1	1	1	1	1	1	1	1	1	1	1	1	1	1	1	1	1	1

FXS=	1.37	1.38	1.39	1.40	1.41	1.42	1.43	1.44	1.45	1.46	1.47	1.48	1.49	1.50	1.51	1.52	1.53	1.54	1.55	1.56
PLASMA=	0.76	0.77	0.78	0.79	0.81	0.82	0.83	0.84	0.85	0.86	0.87	0.89	0.90	0.91	0.92	0.93	0.94	0.95	0.96	0.98
ZMODE=	0.42	0.43	0.44	0.45	0.46	0.47	0.48	0.49	0.50	0.51	0.52	0.53	0.54	0.55	0.56	0.57	0.58	0.59	0.60	0.61
HYBRID=	1.22	1.22	1.23	1.24	1.25	1.25	1.26	1.27	1.28	1.28	1.29	1.30	1.31	1.31	1.32	1.33	1.34	1.35	1.35	1.36
PATTERN=	1	1	1	1	1	1	1	1	1	1	1	1	1	1	1	2	2	2	2	2

FXS=	1.57	1.58	1.59	1.60	1.61	1.62	1.63	1.64	1.65	1.66	1.67	1.68	1.69	1.70	1.71	1.72	1.73	1.74	1.75	1.76
PLASMA=	0.99	1.00	1.01	1.02	1.03	1.04	1.05	1.06	1.07	1.09	1.10	1.11	1.12	1.13	1.14	1.15	1.16	1.17	1.18	1.19
ZMODE=	0.62	0.63	0.64	0.65	0.66	0.67	0.68	0.69	0.70	0.71	0.72	0.73	0.74	0.75	0.76	0.77	0.78	0.79	0.80	0.81
HYBRID=	1.37	1.38	1.39	1.39	1.40	1.41	1.42	1.43	1.43	1.44	1.45	1.46	1.47	1.48	1.48	1.49	1.50	1.51	1.52	1.53
PATTERN=	3	3	3	3	3	3	3	3	3	3	3	3	3	3	3	3	3	3	3	3

FXS=	1.77	1.78	1.79	1.80	1.81	1.82	1.83	1.84	1.85	1.86	1.87	1.88	1.89	1.90	1.91	1.92	1.93	1.94	1.95	1.96
PLASMA=	1.20	1.22	1.23	1.24	1.25	1.26	1.27	1.28	1.29	1.30	1.31	1.32	1.33	1.34	1.35	1.36	1.38	1.39	1.40	1.41
ZMODE=	0.82	0.83	0.84	0.85	0.86	0.87	0.88	0.89	0.90	0.91	0.92	0.93	0.94	0.95	0.96	0.97	0.98	0.99	1.00	1.01
HYBRID=	1.53	1.54	1.55	1.56	1.57	1.58	1.59	1.59	1.60	1.61	1.62	1.63	1.64	1.65	1.65	1.66	1.67	1.68	1.69	1.70
PATTERN=	3	3	3	3	3	3	3	3	3	3	3	4	4	4	4	4	4	5	5	5

FXS=	1.97	1.98	1.99	2.00	2.01	2.02	2.03	2.04	2.05	2.06	2.07	2.08	2.09	2.10	2.11	2.12	2.13	2.14	2.15	2.16
PLASMA=	1.42	1.43	1.44	1.45	1.46	1.47	1.48	1.49	1.50	1.51	1.52	1.53	1.54	1.55	1.56	1.57	1.59	1.60	1.61	1.62
ZMODE=	1.02	1.03	1.04	1.05	1.06	1.07	1.08	1.09	1.10	1.11	1.12	1.13	1.14	1.15	1.16	1.17	1.18	1.19	1.20	1.21
HYBRID=	1.71	1.72	1.72	1.73	1.74	1.75	1.76	1.77	1.78	1.79	1.79	1.80	1.81	1.82	1.83	1.84	1.85	1.86	1.87	1.88
PATTERN=	5	5	5	5	5	5	5	5	5	5	5	5	5	5	5	5	5	5	5	6

FXS=	2.17	2.18	2.19	2.20	2.21	2.22	2.23	2.24	2.25	2.26	2.27	2.28	2.29	2.30	2.31	2.32	2.33	2.34	2.35	2.36
PLASMA=	1.63	1.64	1.65	1.66	1.67	1.68	1.69	1.70	1.71	1.72	1.73	1.74	1.75	1.76	1.77	1.78	1.79	1.80	1.81	1.82
ZMODE=	1.22	1.23	1.24	1.25	1.26	1.27	1.28	1.29	1.30	1.31	1.32	1.33	1.34	1.35	1.36	1.37	1.38	1.39	1.40	1.41
HYBRID=	1.88	1.89	1.90	1.91	1.92	1.93	1.94	1.95	1.96	1.97	1.97	1.98	1.99	2.00	2.01	2.02	2.03	2.04	2.05	2.06
PATTERN=	6	6	6	6	6	6	7	7	7	7	7	7	7	7	7	7	7	7	7	7

FIGURE B-3

FIGURE B-4

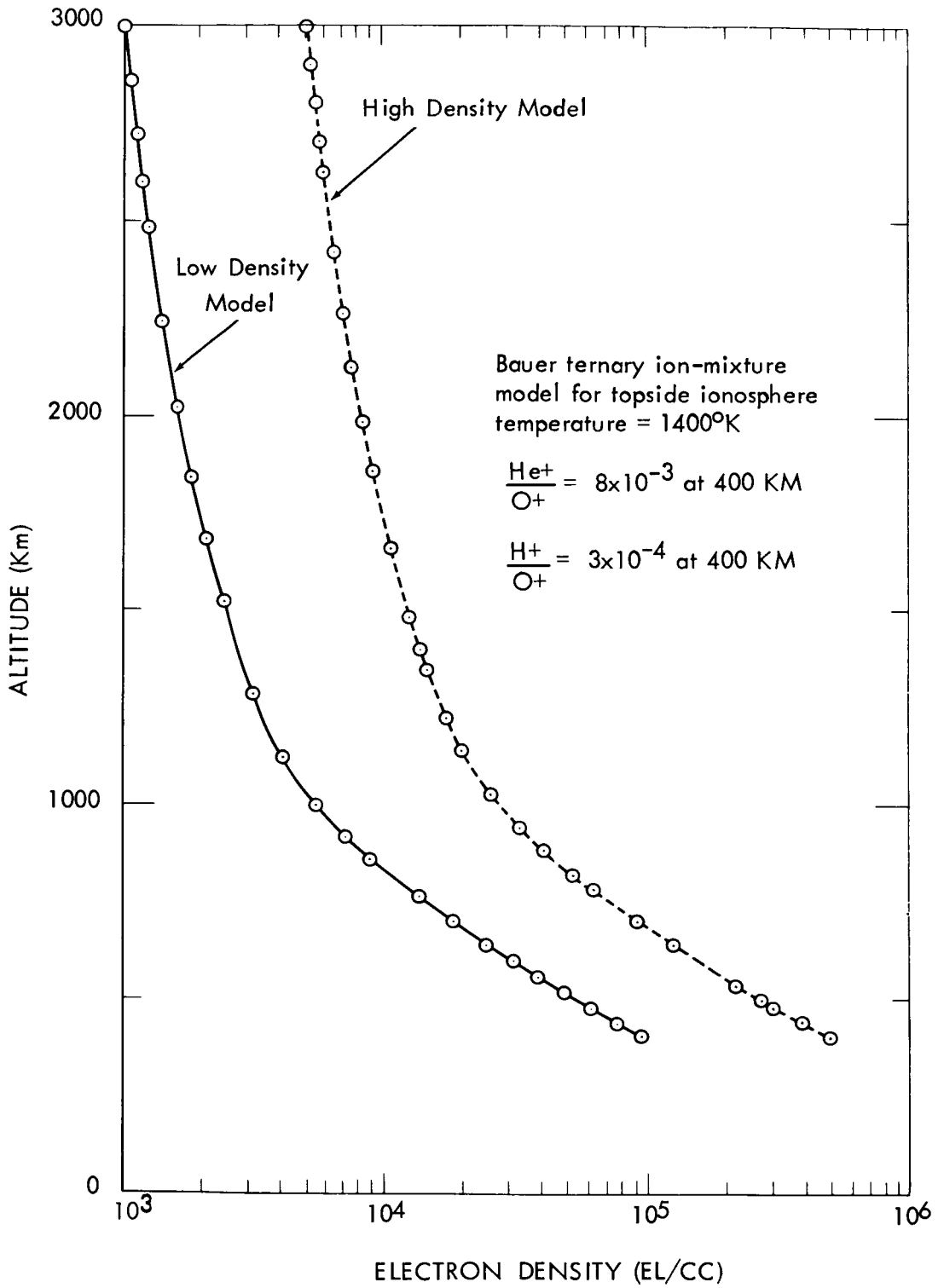
3000
2000
1000
0
ALTITUDE (Km)
High Density Model
Low Density Model
Bauer ternary ion-mixture model for topside ionosphere temperature = 1400°K
He+/O+ = 8x10^-3 at 400 KM
H+/O+ = 3x10^-4 at 400 KM
10^3
10^4
10^5
10^6
ELECTRON DENSITY (EL/CC)

FIGURE B-5

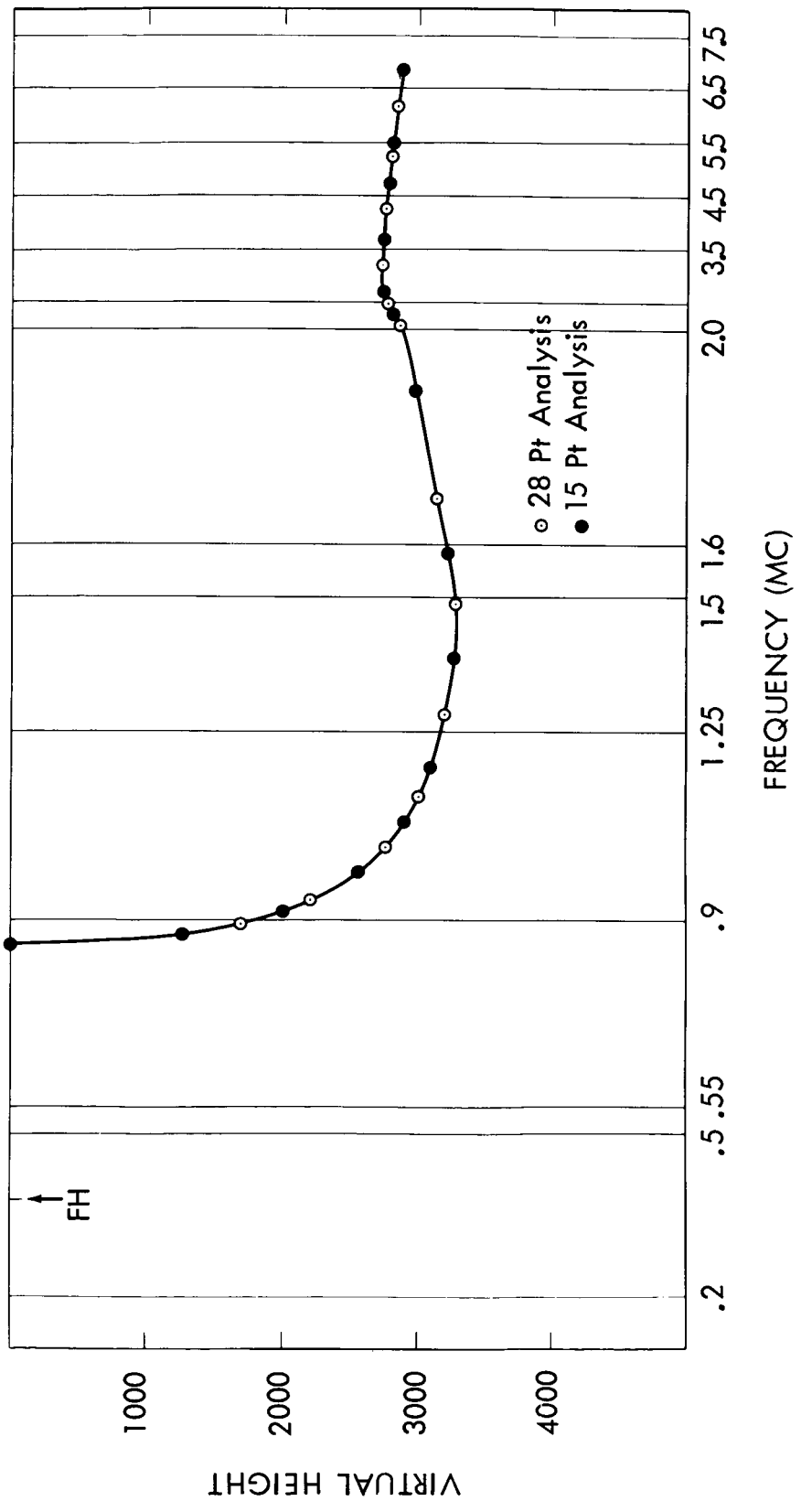
VIRTUAL HEIGHT
1000
2000
3000
4000
FREQUENCY (MC)
.2
.5
.55
.9
1.25
1.5
1.6
2.0
3.5
4.5
5.5
6.5
7.5
FH
⊙ 28 Pt Analysis
● 15 Pt Analysis

FIGURE B-6

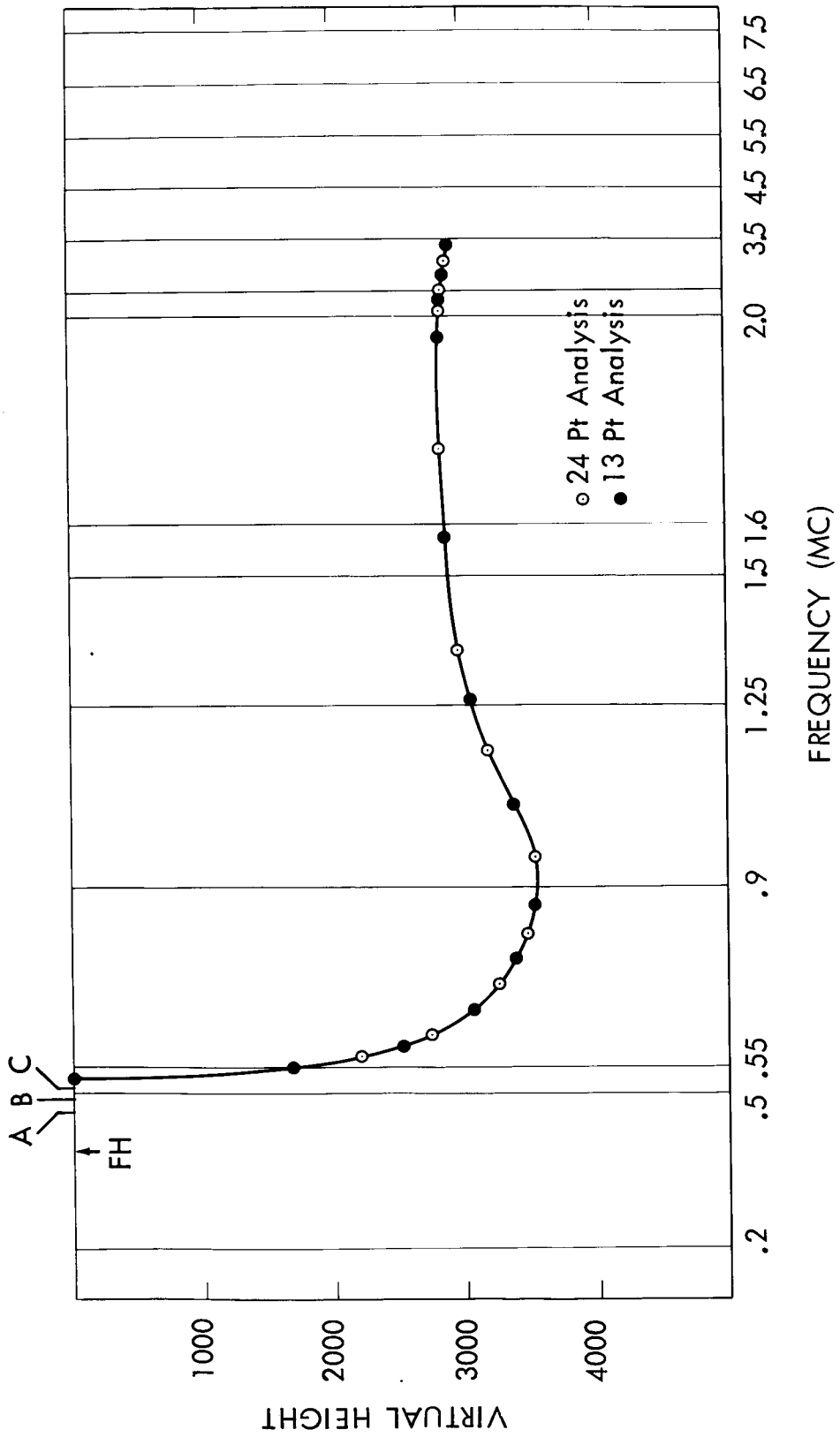
VIRTUAL HEIGHT
1000
2000
3000
4000
A B C
FH
.2
.5
.55
.9
1.25
1.5
1.6
2.0
3.5
4.5
5.5
6.5
7.5
FREQUENCY (MC)
○ 24 Pt Analysis
● 13 Pt Analysis

FIGURE B-7

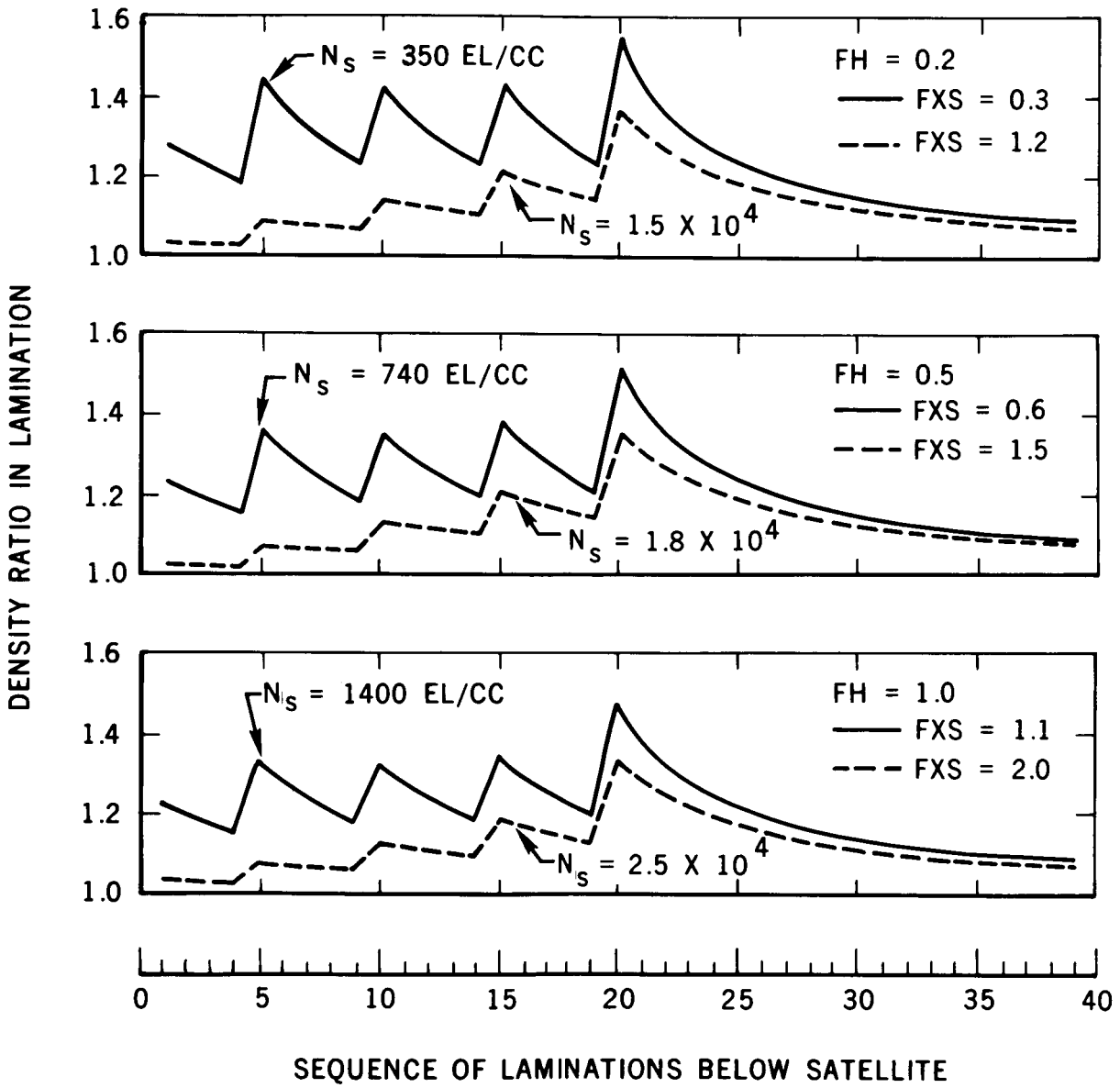
DENSITY RATIO IN LAMINATION
1.6
1.4
1.2
1.0
N_S = 350 EL/CC
FH = 0.2
FXS = 0.3
FXS = 1.2
N_S = 1.5 X 10^4
N_S = 740 EL/CC
FH = 0.5
FXS = 0.6
FXS = 1.5
N_S = 1.8 X 10^4
N_S = 1400 EL/CC
FH = 1.0
FXS = 1.1
FXS = 2.0
N_S = 2.5 X 10^4
0
5
10
15
20
25
30
35
40
SEQUENCE OF LAMINATIONS BELOW SATELLITE

FIGURE B-8

1962 DAY HR. MIN. SEC. STA.
2 3 1 9 0 7 3 1 2 8 12
8 4 2 1
0 7 3 1 1 0
(TIME)
07/31/13
2 MHz Marker

ACCURACY OF GROUP HEIGHT INTEGRAL CALCULATIONS

APPENDIX C

The accuracy of the evaluation of $\int_{h_1}^{h_2} n'dh$ requires both accurate values of the group index and an accurate integration technique. The accuracy of the n' calculations can be checked against Becker's tables (1960),which have been found to be quite reliable. The integration technique is critical only for the last lamination, i.e. for the lamination which includes the reflection point (where n' becomes infinite). Hence the method of integration must be checked with an integral of the form:

$$I = \int_{h_{R-\Delta h}}^{h_R} n'dh \qquad \text{(C-1)}$$

where the upper limit of integration h_R is the reflection point. The accuracy of the integration technique can be investigated in two different ways. One way is to perform the numerical integration several times, each time increasing the number of sampling points L. If the results become constant when L is greater than some number K, then K sampling points yield an accurate answer. To minimize computer time K should be as small as possible. Another method is to use as a basis for comparison one of the special cases when the integration can be performed analytically. The test discussed here was done using the n' function for the extraordinary ray, longitudinal propagation and constant Y. This yields an integral which can be evaluated analytically. A linear in log N lamination was used (see Eq. 12) giving:

$$h = h_{j-1} + a_j \, (\ln N - \ln N_{j-1})$$

and

$$dh = a_j \frac{dN}{N} = a_j \frac{dX}{X}$$

changing to the variable X in Eq. (C-1) gives:

$$I = a_j \int_{1-Y-\epsilon}^{1-Y} \frac{n'}{X} dX \qquad (C-2)$$

Since a_j is outside of the integral, it can be assumed to be unity for the purpose of checking the integration technique. In this case n' is given by Equation (A-10), which can be written

$$n' = \frac{1+bX}{\sqrt{1+aX}} \qquad (C-3)$$

where $a = \frac{-1}{1-Y}$ and $b = \frac{Y}{2(1-Y)^2}$

For any specified value of Y, the quantities a and b are constants. Substituting n' from Eq. (B-3) into Eq. (B-2) yields:

$$I = \int_{1-Y-\epsilon}^{1-Y} \left[\frac{1+bX}{X\sqrt{1+aX}}\right] dX \qquad (C-4)$$

The recommended substitution for the numerical evaluation of Eq. (B-4) is to let:

$$t^2 = 1-X/(1-Y)$$

giving: $$2tdt = - dX/(1-Y)$$

The integration limits are:

$$t_1 = (1 - \frac{1-Y-\epsilon}{1-Y})^{\frac{1}{2}} = \sqrt{\frac{\epsilon}{1-Y}}$$

and $$t_2 = 0$$

After making the above change in variable, and noting that for this special longitudinal case $t=\sqrt{1+aX}$, Eq.(B-4) becomes:

$$I = \int_0^{\sqrt{\frac{\epsilon}{1-Y}}} 2(1-Y)\left(\frac{1+bX}{X}\right)\, dt \qquad \text{(C-5)}$$

where: $X = (1-t^2)(1-Y)$.

The analytical solution of Eq. (B-4) is:

$$I = \left[\frac{2b\sqrt{1+aX}}{a} - \ln\left(\frac{1+\sqrt{1+aX}}{1-\sqrt{1+aX}}\right) \right]_{X=1-Y-\epsilon}^{X=1-Y}$$

The numerical and analytical integrations were carried out for values of Y ranging from 0.1 to 0.9 (for routine analysis Y will seldom exceed a value of 0.90) and for electron density ratios $(1-Y)/(1-Y-\epsilon)$ ranging from 1.01 to 2.0. The numerical integration was performed with the indicated change of variable using a 3 point Gaussian technique, and also without making a change of variable with a 7 point and a 16 point Gaussian technique. The calculations were done on a 7094 computer using double-precision arithmetic. The errors arising from the various numerical integration techniques are shown in table C-1. It is seen that the error is roughly constant and quite substantial for each Gaussian integration where no change in variable was made (4.7 to 5.8 percent with the 7 point Gaussian and 2.1 to 2.6 percent with the 16 point Gaussian). Using the GSFC data point selection criterion, the typical density increase per lamination is about 40 percent and the maximum increase is 60 percent. Hence the maximum error obtained using the 3 point Gaussian with change of variable is less than 0.020. Thus this method is at least two (and typically three to four) orders of magnitude more accurate than the 16 point Gaussian with no change in variable.

The remarkable improvement in accuracy which results from the change in variable is due to the fact that the integrand in Eq.(B-5) is a very slowly changing function. For the special case investigated here ($\theta=0$) the curves representing the integrand as a function of t are parallel to each other as the parameter Y is changed. This is readily seen from the fact that when $\theta=0$:

$$2(1-Y)n't/X = \frac{2}{1-t^2} + \frac{Y}{1-Y}$$

However, the integrand obtained for the general case ($\theta \neq 0$) has a similar slow variation as a function of t as can been seen from Fig. C-1. Hence the conclusion reached for this special case can be considered applicable to the general case.

It should be noted that both $\frac{n'}{X}$ and $\frac{n't}{X}$ become infinite as X approaches zero. This presents no problem in the routine reduction of scalable topside ionograms since the existence of a continuous extraordinary trace up to the satellite, implies that the local density is not zero. It is quite evident that more elaborate techniques (such as perhaps using simultaneously O and X traces, as well as various information which might be derived from plasma resonances, and other observations) would be required for the analysis of ionograms where very low local densities (combined with inadequate sounder resolution), cause the initial (low-frequency) portion of the ionogram to be either poorly defined or completely missing. Analysis of incomplete ionograms will not be discussed in the present report. However, a few comments will be made concerning certain limiting cases when ionograms are barely analyzable due to low local densities. To be suitable for routine analysis, the value of fxs-fH should be greater than 50 kc, because when

fxs-fH is less than 50 kc the exit portion of the extra-ordinary trace usually merges with the fH resonance. As seen in Fig. C-2 this corresponds to a typical local density of 500 electrons per cc (and also to a maximum value of Y equal to about 0.9). The uncertainty in the value of fxs-fH can be reduced considerably for densities ranging from 500 to a few thousand electrons/cc by measuring separately the plasma resonance. However since the minimum sounder frequency is about 0.2 Mc, (i.e. the plasma frequency corresponding to 500 el/cc), densities less then 500 el/cc cannot be determined by this method. To go beyond this stage requires trial and error techniques, such as trying several initial f-fH values until the resulting profile appears to be "correct". This method is illustrated in Fig. C-3, which shows the profiles which would be obtained for the ionogram of fig. B-6 for various incorrect values of fxs: (0.452, 0.492 and 0.512 Mc), keeping the other data points unaltered. These incorrect exit frequencies and the corresponding profiles are identified by the letter A, B and C on the ionogram of fig. B-6 and on Fig. C-3. It is seen that the incorrect guesses produce a flattening of the profile directly below the satellite. Hence, one could select as the correct fxs, the minimum value of fxs which causes the flattening to disappear. This method is obviously not well suited to the routine reduction of ionograms.

7 POINT GAUSSIAN - NO CHANGE IN VARIABLE

Y	Percent increase in density within lamination				
	1	10	40	60	100
.1	5.79	5.63	5.23	5.02	4.70
.3	5.79	5.66	5.29	5.11	4.82
.5	5.79	5.68	5.39	5.23	4.98
.7	5.79	5.72	5.51	5.39	5.21
.9	5.80	5.77	5.69	5.64	5.56

16 POINT GAUSSIAN - NO CHANGE IN VARIABLE

.1	2.63	2.56	2.38	2.28	2.14
.3	2.63	2.57	2.41	2.32	2.19
.5	2.63	2.58	2.45	2.38	2.27
.7	2.63	2.60	2.50	2.45	2.37
.9	2.64	2.62	2.50	2.56	2.53

3 POINT GAUSSIAN - CHANGE IN VARIABLE

.1	0.000025	0.000044	0.0041	0.014	0.065
.3	0.000025	0.000038	0.0036	0.013	0.058
.5	0.000025	0.000031	0.0029	0.011	0.048
.7	0.000025	0.000021	0.0021	0.008	0.035
.9	0.000025	0.000007	0.0008	0.003	0.015

Table C-1. Percent error in the evaluation of the group height integral $\int_{1-Y-\varepsilon}^{1-Y} \frac{n'}{x}\,dx$ as a function of Y and of the percent increase in density $(100\,\frac{1-Y}{1-Y-\varepsilon})$ for various integration techniques. Calculations were performed for the case of longitudinal propagation.

FIGURE C-1

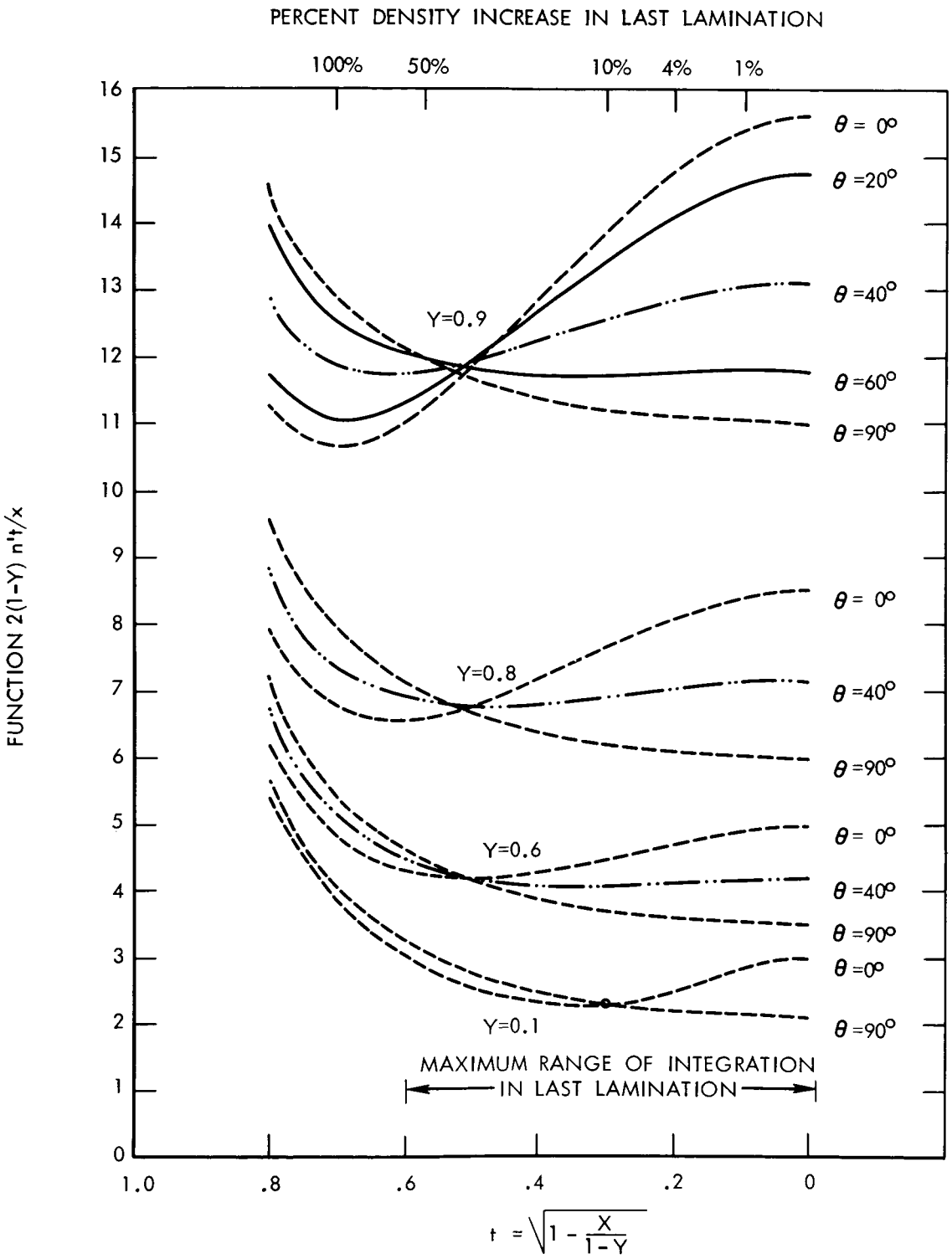
PERCENT DENSITY INCREASE IN LAST LAMINATION
100%
50%
10%
4%
1%
FUNCTION 2(1-Y) n't/x
Y=0.9
θ = 0°
θ =20°
θ =40°
θ =60°
θ =90°
Y=0.8
θ = 0°
θ =40°
θ =90°
Y=0.6
θ = 0°
θ =40°
θ =90°
Y=0.1
θ =0°
θ =90°
MAXIMUM RANGE OF INTEGRATION
IN LAST LAMINATION
t = √(1 - X/(1-Y))

FIGURE C-2

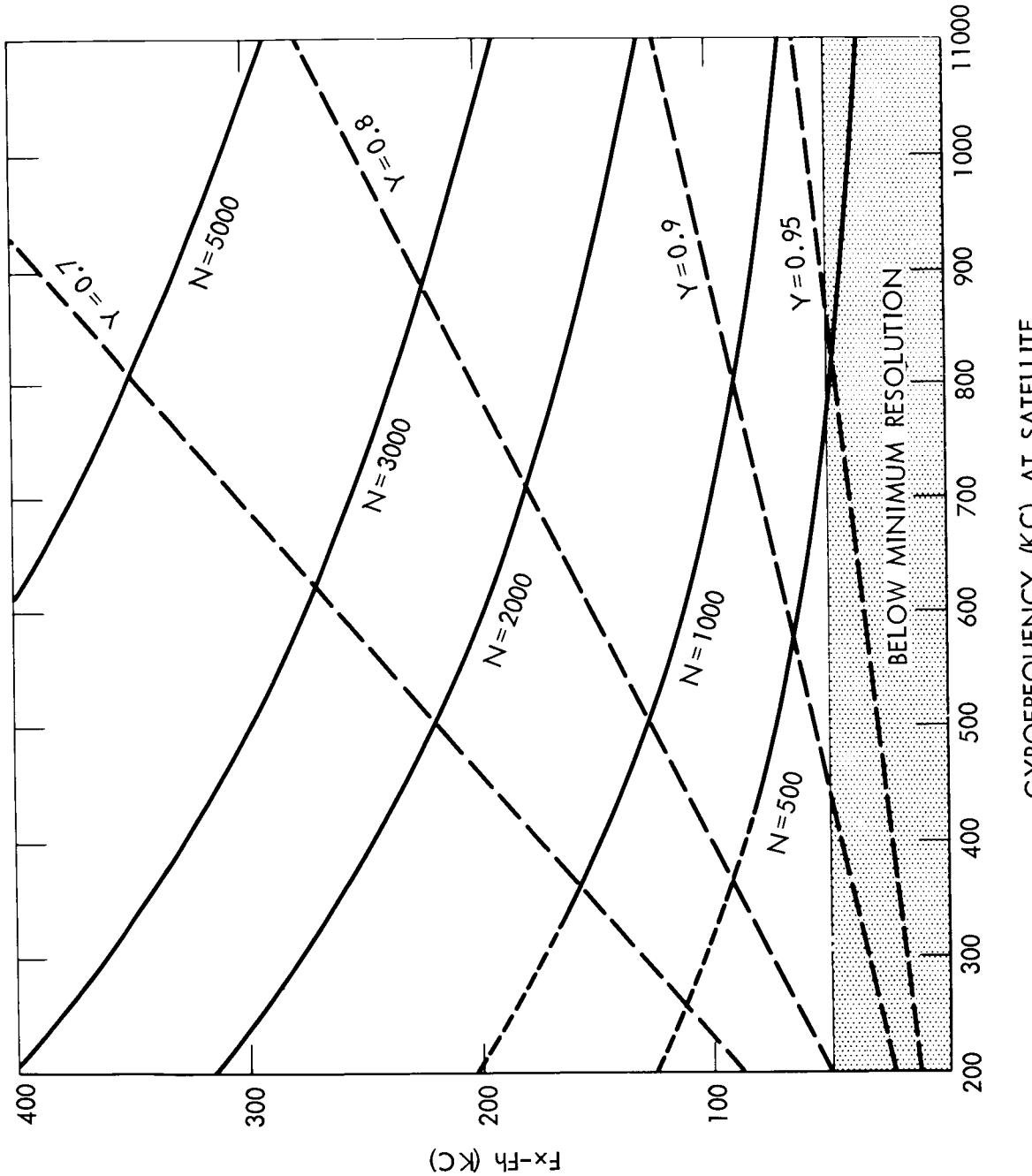
400
300
200
100
Fx-Fh (KC)
200
300
400
500
600
700
800
900
1000
11000
GYROFREQUENCY (KC) AT SATELLITE
N=5000
N=3000
N=2000
N=1000
N=500
Y=0.1
Y=0.8
Y=0.9
Y=0.95
BELOW MINIMUM RESOLUTION

FIGURE C-3

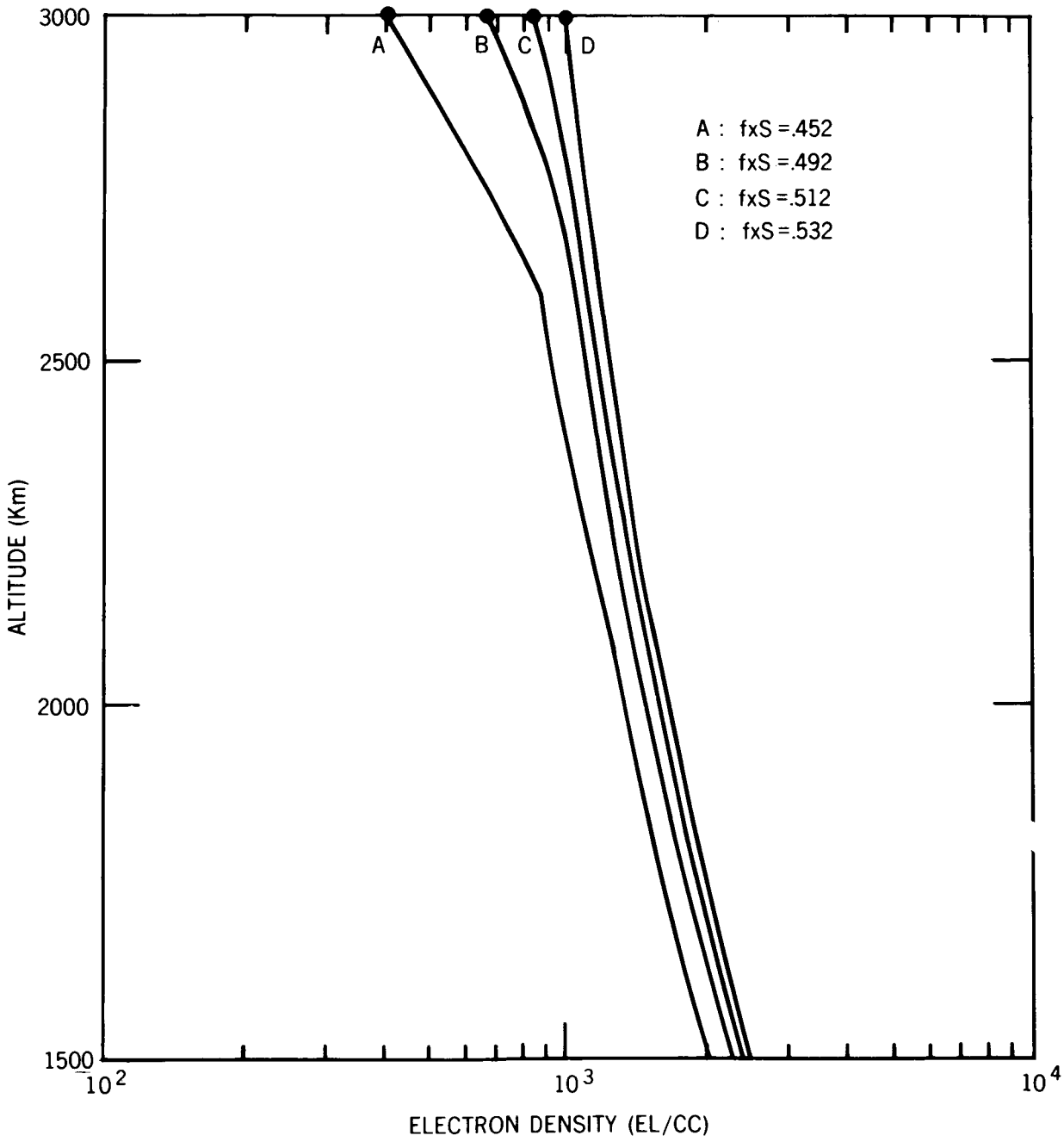
3000
2500
2000
1500
A
B
C
D
A : fxS =.452
B : fxS =.492
C : fxS =.512
D : fxS =.532
ALTITUDE (Km)
10^2
10^3
10^4
ELECTRON DENSITY (EL/CC)

DISCUSSION OF GSFC N-h PROGRAM

1. Basic Assumptions

In the GSFC parabolic-in-log N program, the electron density profile is assumed to consist of k laminations as shown in Fig. D-1. The first lamination (h_o, h_1) which begins at the satellite height h_o and extends down to the height h, is assumed to be linear-in-log N. All other laminations, such as (h_{j-1}, h_j) between heights h_{j-1} and h_j are assumed to be parabolic-in-log N with continuous slopes at the boundaries.

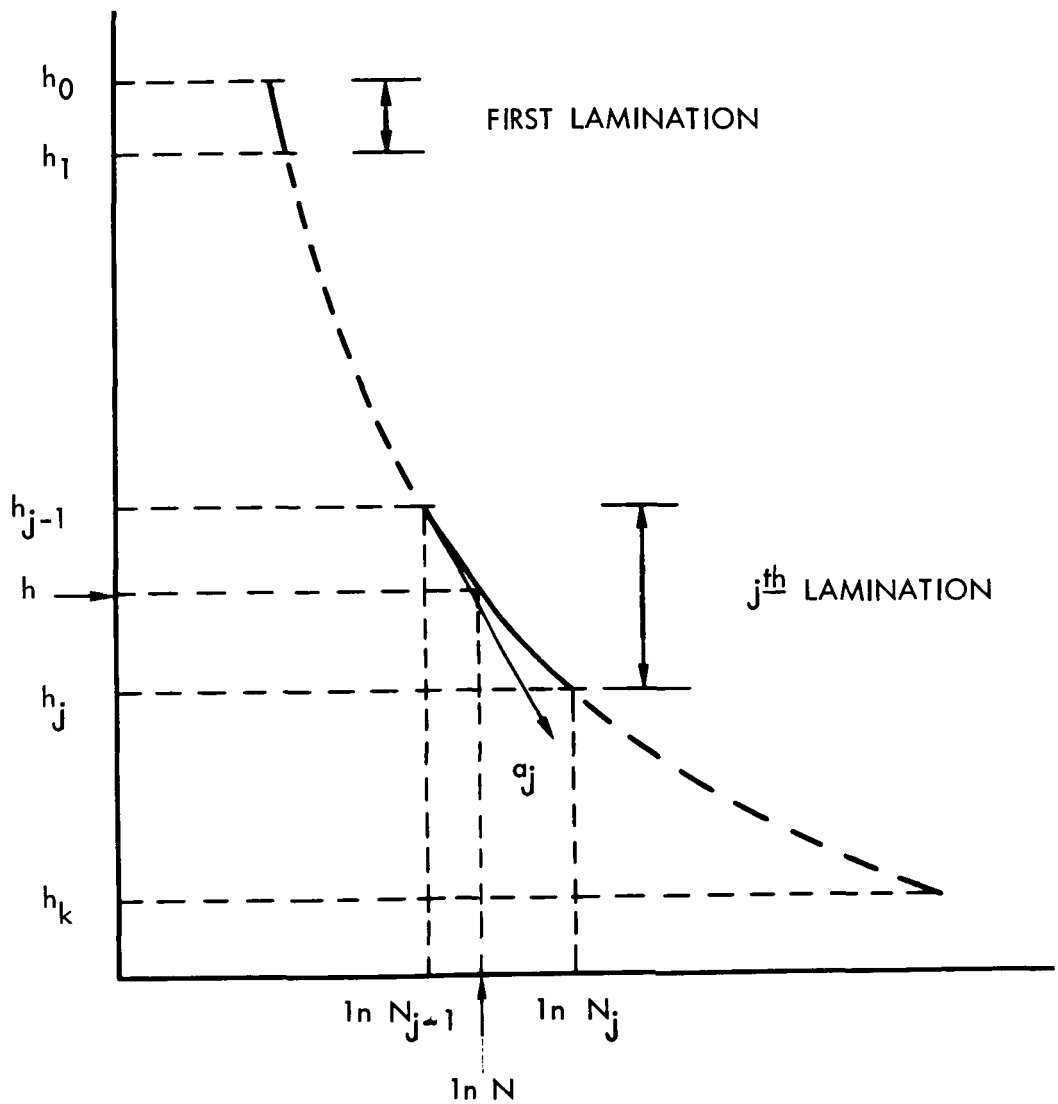

Fig. D-1 Lamination Model

The $j^{\underline{th}}$ lamination is defined by:

$$h = h_{j-1} + a_j \ln \frac{N}{N_{j-1}} + b_j (\ln \frac{N}{N_{j-1}})^2 \qquad \text{(D-1)}$$

where a_j is defined in terms of the a_{j-1} and b_{j-1} parameters of the previous lamination by the relationship:

$$a_j = a_{j-1} + 2b_{j-1} \ln \frac{N_{j-1}}{N_{j-2}} \qquad \text{(D-2)}$$

It should be noted that the assumptions made on the laminations require that the electron density must vary monotonically with altitude. If the topside h vs. lnN profile had a valley, the assumption that the slope be continuous, would require that there is at least one point where dh/d ln N is infinite. Since dh/d ln N = $a_j + 2b_j \ln (N/N_{j-1})$ and since the quantity $\ln (N/N_{j-1})$ is finite, this would require that either a_j or b_j be infinite. The lamination formulas used would then become meaningless.

In the N-h program, the laminations are calculated one at a time, in the order (h_0, h_1), (h_1, h_2), (h_2, h_3) etc... Hence all laminations between the altitudes h_0 and h_{j-1} are known, when the calculation of the $j^{\underline{th}}$ lamination is performed. Let f_j represent the frequency of the extraordinary wave reflected from the unknown height h_j. The virtual height h'_j corresponding to f_j is given by:

$$h'_j = \int_{h_1}^{h_0} n'dh + \int_{h_2}^{h_1} n'dh + \quad + \int_{h_j}^{h_{j-1}} n'dh \qquad \text{(D-3)}$$

$$= DP + \int_{h_j}^{h_{j-1}} n'dh \qquad \text{(D-4)}$$

where DP represents the <u>delay</u> in the <u>previous</u> laminations. The calculation of DP presents no special problem, since it involves calculation of integrals in which all parameters are known. The actual calculation of DP will be made clearer later. For the

present discussion (calculation of $j^{\underline{th}}$ lamination) it will be assumed that DP is known.

2. Initial Calculation of $j^{\underline{th}}$ lamination (Constant Y)

The reflection conditions at the bottom of the $j^{\underline{th}}$ lamination can be written in terms of the X and Y notation of Appendix A as follows:

$$X_j = 1 - Y_j \tag{D-5}$$

where

$$Y_j = \frac{(fH)_j}{f_j} \tag{D-6}$$

Equation D-1 can be expressed in terms of X by noting that

$$\frac{N}{N_{j-1}} = \frac{X}{X_{j-1}} \tag{D-7}$$

Making the substituting indicated by Eq. (D-7) in Eq. (D-1) and differentiating Eq. (D-1) yields:

$$dh = \left[a_j + 2b_j \ln\left(\frac{X}{X_{j-1}}\right)\right] \frac{dX}{X} \tag{D-8}$$

Substituting the above value of dh in Eq. (D-4) yields:

$$h'_j = DP + a_j \int_{X_j}^{X_{j-1}} \frac{n'}{X}\, dX + 2b_j \int_{X_j}^{X_{j-1}} \frac{n'}{X} \ln\left(\frac{X}{X_{j-1}}\right) dX \tag{D-9}$$

Letting $t^2 = 1-X/(1-Y_j)$ and noting that $dX = -2(1-Y_j)t\, dt$ gives

$$h'_j = DP - a_j \int_0^{t_{j-1}} 2(1-Y_j) \frac{n'}{X}\, t\, dt$$

$$- b_j \int_0^{t_{j-1}} 4(1-Y_j) \frac{n'}{X} \ln\left(\frac{X}{X_{j-1}}\right) t\, dt \tag{D-10}$$

To simplify the notation of Eq. D-10, the parameter X was retained in the formula. It must be understood however that in Eq. D-10, X is actually the following function of t:

$$X = (1-t^2)(1-Y_j) \qquad \text{(D-11)}$$

Similarly, since n' is a function of X, Y and θ, the values of X entering into the calculation of n' are those given by Eq. D-11. Since the value of Y_j is not known initially, it is necessary to use an estimated value of Y, to compute the integrals in Eq. (D-10). One method is to let $Y_j = Y_{j-1}$ and to assume that Y is constant within the lamination and equal to Y_{j-1}. All the parameters are then known in Eq. (D-10) and the integrals can be evaluated. Representing the integrals associated with a_j and b_j by S_A and S_B respectively, yields:

$$b_j = (DP - h'_j - a_j S_A)/S_B \qquad \text{(D-12)}$$

3. Iteration With Variable Y

The approximate answer thus obtained for the lamination can be refined by an iteration process, in which Y_j is computed for the calculated value of h_j and in which the values of Y entering into the n' calculations are computed by assuming that Y decreases from the value Y_{j-1} at the top of the lamination to the value Y_j at the bottom of the lamination according to:

$$Y = \frac{K}{(R + h)^3} \qquad \text{(D-13)}$$

The constant K and the earth's radius R in Eq. (D-13) can be eliminated by making use of the boundary conditions:

$$Y_j(R + h_j)^3 = Y_{j-1}\ (R + h_{j-1})^3 = K \qquad \text{(D-14)}$$

To express Y in terms of Y_j, Y_{j-1} and h, Eqs. (D-13) and (D-14) are written:

$$R + h = K/Y^{1/3} \qquad \text{(D-15)}$$

$$R + h_j = K/Y_j^{1/3} \qquad \text{(D-16)}$$

$$R + h_{j-1} = K/Y_{j-1}^{1/3} \qquad \text{(D-17)}$$

from which

$$h - j = K(Y^{-1/3} - Y_j^{-1/3}) \qquad \text{(D-18)}$$

$$h_{j-1} - h_j = K(Y_{j-1}^{1/3} - Y_j^{-1/3}) \qquad \text{(D-19)}$$

The constant K is eliminated by dividing Eq. (D-18) by Eq. (D-19). Solving the resulting equation for Y yields:

$$Y = \frac{Y_j}{\left\{1 + \left[\left(\frac{Y_j}{Y_{j-1}}\right)^{1/3} - 1\right]\frac{(h-h_j)}{(h_{j-1}-h_j)}\right\}^3} \qquad \text{(D-20)}$$

The values of h to be used in Eq. (D-20) should be those corresponding to the values of X. It is therefore important to note that the b_j obtained from Eq. (D-12) was based upon the assumption:

$$X_j = 1-Y_{j-1} \qquad \text{(D-21)}$$

Hence to be consistent the altitude h_j must be calculated according to the formula:

$$h_j = h_{j-1} + a_j \ln\left(\frac{X_j}{X_{j-1}}\right) + b_j \left[\ln\left(\frac{X_j}{X_{j-1}}\right)\right]^2 \qquad \text{(D-22)}$$

where $X_j = 1-Y_{j-1}$

If Y_j is now redefined in terms of h_j, (giving $X_j = 1-Y_j$) Eq. (D-22) will no longer yield the same value of

h_j at the reflection point. In order to proceed with the iteration (and in particular make sure that Eq. (D-20) will keep Y between Y_{j-1} and Y_j), we must either redefine h_j in terms of $X_j = 1-Y_j$, or recompute b_j so that Eq. (D-22) gives the same value of h_j for the new X_j. In the GSFC program, the computed value of h_j is preserved. The parameters Y_j, X_j, and b_j are redefined prior to the iteration process. Iteration is continued until the successive values obtained for h_j agree to within 0.01 km. When this happens the difference between the b_j computed from Eq. (D-12) and the b_j reevaluated prior to iteration becomes insignificant. When the desired convergence is achieved, the final value of b_j is the value computed from Eq. (D-12) and the final value of h_j correspond to the Y_j and X_j obtained from the previous calculation. Hence the final compromise is made on fH_j which is actually computed (and stored in the program) for an altitude slightly different than h_j (the altitude difference, however, being less than 10 meters).

Returning to the posponed discussion of DP of Eq. (D-4), it is seen that DP involves a summation of integrals identical to those of the $j^{\underline{th}}$ lamination, except that the limits are different, but <u>known</u> when the $j^{\underline{th}}$ lamination is calculated. These integrals are also evaluated making use of the change of variable $t^2 = 1 - X\,(1-Y_j)$, and using Eq. (D-20) to vary Y within the lamination.

For the first lamination, which is assumed linear-in-log N, the coefficient <u>b</u> is zero and Eq. (D-10) is solved for the coefficient <u>a</u>. Actually the first calculation made on the $j^{\underline{th}}$ lamination is also based upon a linear-in-log N method; this yields a good estimate of the value of h_j, which is then used as the starting point for the iteration using the parabolic-in-log N technique.

4. Miscellaneous Comments

The existence of a continuous extraordinary trace on a topside ionogram usually implies that the electron density decreases monotonically with altitude. It is theoretically possible, however, to obtain continuous extraordinary echoes at the satellite from a region below the satellite where the electron density is constant or even increasing with altitude. The formula for fx:

$$fx = \frac{fH}{2} + \tfrac{1}{2}\sqrt{4fN^2 + fH^2}$$

shows that for a constant fN, the value of fx will increase monotonically as a function of the distance below the satellite, simply because fH is increasing. This can also be true if fN decreases monotonically with depth below the satellite, provided the decrease is over-compensated by the increase in fH.

It was pointed out earlier that the lamination formulas used for the parabolic-in-log N program require that the electron density variation be monotonic. In fact, since the density cannot be continuously decreasing below the satellite, the parabolic-in-log N assumptions imply that the topside electron density must decrease monotonically with altitude. This assumption is also implicit in the transformation $t^2 \doteq 1-X/(1-Y_j)$.

Even if the profile decreases monotonically with altitude, the iteration process (based upon the initial assumption $Y_j = Y_{j-1}$) may not converge if the profile is sufficiently steep. The permissible values of gyrofrequencies at the bottom of the lamination range from the value at the top of the lamination fH_{j-1} to a maximum value fH_{jM} corresponding to the minimum permissible increase in density. Thus, if we define the minimum permissible increase in density as 0.1 per cent, the quantity fH_{jM} is defined by:

$$fx_j\,(fx_j - fH_{jM}) = (1.001)\; fx_{j-1}(fx_{j-1} - fH_{j-1}) \qquad (D\text{-}23)$$

True height calculations yield different answers for h_j as fH_j is varied from fH_{j-1} to fH_{jM}. The basic purpose of the iteration process is to find from all the permissible values of h_j, the particular height h_j at which the fH_j used in the true height calculation is the same as the actual value of fH_j at the altitude h_j. The calculations were performed for hS = 2000 km, fHS = 0.45 MHz, fH varying according to the inverse cube law, $\theta = 45^o$, fxS = 0.50 MHz, and at the bottom of the first lamination f_1 = 0.52 MHz. The resulting heights h_1 at the bottom of the first lamination are shown on Fig. D-2 as a function of fH_1 (fH at bottom of the first lamination) for various assumed values of virtual heights (h_1). For example if h'_1 = 1800 km, the resulting heights are given by the curve L_1. Curve M shows the actual gyrofrequency at the altitudes shown. The correct height is therefore given by the intersection of curves L_1 and M. If the initial assumption is fH_1 = fHS, the first value of h_1 would correspond to A_1. The iteration would then be performed using fH at B_1, which is the correct fH at the altitude of A_1. This would yield a new value of h_1, namely that corresponding to C_1. The second iteration is performed using the fH value at D_1. It is seen graphically that the process converges to the point O_1. The same process, however, will not converge on curve L_2, although there is a solution at O_2. If the calculation is started with the maximum permissible value of fH, the initial height will be at P_1 on curve L_1 and at P_2 on curve L_2. It is seen that the process will then always converge, if there is a solution. Curve L_3 is an example in which there is no solution such that the density at the bottom of the first lamination is greater than the density at the satellite.

In view of the above consideration, the GSFC program performs the initial calculation of the laminations using the value of fH_j defined by Eq. (D-23), provided fH_{jM} is less than 1.15 fH_{j-1}. This upper limit was set for fH_{jM} because at lower altitudes where the density increases rapidly with depth, Eq. (D-23) leads to unreasonably high values of fH_{jM}.

FIGURE D-2

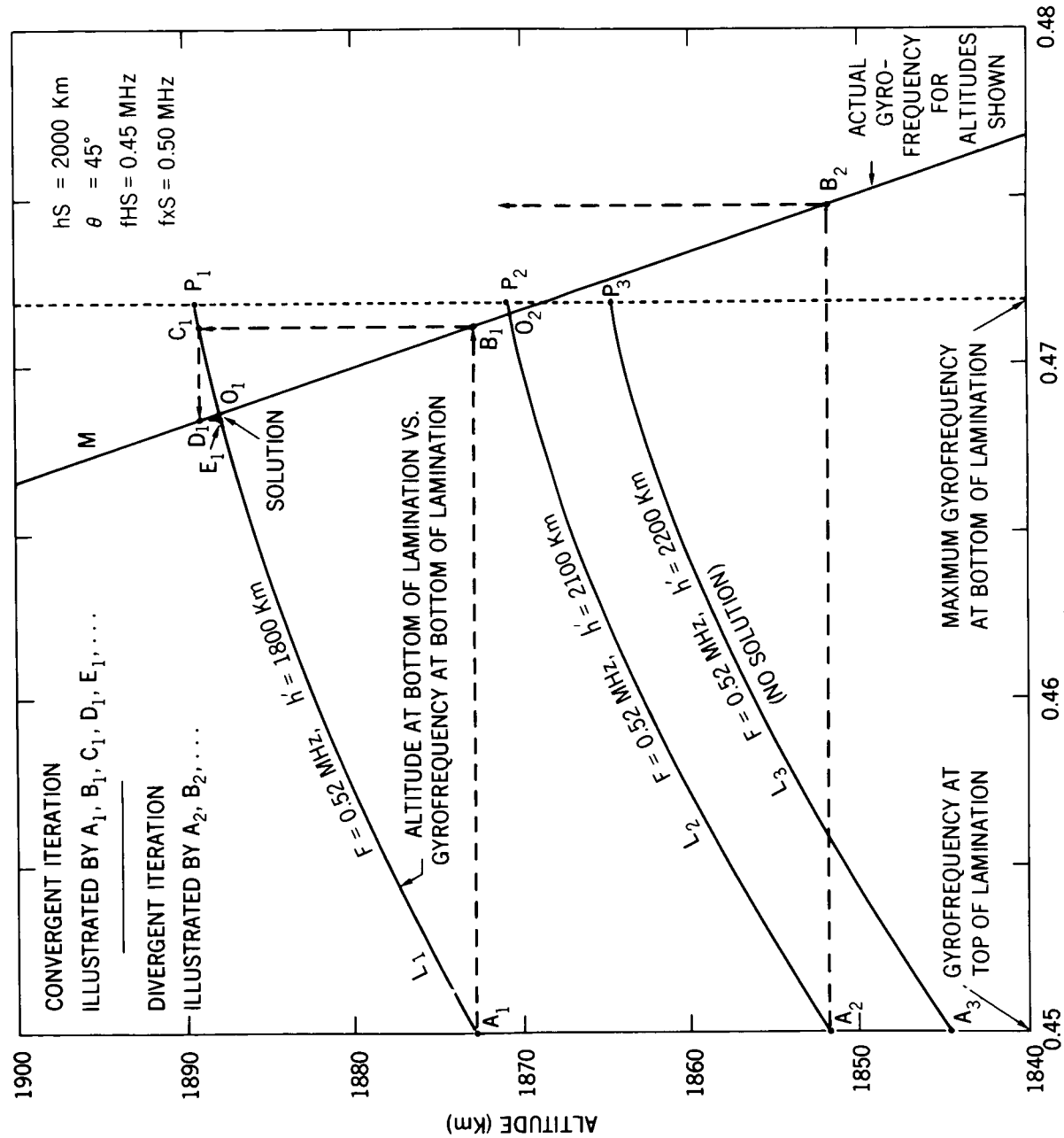
CONVERGENT ITERATION
ILLUSTRATED BY $A_1, B_1, C_1, D_1, E_1, \ldots$
DIVERGENT ITERATION
ILLUSTRATED BY $A_2, B_2, \ldots$
hS = 2000 Km
θ = 45°
fHS = 0.45 MHz
fxS = 0.50 MHz
M
P_1
C_1
D_1
E_1
O_1
SOLUTION
L_1
F = 0.52 MHz, h' = 1800 Km
ALTITUDE AT BOTTOM OF LAMINATION VS. GYROFREQUENCY AT BOTTOM OF LAMINATION
A_1
B_1
P_2
O_2
L_2
F = 0.52 MHz, h' = 2100 Km
P_3
L_3
F = 0.52 MHz, h' = 2200 Km
(NO SOLUTION)
A_2
B_2
ACTUAL GYRO-FREQUENCY FOR ALTITUDES SHOWN
MAXIMUM GYROFREQUENCY AT BOTTOM OF LAMINATION
GYROFREQUENCY AT TOP OF LAMINATION
A_3
1900
1890
1880
1870
1860
1850
1840
ALTITUDE (Km)
0.45
0.46
0.47
0.48
GYROFREQUENCY (MHz)

APPENDIX E

SPATIAL AND TEMPORAL COVERAGE OF TOPSIDE SOUNDINGS

Introduction

Ground-based soundings provide continuous (24 hours per day) monitoring of the ionosphere below F2max at the various sites where ionospheric sounding stations are located. The situation is quite different with the topside sounder, since the soundings can take place only at the specific locations and times dictated by the orbit. Thus, if an observer wanted topside data for a given location on a given day, the nearest subsatellite point could be 1000 km away from the location of interest. Furthermore, assuming that the satellite sounder was turned on when this nearest approach occurred, the available sounding would have been at only one of the two possible local mean times for that particular date. Due to limitations imposed by the satellite power systems, Alouette I and Alouette II operated initially a maximum of 7 hours per day. Solar cell degradation produces further reduction in available power, and after one year, 4 hours of operation per day is typical for the topside sounder. Fortunately, the subsequent solar cell decay is less severe, and in its 5th year of operation, Alouette I could still provide $2\frac{1}{2}$ hours of soundings per day.

In view of the satellite power limitation, topside soundings prior to 1965 have been concentrated in certain geographical areas. Most of the soundings were conducted over the American continents. These data were supplemented with observations obtained near Winkfield, (England), Singapore, Woomera (Australia) and Hawaii. Since 1965, the geographical coverage has been gradually increased to include West-Africa, Norway, Antarctica and Japan.

Hence in order to utilize topside sounder data for correlative studies, it is necessary to know the satellite orbit (location and local mean time of subsatellite point) and also the satellite

schedule (planned geographical coverage for topside soundings and actual times when the satellite sounder was operating).

One additional comment should be made concerning the availability of topside soundings. As is the case for other satellite experiments, the scientific teams responsible for the planning and execution of the project have first rights to the acquired data. The period of time during which these rights are exercised is a nominal year after acquisition of the topside ionograms. One year after the topside ionograms have been processed, copies are deposited at the World Data Center in Boulder, Colorado, and these copies are available to anyone who would like to use them.

The following discussion will provide some indication of the topside data which might be available for correlative studies, i.e. for studies in which time and space simultaneity is an important factor.

Alouette I

Topside soundings of the upper ionosphere were initiated on September 29, 1962 with the successful launching of Alouette I. This satellite was placed in a nearly circular orbit (apogee 1033 km, perigee 994 km), at an inclination of 80.47 degrees. For any given day and latitude the soundings can be made at only two local times 12 hours apart. The local time would be the same at all latitudes, if the orbit were polar. Due to the 80.5 degree inclination, the local time at the subsatellite point is not constant with latitude. However the change in local time is small at low and mid-latitudes (typically 1 hr. 15 min. over the latitude range from 45^{o} South to 45^{o} North). Since the local mean time varies by 24 hours along the entire orbit, and since this change is continuous, most of the variation in LMT on a given day takes place between 60 and 80 degrees of latitude.

The combined effect of the earth motion around the sun and of the orbit plane precession, causes the two daily local

mean times to change gradually from one day to the next day in such a way that a complete diurnal coverage is achieved in a period of 3 months. This variation repeats itself almost exactly from year to year. Hence a single graph, such as the one shown in Fig. E-1, can be used to estimate the local time at which data is available for a given month and day. The graph of Fig. E-1, provides also this information for Alouette II, but valid only for the year 1966. The graph of Fig. E-1 is for 0 degrees of latitude, however the LMT shown are still correct to within $\pm$1 hour for latitudes ranging from -60 to +60 degrees.

Returning to the problem of correlative studies where not only time simultaneity, but also space simultaneity must be achieved, it is important to know how the position of the nearest subsatellite point varies with respect to a location of interest. On a given day the two nearest subsatellite tracks (for one of the two available local mean times) would be spaced by 26.52 degrees of longitudes. The worst situation would be to have one orbit 13.26 degrees West of the desired location and the other orbit 13.26 degrees East. However, if the nearest daily crossings (at the latitude of the location of interest) are plotted for a period of 7 days, it is seen that the complete set of nearest crossings are almost uniformly spaced in longitude (the spacing is either 3.7 or 3.8 degrees). Hence, in any given week there will be at least one subsatellite track within 2 degrees of the desired longitude. This is illustrated in Figure E-2 which shows the set of (nighttime) equatorial crossings nearest to the Greenwich meridian for an arbitrarily selected one week period beginning on Sept 20, 1964. The following week (not shown on Fig. E-2) the entire pattern is repeated, with a very slight longitude displacement (0.128 degrees). For the example shown the nearest crossing during the first week occurred on the 6th day and it was 1.05 degrees West of the desired location (0 degree latitude, 0 degree longitude). On the 6th day of the second week the corresponding crossing would be 0.128 degrees closer to the Greenwich meridian. The upper portion of Fig. E-2

shows (on an enlarged longitude scale) the position of the two nearest weekly crossings for the 3rd, 5th, 7th, 9th and 11th consecutive weeks. It is seen that on the 6th day of the 9th week the crossing comes the nearest to the Greenwich meridian (in this particular case 0.04 degrees).

The pattern shown on Fig. E-2 changes slightly from year to year. The 7-day cycle holds true for the first four years of Alouette I (and most likely for its subsequent life). Thus, once each week, a subsatellite track can be found which is within 2 degrees of longitude of any point on the earth surface between -80 degrees and + 80 degrees of latitude. The rate at which the pattern of Fig. E-2 shifts varies slightly from year-to-year. For the example shown (4th quarter of 1964) the rate was 0.13 degree per week. One year earlier (Oct 1963) the rate was 0.08^{o}/W and one year later (Oct 1965) the rate was 0.18^{o}/W. An experimenter wishing to find the nearest subsatellite track to a desired location can find in the satellite World Maps the necessary data to construct a graph such as Fig. E-2 for any latitude and longitude of interest.

Alouette II

Alouette II was launched Nov. 11, 1965 in an eccentric orbit (apogee: 2983 km, perigee: 501 km) inclined at 79.83 degrees. The general comments made on the Alouette I data coverage are also applicable to Alouette II. The local time variation (see Fig. E-1 and E-3) is similar to that of Alouette I, but since the Alouette II diurnal variation takes about 102 days, the variation does not repeat itself from year to year. The procedure illustrated in Fig. E-2 for finding data suitable for correlations requiring space simultaneity can be used with Alouette II. For the first year of Alouette II operation, the recurrent pattern corresponds to a 5 day cycle, giving a longitude spacing of about 6 degrees. Thus once every 5 days there will be at least one subsatellite track within 3 degrees of a desired location. The rate at which the pattern shifts varies much more rapidly than for Alouette I. In December 1965, the 5-day Alouette II pattern was moving westward at a rate of 0.80 degrees/week. The westward drift slowed

down gradually (0.54^{o}/W in April 1966, 0.14^{o}/W in Oct 1966) and in January 1967 the drift had reversed its direction and become eastward with a rate 0.07 degrees/week.

In view of its eccentric orbit, another question which may be raised on Alouette II is the altitude range over which data is acquired. Due to the rotation of the line of apsides the position of apogee and perigee changes periodically.

The argument of perigee is indicated on Figures E-1 and E-3. Since perigee is measured from the ascending node, a perigee of 0 degrees occurs on a North - bound pass. Similarly a perigee of 180 degrees occurs on a South - bound pass at the descending node. When perigee is at 90 degrees, it coincides with the North point(i.e. it is where the north bound pass becomes a south bound pass). Similarly, a perigee at 270 degrees coincides with the South point. Since the local mean time scale on Figures E-1 and E-3 corresponds to the equatorial crossings, the indicated local mean times are correct at perigee whenever perigee is at 0 or 180 degrees. The local mean time when perigee is at 90^{o} (i.e. at the north point) is 6 hours later than the time at the North bound equatorial crossing (ascending node). The local mean time when perigee is at 270 degrees (i.e. at the **south** point) is 6 hours earlier than the time at the ascending node. It is seen from Figure E-1 that apogee at the equator occurred at approximately midnight in February 1966. In March 1967, apogee occurred at the equator at approximately 3 A.M. local mean time. Thence one can expect that apogee will occur at the equator at noon in 1970. Typical height variations as a function of altitude are shown on Figure E-4. Since apogee at the equator can occur for either perigee at 0 degree or perigee at 180 degrees, it is necessary to indicate how the graph should be read as a function of time. For increasing time, the curve of Fig. E-4 is traced clockwise when perigee is at 0 degree and counterclockwise when perigee is at 180 degrees. Electron density oontours obtained when perigee is near the South point are given in Fig. **8.**

FIGURE E-1

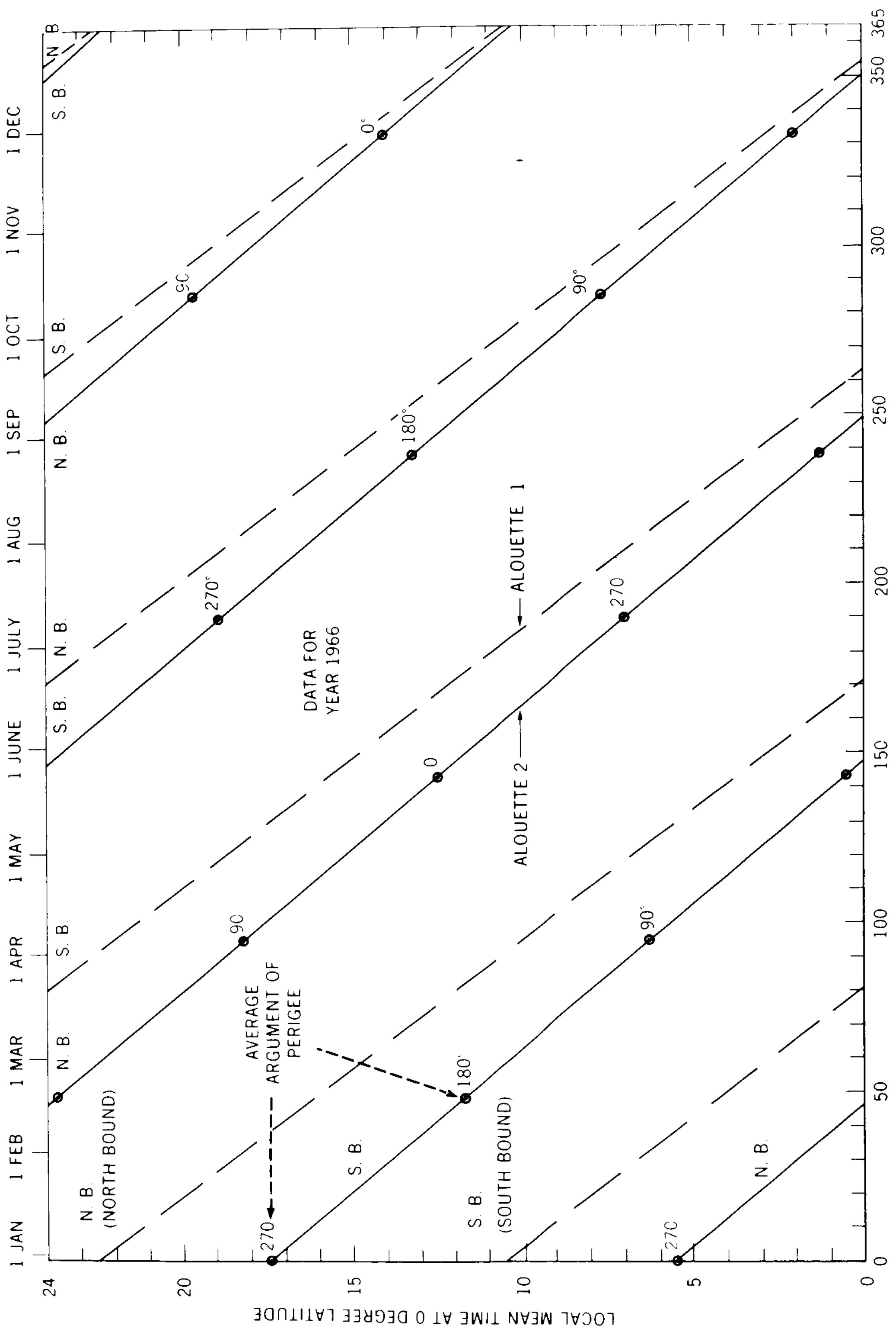

DATA FOR YEAR 1966
ALOUETTE 1
ALOUETTE 2
AVERAGE ARGUMENT OF PERIGEE
N. B. (NORTH BOUND)
S. B. (SOUTH BOUND)
N. B.
S. B.
1 JAN
1 FEB
1 MAR
1 APR
1 MAY
1 JUNE
1 JULY
1 AUG
1 SEP
1 OCT
1 NOV
1 DEC
DAY NUMBER
0
50
100
150
200
250
300
350
365
LOCAL MEAN TIME AT 0 DEGREE LATITUDE
0
5
10
15
20
24
270
90
0
180

FIGURE E-2

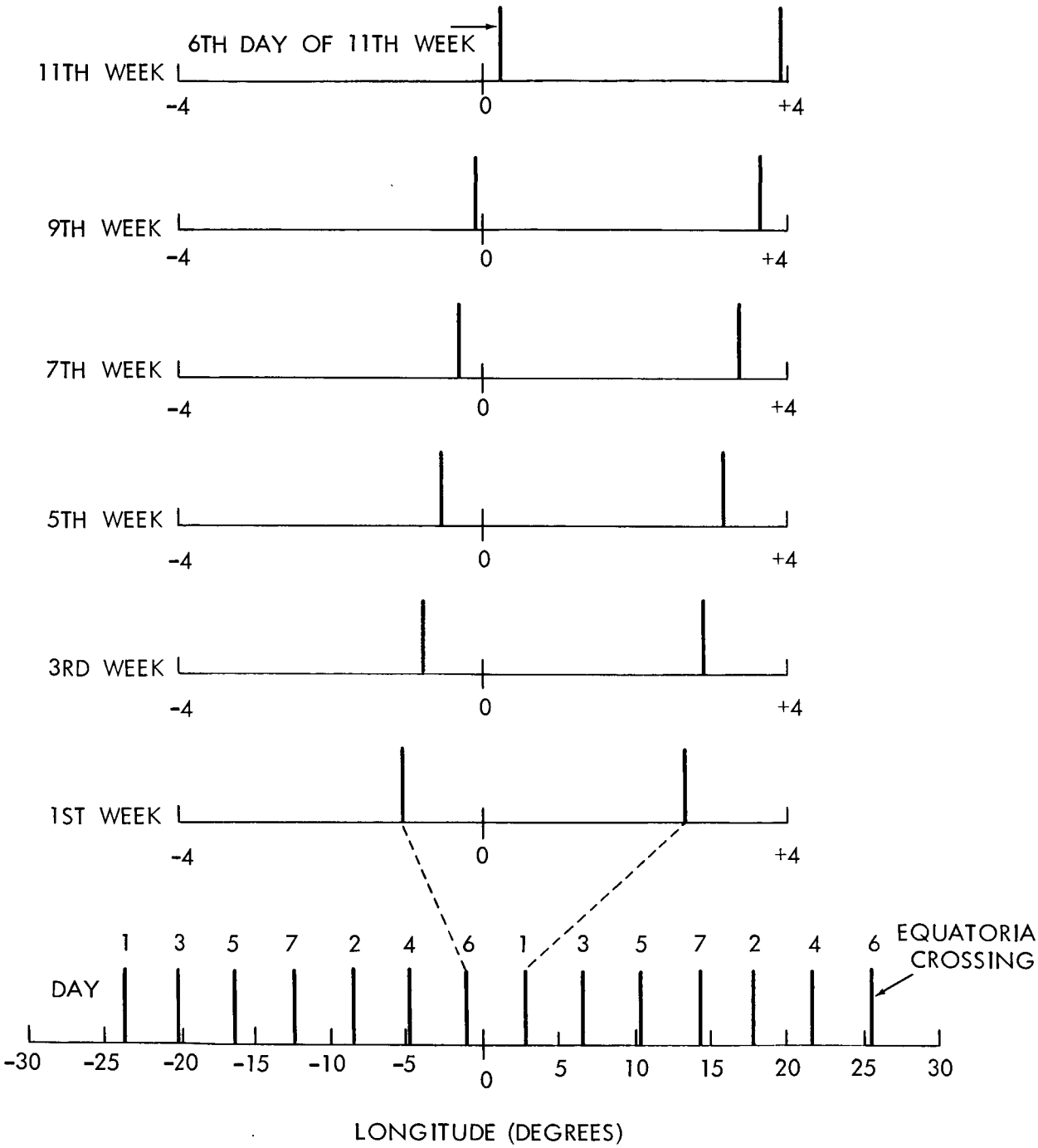

1st week selected arbitrarily as period from
64-09-20 (Day 1) to 64-09-26 (Day 7)

FIGURE E-3

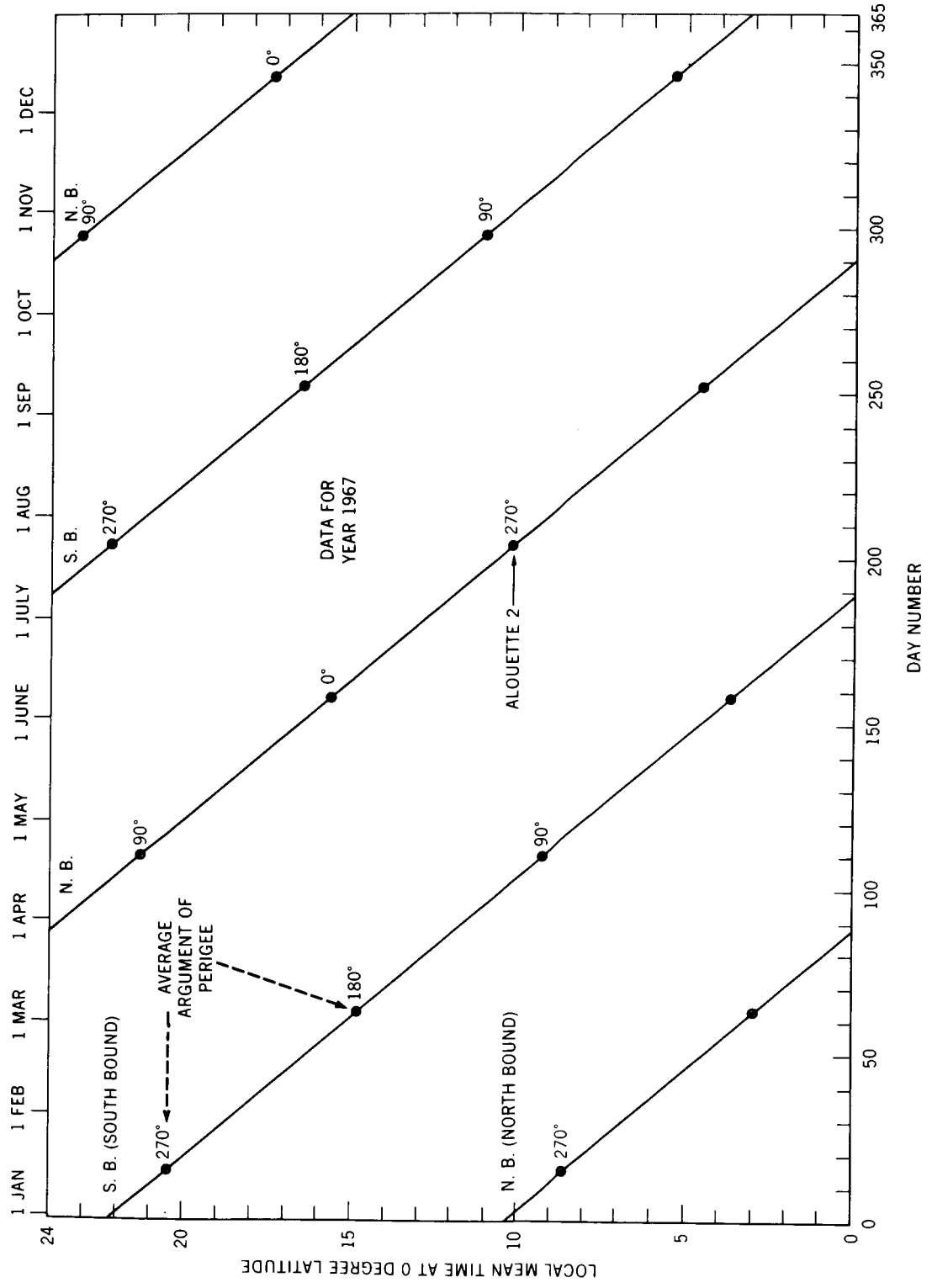
1 JAN
1 FEB
1 MAR
1 APR
1 MAY
1 JUNE
1 JULY
1 AUG
1 SEP
1 OCT
1 NOV
1 DEC
0
50
100
150
200
250
300
350
365
DAY NUMBER
24
20
15
10
5
0
LOCAL MEAN TIME AT 0 DEGREE LATITUDE
S. B. (SOUTH BOUND)
N. B. (NORTH BOUND)
AVERAGE ARGUMENT OF PERIGEE
ALOUETTE 2
DATA FOR YEAR 1967
0°
90°
180°
270°
N. B.
S. B.

FIGURE E-4

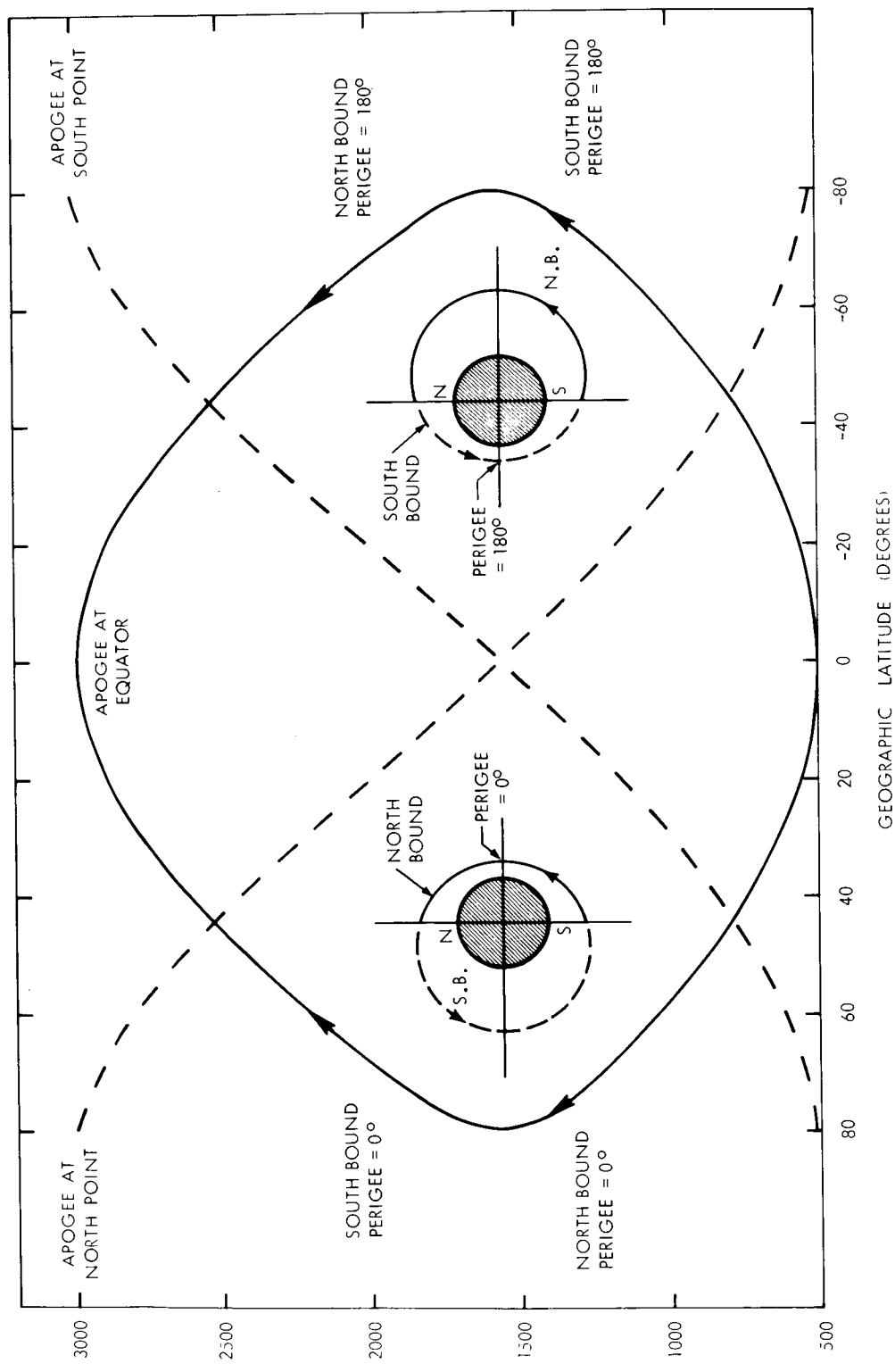
APOGEE AT SOUTH POINT
NORTH BOUND PERIGEE = 180°
SOUTH BOUND PERIGEE = 180°
APOGEE AT EQUATOR
SOUTH BOUND
PERIGEE = 180°
N.B.
N
S
NORTH BOUND
PERIGEE = 0°
S.B.
APOGEE AT NORTH POINT
SOUTH BOUND PERIGEE = 0°
NORTH BOUND PERIGEE = 0°
3000
2500
2000
1500
1000
500
ALTITUDE (KM)
-80
-60
-40
-20
0
20
40
60
80
GEOGRAPHIC LATITUDE (DEGREES)